

Ultra-light axions and the S_8 tension: joint constraints from the cosmic microwave background and galaxy clustering

Keir K. Rogers,^{a,1} Renée Hložek,^{a,b} Alex Laguë,^{c,d,b,a} Mikhail M. Ivanov,^{e,f} Oliver H. E. Philcox,^{g,h,i,e} Giovanni Cabass,^e Kazuyuki Akitsu^e and David J. E. Marsh^j

^aDunlap Institute for Astronomy & Astrophysics, University of Toronto,
50 St. George Street, Toronto, ON M5S 3H4, Canada

^bDavid A. Dunlap Department of Astronomy & Astrophysics, University of Toronto,
50 St. George Street, Toronto, ON M5S 3H4, Canada

^cDepartment of Physics and Astronomy, University of Pennsylvania,
209 South 33rd Street, Philadelphia, PA 19104-6396, USA

^dCanadian Institute for Theoretical Astrophysics, University of Toronto,
60 St. George Street, Toronto, ON M5S 3H8, Canada

^eSchool of Natural Sciences, Institute for Advanced Study,
1 Einstein Drive, Princeton, NJ 08540, USA

^fNASA Hubble Fellowship Program Einstein Postdoctoral Fellow

^gCenter for Theoretical Physics, Department of Physics, Columbia University,
538 West 120th Street, New York, NY 10027, USA

^hSimons Society of Fellows, Simons Foundation, New York, NY 10010, USA

ⁱDepartment of Astrophysical Sciences, Princeton University,
Peyton Hall, 4 Ivy Lane, Princeton, NJ 08544, USA

^jTheoretical Particle Physics and Cosmology, King's College London,
Strand, London WC2R 2LS, UK

¹Corresponding author.

E-mail: keir.rogers@utoronto.ca, hlozek@dunlap.utoronto.ca,
alague@sas.upenn.edu, ivanov@ias.edu, ohep2@cantab.ac.uk, gcabass@ias.edu,
kakitsu@ias.edu, david.j.marsh@kcl.ac.uk

Abstract. We search for ultra-light axions as dark matter (DM) and dark energy particle candidates, for axion masses $10^{-32} \text{ eV} \leq m_a \leq 10^{-24} \text{ eV}$, by a joint analysis of cosmic microwave background (CMB) and galaxy clustering data – and consider if axions can resolve the tension in inferred values of the matter clustering parameter S_8 . We give legacy constraints from *Planck* 2018 CMB data, improving 2015 limits on the axion density $\Omega_a h^2$ by up to a factor of three; CMB data from the Atacama Cosmology Telescope and the South Pole Telescope marginally weaken *Planck* bounds at $m_a = 10^{-25} \text{ eV}$, owing to lower (and theoretically-consistent) gravitational lensing signals. We jointly infer, from *Planck* CMB and full-shape galaxy power spectrum and bispectrum data from the Baryon Oscillation Spectroscopic Survey (BOSS), that axions are, today, $< 10\%$ of the DM for $m_a \leq 10^{-26} \text{ eV}$ and $< 1\%$ for $10^{-30} \text{ eV} \leq m_a \leq 10^{-28} \text{ eV}$. BOSS data strengthen limits, in particular at higher m_a by probing high-wavenumber modes ($k < 0.4h \text{ Mpc}^{-1}$). BOSS alone finds a preference for axions at 2.7σ , for $m_a = 10^{-26} \text{ eV}$, but *Planck* disfavours this result. Nonetheless, axions in a window $10^{-28} \text{ eV} \leq m_a \leq 10^{-25} \text{ eV}$ can improve consistency between CMB and galaxy clustering data, e. g., reducing the S_8 discrepancy from 2.7σ to 1.6σ , since these axions suppress structure growth at the $8h^{-1} \text{ Mpc}$ scales to which S_8 is sensitive. We expect improved constraints with upcoming high-resolution CMB and galaxy lensing and future galaxy clustering data, where we will further assess if axions can restore cosmic concordance.

Contents

1	Introduction	1
2	Axion structure formation model	4
2.1	Linear theory	4
2.1.1	Axion cosmology	4
2.1.2	S_8 and the linear matter power spectrum	5
2.1.3	Cosmic microwave background	7
2.2	Galaxy clustering and the effective field theory of large-scale structure	7
2.2.1	Galaxy power spectrum and bispectrum multipoles	7
2.2.2	Introduction to the effective field theory of large-scale structure	10
2.2.3	Axions and the effective field theory of large-scale structure	10
3	Data	11
3.1	Cosmic microwave background	12
3.1.1	<i>Planck</i>	12
3.1.2	Atacama Cosmology Telescope	13
3.1.3	South Pole Telescope	14
3.2	Baryon acoustic oscillations & supernovae	14
3.3	Baryon Oscillation Spectroscopic Survey galaxy power spectrum & bispectrum	15
3.4	Parameter inference	15
4	Results	16
4.1	Cosmic microwave background, baryon acoustic oscillations & supernovae	16
4.1.1	<i>Planck</i>	16
4.1.2	All CMB, BAO & supernovae	20
4.2	Baryon Oscillation Spectroscopic Survey galaxy power spectrum & bispectrum	26
4.2.1	Λ CDM	26
4.2.2	Parameter tension metrics	26
4.2.3	BOSS-only axion constraints	28
4.2.4	Joint <i>Planck</i> and BOSS axion constraints	31
5	Discussion	36
5.1	Comparison to previous work	39
5.2	$m_a = 10^{-26}$ eV	39
5.3	Comparison to other axion probes and future prospects	40
5.4	Axions as a resolution to the S_8 parameter tension	41
6	Conclusions	43

1 Introduction

While evidence for dark matter (DM) exists observationally [1–6], the fundamental nature of dark matter remains one of the greatest unsolved problems in science. Axions are a well-motivated particle candidate for DM [7–15]. Axions were proposed to solve the strong CP

problem [16–18] and can arise in a string theory “axiverse” where many axions of different masses are produced, suggesting that no single axion, but rather a mixture, can dominate the dark sector [16, 18–22]. Depending on their particle mass, axions behave either as DM or as a scalar field dark energy (DE) component [23]. Axions are proposed to resolve the so-called “small-scale crisis” in the clustering of matter [24–26], as they suppress the growth of small-scale (sub-Mpc) structure depending on the mass of the axion. Improvements in our ability to model astrophysical effects in the formation of Galactic and sub-Galactic structure [e.g., 27] and a more complete census of the Milky Way (MW) satellite galaxy population [e.g., 28] have demonstrated the viability of astrophysical solutions to the “small-scale crisis.” Further, complementary constraints from e.g., the Lyman-alpha forest [29] and the MW sub-halo mass function [30] have ruled out the axion mass $\sim 10^{-22}$ eV as being all the DM that is invoked to address small-scale issues. Nonetheless, advances in our understanding of axion structure formation including astrophysical effects [e.g., 31–36] now allows us to test empirically using cosmological data the existence of ultra-light axions, as motivated from fundamental theory, across the full mass range where their wavelength is astrophysically large (10^{-32} eV $\leq m_a \leq 10^{-18}$ eV).

Observational constraints on the axion typically limit a combination of the axion mass and the axion energy density (or the fraction that axions make up of the total DM energy density). Multiple tracers have been used to constrain the allowed mass and density of axions including, e.g., the cosmic microwave background [CMB; 23, 37, 38], galaxy clustering [39], galaxy weak lensing [40, 41], the Lyman-alpha forest [29, 32, 42–45], dwarf galaxies [30, 46, 47], 21 cm observations [48–50]. A single axion species as the *only* DM candidate is ruled out by the Lyman-alpha forest for masses less than 2×10^{-20} eV (at 95% c.l.) [29]. However, axions as a component of the DM or DE (either as a mixture of axions of different masses or in combination with other dark sector species) is still viable across the ultra-light mass range (10^{-32} eV $\leq m_a \leq 10^{-18}$ eV) and above (see, e.g., Refs. [51, 52] for reviews of searches for axion-like particles). In this work, we search for axions through their gravitational imprint in a compendium of CMB and large-scale structure data for $m_a \leq 10^{-25}$ eV and allowing for sub-dominant axion energy densities $\Omega_a h^2$. We present legacy constraints from *Planck* 2018 CMB data [53], the first study of high-resolution CMB data from the Atacama Cosmology Telescope [ACT; 54] and the South Pole Telescope [SPT; 55], and a full joint analysis of *Planck* CMB and full-shape galaxy power spectrum and bispectrum data from the Baryon Oscillation Spectroscopic Survey [BOSS, 56, 57].

We include high-resolution CMB data and we model axions in galaxy power spectrum data to smaller scales than previously considered (wavenumbers $k < 0.4 h \text{ Mpc}^{-1}$) as probing smaller scales gains sensitivity to the scale-dependent suppression of heavier axions. The challenge is that exploiting smaller scales typically requires robust modelling of axion structure formation into the non-linear regime, moving beyond the well-established linear-order theory (e.g., *axionCAMB* [23, 58], *AxiCLASS* [59]) that is sufficient for *Planck* analyses¹. Ref. [39] modelled axions into the mildly non-linear regime using the effective field theory of large-scale structure [EFT of LSS; 62–71], finding that, similarly to massive neutrinos [69, 72], the galaxy bias and counterterm parameters capture non-linear effects after modifying the input linear matter power spectrum. Axion-induced wave effects are suppressed as they manifest on scales suppressed in the linear power spectrum.

In this work, we find that current high-resolution CMB data from ACT-DR4 and SPT-

¹Refs. [60, 61] discuss the robustness of the fluid approximations that are typically required to make linear-order axion perturbation calculations computationally tractable.

3G can be modelled by linear theory. However, upcoming and proposed future high-resolution CMB lensing data from, e.g., ACT, SPT, Simons Observatory, CMB-S4, and galaxy weak lensing data from, e.g., the Dark Energy Survey (DES), *Rubin* Observatory, *Euclid* will gain sensitivity to heavier axions ($m_a > 10^{-25}$ eV) but will probe fully non-linear scales. Ref. [40] searched for axions as the only DM species in DES-Y1 galaxy shear data using an axion halo model that analytically captures the effect of axions on the formation and clustering of DM halos [73]. Ref. [74] extended this model to the case of mixed axion and cold DM. A complementary approach is to capture non-linear modes using machine learning models called emulators which are trained on the outputs of cosmological simulations [e.g., 75–82]. Emulators have been used successfully to set DM constraints, e.g., with the Lyman-alpha forest [29, 32, 83], where astrophysical effects can be captured in training simulations. Accurate emulator predictions rely on accurate input simulations. There is much progress in our ability to simulate axion structure formation using fluid approximations [84] and by solving the full axion field equations [33–35, 85–89].

There are discrepancies between CMB, galaxy clustering and galaxy shear inferences on the amplitude of matter density fluctuations [see 90, for a recent review]. This is typically characterised by the matter clustering parameter σ_8 , the amplitude at redshift $z = 0$ when averaged over $8 h^{-1}$ Mpc scales, or by the degenerate combination $S_8 \equiv \sqrt{\frac{\Omega_m}{0.3}} \sigma_8$ (where Ω_m is the matter energy density), which is well constrained by large-scale structure experiments. The statistical significance of the so-called S_8 tension ranges from 2 to 3 σ depending on the data considered; galaxy shear, in particular, drives the largest discrepancies with CMB data. Notwithstanding undetected systematic errors in the data, the S_8 tension has proposed solutions based on physics beyond Λ CDM typically by introducing either a time-dependence or a scale-dependence in the DM dynamics. This can be achieved by, e.g., coupling DM to DE [91, 92], a complex dark sector (e.g., atomic DM [93–95]), decaying DM [96–100], or baryon-DM interactions [101]; Ref. [102] more generally considers modifications to non-linear clustering including the effects of baryonic feedback.

Ultra-light axions form a component of the dark sector with a scale-dependent growth factor. We therefore hypothesise that axions could alleviate the S_8 tension, by behaving like standard cold DM at the scales probed by current CMB surveys, while suppressing the growth of structure at the smaller scales to which galaxy surveys are sensitive. We investigate this hypothesis by jointly analysing CMB and galaxy clustering data. The inclusion of galaxy shear measurements is left for future work. Another discrepancy in the Λ CDM model is the H_0 tension, the $\sim 5\sigma$ difference in the Hubble expansion rate today H_0 as inferred from different direct and indirect distance ladders [see, e.g., 90]. Many proposed solutions to the H_0 tension based on new physics, however, exacerbate the discrepancy in S_8 [e.g., 103]. Models of ultra-light axions, with $m_a \sim (10^{-27} - 10^{-26})$ eV, combined with modifications to the dynamics of the DE component [104–106] are invoked to alleviate simultaneously both parameter tensions. In this work, we stress the importance of assessing tension in the full parameter space. In testing the extent to which ultra-light axions can improve consistency between CMB and large-scale structure data, we therefore use metrics of tension that account for the full non-Gaussian posterior distribution.

In § 2, we introduce our model for axion structure formation: the linear theory in § 2.1 and the EFT of LSS that we use as our non-linear theory in § 2.2. We discuss our data in § 3: CMB in § 3.1, baryon acoustic oscillations (BAO) and supernovae in § 3.2, full-shape BOSS galaxy clustering in § 3.3 and our parameter inference methods in § 3.4. We present results from the CMB, BAO and supernovae in § 4.1 and from BOSS galaxy clustering in § 4.2. In

§ 5, we discuss these results and draw conclusions in § 6.

2 Axion structure formation model

2.1 Linear theory

2.1.1 Axion cosmology

In order to model the effect of ultra-light axions (ULAs) on the cosmic microwave background (CMB), we calculate linear-order perturbations using the Einstein-Boltzmann solver **axionCAMB**² [23, 58]. The fundamental equation governing the axion field ϕ is the Klein-Gordon equation:

$$\square\phi - m_a^2\phi = 0, \quad (2.1)$$

where \square is the d'Alembert operator. We consider a temperature-independent axion mass, which is appropriate for string theory axions, where the mass switches on at a high energy scale (typically the geometric mean of the supersymmetry scale and the Planck scale [20]). We ignore self-interactions of the axion (valid for initial field misalignment angles that are not tuned close to π [107–110]). The axion-photon coupling can affect CMB polarisation if it is large (see e.g., Refs. [111–114]), but does not back-react significantly on the axion DM density (although see Ref. [115]). Cosmologically, all other axion couplings can lead only to a small thermal population of axions, which is negligible for couplings consistent with astrophysical limits, current constraints on the effective number of relativistic species N_{eff} , and in the mass range that we consider (for related discussion, see, e.g., Refs. [116, 117]). Thus, we set the axion couplings to zero and consider only gravitational effects. The gravitational couplings of the axion are contained in the metric dependence of \square .

Under the above approximations, the relic density of axions arises from the solution of Eq. (2.1) for a spatially-homogeneous axion field $\phi = \phi(t)$ coupled to the Friedmann equation governing the evolution of the scale factor $a(t)$. The field is assumed to have an initial value $\phi_i = \theta_i f_a$, where θ_i is the initial field misalignment angle and f_a is the decay constant. **axionCAMB** solves a shooting problem to fix ϕ_i given $\Omega_a h^2$, m_a and cosmological parameters. In the mass range that we probe in this work, the relic density can be approximated as

$$\Omega_a h^2 \approx \begin{cases} 5.23 \times 10^{-2} \left(\frac{\Omega_m h^2}{0.143} \right)^{\frac{3}{4}} \left(\frac{\phi_i}{10^{17} \text{ GeV}} \right)^2 \left(\frac{1+z_{\text{eq}}}{3400} \right)^{-\frac{3}{4}} \left(\frac{m_a}{10^{-23} \text{ eV}} \right)^{\frac{1}{2}} & \text{if } m_a \gtrsim H(z_{\text{eq}}), \\ 3.62 \times 10^{-3} \left(\frac{\Omega_m h^2}{0.143} \right) \left(\frac{\phi_i}{10^{17} \text{ GeV}} \right)^2 & \text{if } H_0 \lesssim m_a \lesssim H(z_{\text{eq}}), \end{cases} \quad (2.2)$$

where $\Omega_m h^2$ is the total matter energy density, z_{eq} is the redshift of matter – radiation equality, $H(z)$ is the Hubble expansion rate and H_0 is its value today. The initial misalignment angle is expected to be determined by a random process, while the decay constant is a physical constant (possibly itself determined by a vacuum expectation value of some other scalar field). Taking the random θ_i to be of order unity, $\Omega_a h^2$, for given axion mass and cosmological parameters, is a function of f_a . For f_a near the Grand Unified Theory scale (between 10^{16} GeV and 10^{17} GeV), $\Omega_a h^2$ is large enough to contribute significantly to the total energy density (as shown in Eq. (2.2)).

At early times, defined as when $H \gg m_a$, **axionCAMB** solves fluid equations, equivalent to the full Klein-Gordon equation (Eq. 2.1) at linear order in spatial fluctuations of ϕ and metric perturbations, in the synchronous gauge. The homogeneous axion field begins to oscillate

²<https://github.com/dgrin1/axionCAMB>.

when $H \approx m_a$. After this time, `axionCAMB` uses the WKB approximation to adopt an effective fluid description [118–121]. The fluid model is equivalent to the Madelung formulation [122] and is accurate up to shell crossing. For further discussion of the accuracy of the adopted approximations, see Refs. [23, 60, 61].

The main physical features that distinguish ULAs from standard Λ CDM components, as pertains to cosmological observables, are two-fold [23]. First, the slow roll of the axion field when $H \gg m_a$ leads to a distinctive background evolution equivalent to a fraction of the matter component behaving like an early form of dark energy. This leads to differences in the diffusion damping and Sachs-Wolfe contributions to the CMB, changes the sound horizon, and changes the distance to the surface of last scattering (if axions begin their oscillation after matter-radiation equality, i. e., for $m_a \lesssim 10^{-28}$ eV).

Second, the gradient terms in the Klein-Gordon equation appear as an effective pressure opposing gravitational collapse, leading to a Jeans scale for the ULAs and, consequently, a suppression in the amplitude of density perturbations on small scales [22, 119, 123, 124]. If axions contribute non-negligibly to the total DM density, the Jeans scale can be approximated as

$$\lambda_J \approx 12.3 (1+z)^{\frac{1}{4}} \left(\frac{\Omega_a h^2}{0.01} \right)^{-\frac{1}{4}} \left(\frac{m_a}{10^{-26} \text{ eV}} \right)^{-\frac{1}{2}} h^{-1} \text{ Mpc}. \quad (2.3)$$

If ULAs begin to oscillate prior to matter – radiation equality ($m_a \gtrsim 10^{-28}$ eV), there is strong suppression of the matter power spectrum, compared to a pure cold DM model, for wavelengths smaller than the Jeans scale evaluated at matter – radiation equality [125]. If $m_a \lesssim 10^{-28}$ eV, the physics of the Jeans scale (suppression of density perturbations relative to pure cold DM) is related to the horizon size at the time when the axion becomes non-relativistic. The magnitude of the relative suppression of the power spectrum, with respect to the cold DM limit, increases with the fraction of the DM composed of axions.

2.1.2 S_8 and the linear matter power spectrum

Figure 1 illustrates this Jeans scale (for wavenumbers k above the Jeans wavenumber, the linear matter power spectrum $P^{\text{linear}}(k)$ is suppressed relative to the Λ CDM limit) and how it depends on axion mass m_a : the lighter the axion, the larger the power suppression scale (the smaller the suppression wavenumber). In Fig. 1, we show linear matter power spectra at the 95 % upper limits on the axion energy density $\Omega_a h^2$ given a combination of *Planck* CMB and BOSS galaxy clustering data (see § 4.2). As will be expanded later, these data set stronger constraints on the amount of axions at lower mass; Fig. 1 thereby illustrates how a lower $\Omega_a h^2$ reduces the strength of the power suppression. The amplitude of the linear matter power spectrum today (redshift $z = 0$) is often summarised by the cosmological parameter

$$\sigma_8 = \int d\ln k \frac{k^3}{2\pi} W^2(k) P^{\text{linear}}(k), \quad (2.4)$$

where $W(k)$ is the Fourier transform of a top-hat filter in real space with radius $8 h^{-1}$ Mpc; large-scale structure (LSS) data are then typically used to constrain the parameter combination $S_8 = \sqrt{\frac{\Omega_m}{0.3}} \sigma_8$, where Ω_m is the total matter energy density³. S_8 is therefore sensitive to

³The parameter combination S_8 was historically optimised to project away parameter degeneracies in galaxy weak lensing experiments. We typically use this parameter combination in this work with galaxy clustering since it still does a good job of projecting away degeneracies and it simplifies comparisons to the literature.

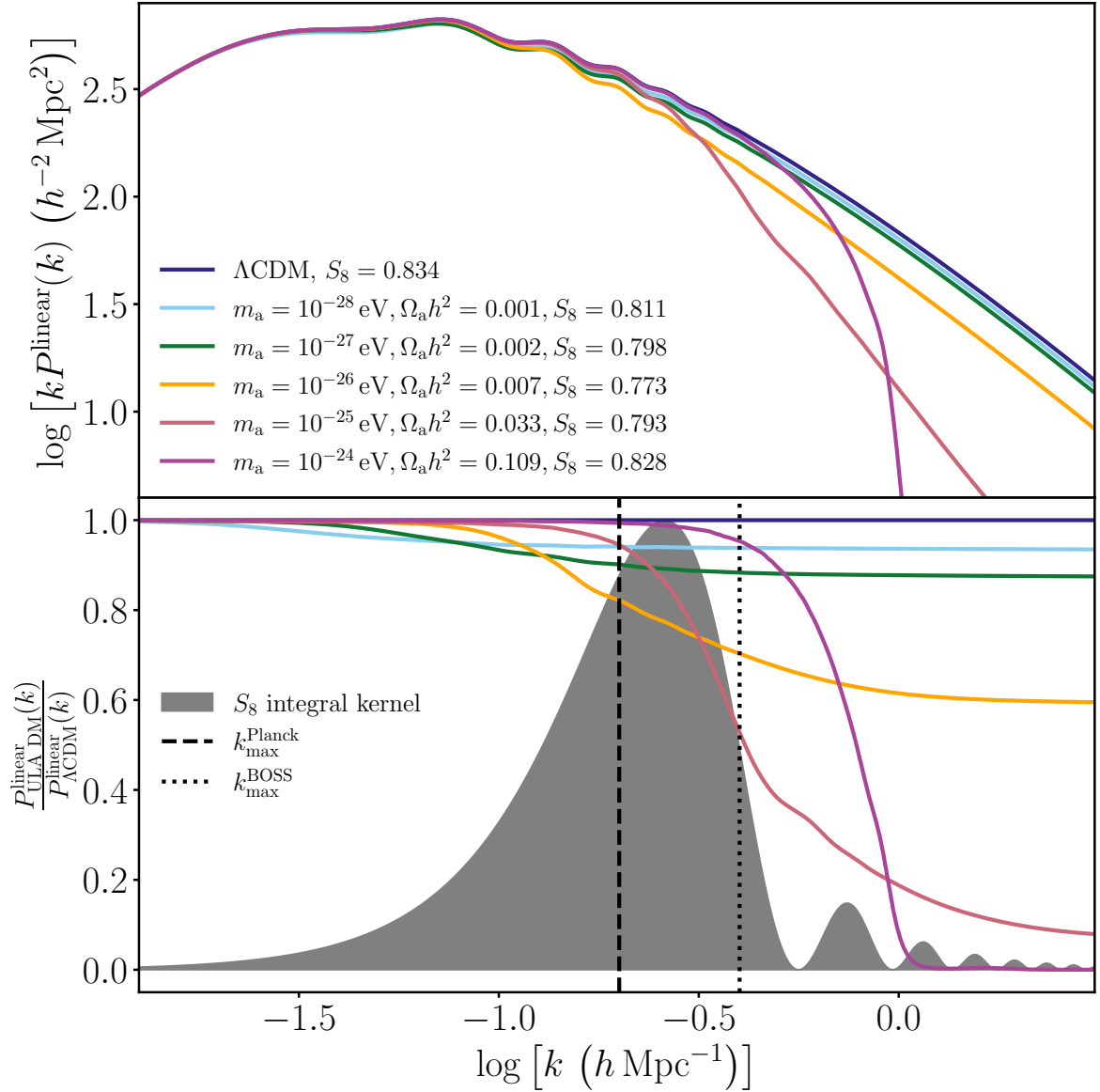


Figure 1. The effect of ultra-light axions on the linear matter power spectrum (*top panel*) and the ratio to the ΛCDM limit (*bottom panel*). Power spectra are shown at the 95% upper limit on the axion energy density $\Omega_a h^2$ given *Planck* CMB and BOSS galaxy clustering data and thus reflect the tightening density constraint at lower axion mass m_a (see Table 2; all parameters fixed apart from m_a , $\Omega_a h^2$, the cold DM density $\Omega_c h^2$ and the dark energy fraction Ω_Λ). In the bottom panel, the shaded area shows the Fourier-space filter $k^2 W^2(k)$ (in arbitrary units) of $k P^{\text{linear}}(k)$ in the integral calculation of the matter clumping factor S_8 (see Eq. (2.4)), where $W(k)$ is the Fourier transform of a top-hat filter in real space with radius $8 h^{-1} \text{Mpc}$ and Ω_m is the (fixed) total matter energy density. The shaded area thus indicates the wavenumbers to which S_8 is most sensitive; for $m_a \leq 10^{-25} \text{ eV}$, axions suppress power and thus lower S_8 ; for $m_a \geq 10^{-24} \text{ eV}$, the axion-induced power suppression is at too large a wavenumber to change S_8 significantly. The dashed line indicates the maximum wavenumber which we probe in the *Planck* likelihood (see § 3.1.1); the dotted line indicates the maximum wavenumber which we model in the BOSS galaxy power spectrum (see § 3.3).

a filtered integral of the linear matter power spectrum; the bottom panel of Fig. 1 shows this filter and indicates the scales to which S_8 is sensitive. It can be seen that, for $m_a \geq 10^{-24}$ eV, the power suppression is on too small scales to lower significantly S_8 . For $m_a \leq 10^{-28}$ eV, the data constraint is too strong to leave an appreciable amount of axions that significantly lowers S_8 . However, there is a window for $m_a \in [10^{-27}, 10^{-25}]$ eV, where the presence of axions significantly lowers S_8 and is allowed by the data we consider. S_8 is lowered because the Jeans scale today for $m_a = 10^{-25} - 10^{-26}$ eV is about $4 - 12 h^{-1}$ Mpc (see Eq. (2.3)). We therefore discuss the prospects of axions resolving discrepancies in the inferred values of S_8 given CMB and LSS data in § 5.

2.1.3 Cosmic microwave background

In modelling CMB anisotropies, we consider only adiabatic initial perturbations; we defer a search for isocurvature perturbations to future work [see 37, 126, for consequences on the energy scale of inflation]. Fig. 2 illustrates how axions change the CMB temperature TT , polarisation EE , cross TE and lensing potential $\phi\phi$ angular power spectra C_ℓ as a function of multipole ℓ . For the multipoles probed by current data (*Planck*, ACT-DR4, SPT-3G; see § 3), the impact of axions for $m_a \geq 10^{-25}$ eV on these data is small compared to statistical uncertainties. For axions that become a dark matter component before matter-radiation equality ($m_a \geq 10^{-27}$ eV), much of the data constraint comes from the change in the relative heights of acoustic peaks arising from the change in the matter-to-radiation ratio (see Fig. 2). For axions that still behave like dark energy after matter-radiation equality ($m_a \leq 10^{-28}$ eV), much of the data constraint (once the angular size of the sound horizon is constrained) comes from the change in the integrated Sachs-Wolfe effect at the smallest multipoles. The lensing power spectrum is sensitive to all axion masses through a scale (multipole)-dependent suppression arising from the matter power spectrum (see Fig. 1; see Refs. [23, 37, 127] for summaries of the effects of axions on the CMB).

Since we conservatively ignore small-scale CMB lensing anisotropies (we use only multipoles $8 \leq L \leq 400$ as recommended by the Planck Collaboration; see § 3.1.1), we ignore non-linear effects in the lensing power spectrum. Refs. [49, 74, 127] indicated that this is a good approximation as, for axion mass $m_a < 10^{-25}$ eV, axions with observationally-allowed energy densities do not non-linearly cluster at observationally-relevant wavenumbers and redshifts. For $m_a \geq 10^{-25}$ eV, the non-linear effects are only significant for larger multipoles than we use. A halo model was developed to capture the effects of ultra-light axions on non-linear scales in CMB and galaxy lensing [74]. Using this halo model, we reconsider the impact of ignoring non-linear effects in our *Planck* CMB lensing analysis (Fig. 3). We conclude that this observable is well captured using linear theory for the L range considered in this work. Forthcoming measurements of small-scale lensing anisotropies from ground-based CMB (and future galaxy weak lensing) experiments will increase sensitivity to smaller axion suppression scales and, hence, larger m_a . We anticipate that non-linear modelling will become necessary in this regime.

2.2 Galaxy clustering and the effective field theory of large-scale structure

2.2.1 Galaxy power spectrum and bispectrum multipoles

In order to capture the anisotropic clustering in the galaxy distribution arising from redshift-space effects, we model galaxy power spectrum multipoles [e.g., 70]:

$$P_\ell(k, z) \equiv \frac{2\ell + 1}{2} \int_{-1}^1 d\mu \mathcal{L}_\ell(\mu) P_g(k, \mu, z). \quad (2.5)$$

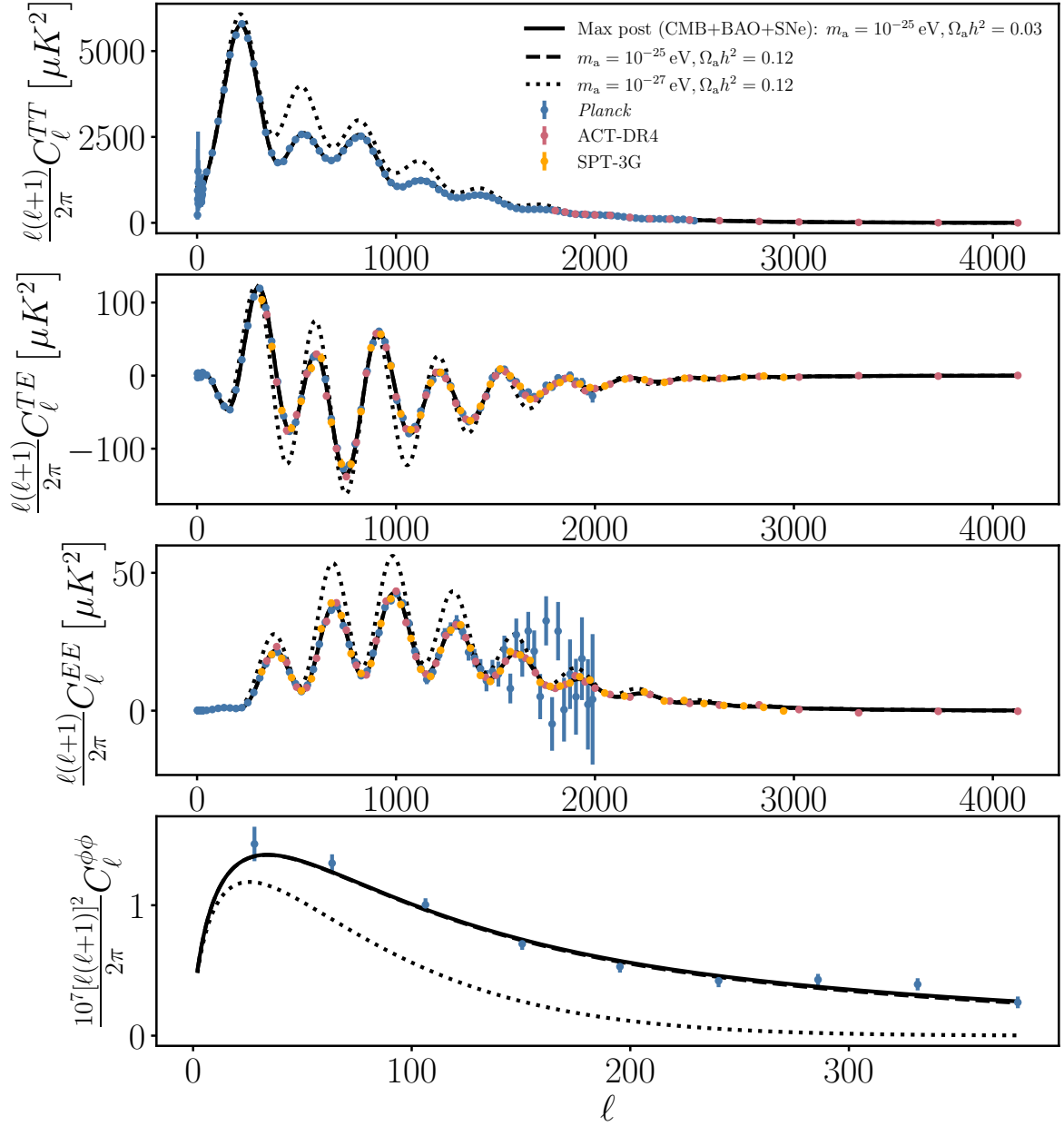


Figure 2. The effect of ultra-light axions on (from top to bottom) the cosmic microwave background (CMB) TT , TE , EE and $\phi\phi$ angular power spectra, compared to data from *Planck* (blue), the Atacama Cosmology Telescope (ACT-DR4; red) and the South Pole Telescope (SPT-3G; orange). We show the maximum posterior model (solid) given *Planck*, ACT and SPT CMB, galaxy baryon acoustic oscillation (BAO) and supernovae (SNe) data for axion mass $m_a = 10^{-25}$ eV. We compare this to the cases where the axion energy density $\Omega_a h^2 = 0.12$ for $m_a = 10^{-25}, 10^{-27}$ eV (all other parameters fixed to their maximum posterior values). At the multipoles currently probed, axions for $m_a \geq 10^{-25}$ eV are poorly constrained by these data; upcoming high-resolution CMB lensing measurements will increase sensitivity to heavier axions. Data are shown as points with 68% c.l. errorbars.

Here, $P_g(k, \mu, z)$ is the full anisotropic galaxy power spectrum depending on wavenumber k , the cosine of the angle between the wavenumber and the line-of-sight μ , and redshift z ;

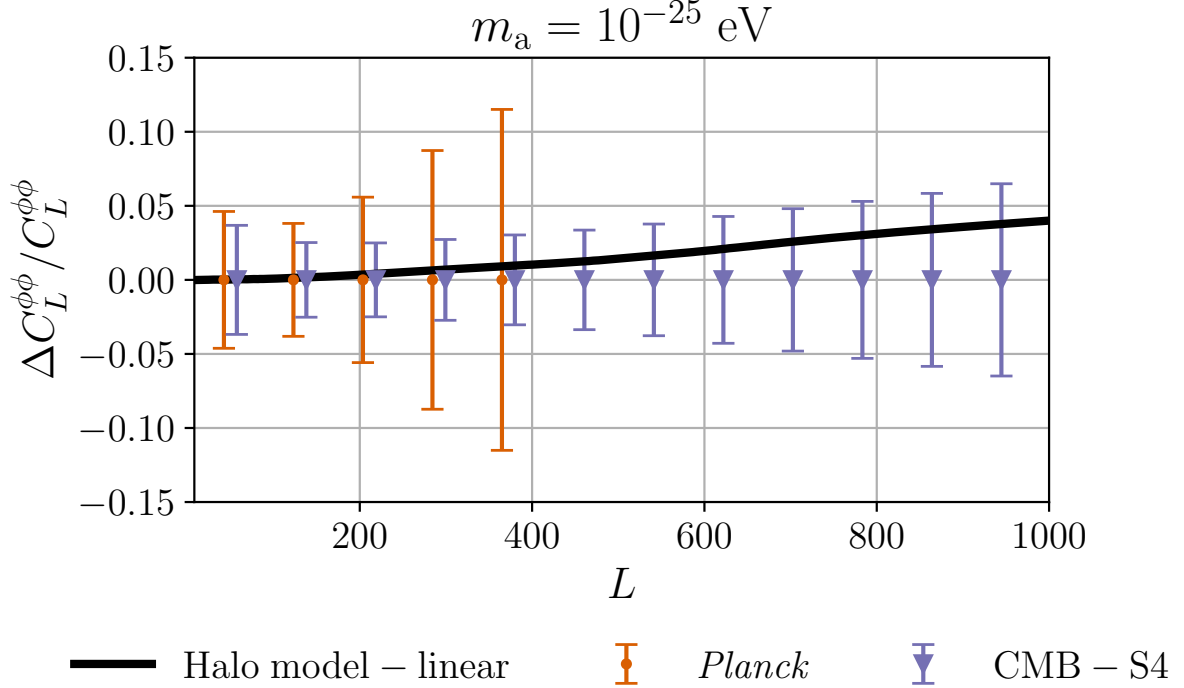


Figure 3. Fractional difference in the cosmic microwave background (CMB) lensing potential angular power spectrum $C_L^{\phi\phi}$ as a function of multipole L between a non-linear axion halo model [74] and the linear theory prediction from **axionCMB** [23, 58] (*black line*). We show the difference in the theoretical prediction for an axion of mass $m_a = 10^{-25} \text{ eV}$ which constitutes 50% of the total dark matter energy density. There is a negligible difference for $L \leq 400$ compared to the error in the *Planck* data that we use (*orange*; see § 3.1.1). The inclusion of non-linearities will however be necessary for future CMB surveys such as CMB-S4 (*purple*; forecasted data error from Ref. [37]).

$\mathcal{L}_\ell(\mu)$ are Legendre polynomials indexed by multipole ℓ . Non-linear redshift-space distortions (“fingers of God” [128]) are non-trivial to model with accuracy on small scales, while the power suppression effect of axions is stronger as wavenumber increases. Therefore, to increase the constraining power from galaxy data and following Ref. [129], we estimate the reconstructed real-space⁴ galaxy power spectrum $Q_0(k, z) \equiv P_0(k, z) - \frac{1}{2}P_2(k, z) + \frac{3}{8}P_4(k, z)$ [see also 130]. Ref. [129] demonstrates that this estimator effectively down-weights information in line-of-sight modes ($\mu > 0.3$) that are heavily contaminated by redshift-space distortions. Further, we extract information on the post-reconstructed baryon acoustic oscillation feature using the Alcock-Paczynski (AP) parameters:

$$\alpha_{\parallel}(z) \equiv \frac{H^{\text{fid}}(z)r_s^{\text{fid}}(z_d)}{H(z)r_s(z_d)}, \quad \alpha_{\perp}(z) \equiv \frac{D_A(z)r_s^{\text{fid}}(z_d)}{D_A^{\text{fid}}(z)r_s(z_d)}. \quad (2.6)$$

Here, $H(z)$ is the Hubble parameter, $r_s(z_d)$ is the sound horizon at the redshift of decoupling, $D_A(z)$ is the angular diameter distance, and “fid” indicates a fiducial cosmology. For the first time, in order to extract information beyond the two-point statistics described above, we model the effect of axions on the galaxy bispectrum (Fourier transform of the three-point correlation function). In this work, we consider only the angle-averaged bispectrum monopole ($\ell = 0$) $B_0(k_1, k_2, k_3)$.

⁴I. e., without redshift-space distortions.

2.2.2 Introduction to the effective field theory of large-scale structure

In order to model the effect of ULAs on the redshift-space galaxy power spectrum and bispectrum, we calculate mildly non-linear perturbations using the effective field theory of large-scale structure [EFT of LSS; 62–64, 71] as implemented in the Einstein-Boltzmann solver CLASS-PT⁵ [70]. Following the effective field theory of large-scale structure, this is a schematic view of our power spectrum model [68, 70]:

$$P_\ell(k, z) = P_\ell^{\text{tree}}(k, z) + P_\ell^{\text{one-loop}}(k, z) + P_\ell^{\text{counterterms}}(k, z) + P_\ell^{\text{stochastic}}(k, z). \quad (2.7)$$

Here, $P_\ell^{\text{tree}}(k, z)$ captures linear bias and redshift-space distortions ($\propto P^{\text{linear}}(k, z)$, which is the linear matter power spectrum) [131]; $P_\ell^{\text{one-loop}}(k, z)$ captures perturbative corrections up to one loop in order ($\propto k^2 P^{\text{linear}}(k, z)$ on large scales); $P_\ell^{\text{counterterms}}(k, z)$ captures ultra-violet counterterms that consistently account for small-scale physics ($\propto k^2 P^{\text{linear}}(k, z)$); and $P_\ell^{\text{stochastic}}(k, z)$ captures stochastic effects including shot noise and fingers of God ($\propto \text{constant}$, plus corrections). We also include infrared resummation to account for non-perturbative long-wavelength displacements [70, 132–134], and account for the so-called Alcock-Paczynski distortion [135] (i.e., the effects of an incorrect fiducial cosmology above) by wavevector rescalings [see e.g., 56, 110].

The bispectrum model can be given schematically in 3D space [136]:

$$B(\mathbf{k}_1, \mathbf{k}_2, z) = B^{\text{tree}}(\mathbf{k}_1, \mathbf{k}_2, z) + B^{\text{counterterms}}(\mathbf{k}_1, \mathbf{k}_2, z) + B^{\text{stochastic}}(\mathbf{k}_1, \mathbf{k}_2, z), \quad (2.8)$$

for wavevectors $\mathbf{k}_1, \mathbf{k}_2$. Here, $B^{\text{tree}}(\mathbf{k}_1, \mathbf{k}_2, z)$ captures tree-level perturbations ($\propto P_{\text{linear}}^2(k, z)$); $B^{\text{counterterms}}(\mathbf{k}_1, \mathbf{k}_2, z)$ is a proxy for ultraviolet fingers-of-God counterterms ($\propto k_{\parallel}^2 P_{\text{linear}}^2(k, z)$, where k_{\parallel} is the wavenumber for modes parallel to the line of sight); and $B^{\text{stochastic}}(\mathbf{k}_1, \mathbf{k}_2, z)$ captures stochastic effects ($\propto P_{\text{linear}}(k, z) + \text{constant}$). For the bispectrum, the tree-level model is sufficiently accurate for the small wavenumbers that we consider in our data ($k < 0.08 h \text{ Mpc}^{-1}$; see § 3.3). We again account for infrared resummation [134] and the Alcock-Paczynski distortion as above. We then integrate over external angles to calculate the bispectrum monopole $B_0(k_1, k_2, k_3)$, which can be compared to data without additional window convolutions. In comparing to BOSS data, we multiply B_0 by a discreteness weight vector to account for the finite resolution of the Fourier grid⁶.

2.2.3 Axions and the effective field theory of large-scale structure

The EFT of LSS was originally developed with the assumption of cold, collisionless dark matter (CDM). However, we follow Ref. [39] in noting that the effect of ultra-light axion dark matter (not to cluster below a characteristic scale) is qualitatively the same as for free-streaming neutrinos (although the physical reason is different). Ref. [72] found that, to first order, the additional counterterms needed to account for the effect of neutrinos have the same functional form as existing CDM counterterms. We therefore assume that the additional axion-induced counterterms will also have the same functional form, although with different constants of proportionality which must be marginalised. Further, Ref. [39] demonstrated that linear-order axion-wave corrections are negligible since they manifest on scales that are

⁵<https://github.com/Michalychforever/CLASS-PT>. Background evolution and linear matter power spectrum calculations are done in axionCAMB, which are passed to CLASS-PT for non-linear corrections.

⁶BOSS discreteness weight vectors can be found at https://github.com/oliverphilcox/full_shape_likelihoods.

Data	Description	Nuisance pars.	§	Refs.
<i>Planck</i> 2018	$C_\ell^{TT,TE,EE,\phi\phi}: \ell \leq 2508, L \leq 400$	a_{Planck}	3.1.1	[2]
ACT-DR4	$C_\ell^{TT,TE,EE}: 326 \leq \ell \leq 4325$	y_{p}	3.1.2	[54]
SPT-3G	$C_\ell^{TE,EE}: 300 \leq \ell \leq 2999$	Fixed	3.1.3	[55]
BAO + SNe	6dFGS, MGS, BOSS DR12, JLA	$\alpha, \beta, \delta M$	3.2	[139–142]
BOSS full-shape	$P_{0,2,4}(k, z), Q_0(k, z), B_0(k, z), \text{AP}$	EFT of LSS	3.3	[56]

Table 1. A summary of the data used in this work.

already heavily suppressed in the linear matter power spectrum. Ref. [39] also demonstrated that axion and cosmological parameters can be inferred without bias from a simulated BOSS galaxy catalogue in the presence of axions, when marginalising over the EFT of LSS model presented above. It follows that phenomenology of axions can be captured by only modifying the background evolution and linear matter power spectrum (presented in § 2.1 and calculated using `axionCAMB`) as input to the EFT of LSS model presented in Eqs. (2.7) and (2.8).

We marginalise over a full set of EFT of LSS nuisance parameters: linear b_1 , quadratic b_2 , tidal $b_{\mathcal{G}_2}$ and third-order b_{Γ_3} galaxy biases; monopole c_0 , quadrupole c_2 , hexadecapole c_4 , fingers-of-God \tilde{c} and bispectrum c_1 counterterms; power spectrum P_{shot} and bispectrum B_{shot} shot noise parameters; and power spectrum scale-dependent stochastic parameters a_0 and a_2 [more details are given in 136].

Figure 4 shows the effect of ultra-light axions on the galaxy power spectrum, for $m_{\text{a}} = 10^{-25}$ eV. The solid line shows the power spectrum for axion energy density $\Omega_{\text{a}} h^2 = 0.03$, while the dashed line shows the power spectrum for $\Omega_{\text{a}} h^2 = 0.09$ (all other parameters fixed to the same values as for the solid line). There are two main effects. The first is a scale-dependent suppression in the power spectrum, which gets stronger on smaller scales (and so is most significantly seen in the Q_0 statistic). This is qualitatively similar to the effect in the linear matter power spectrum. The effect is physically caused by axions not clustering on scales below their Jeans wavelength at matter-radiation equality. The second effect is a small-scale enhancement in the galaxy quadrupole (and, to a much-lesser extent, hexadecapole). This effect is caused by a reduction in the fingers of God effect owing to lower peculiar velocities at weaker matter over-densities, although this is degenerate with the EFT of LSS counterterm parameter that controls the fingers of God amplitude. These effects are discussed in further detail in Ref. [39]. The dotted lines lower the primordial power spectrum amplitude A_{s} with respect to the solid lines and thus suppress the galaxy power spectrum at all wavenumbers.

Fig. 5 shows the effect of ultra-light axions on the galaxy bispectrum monopole, for $m_{\text{a}} = 10^{-25}$ eV. As above, the dashed line shows the effect of increasing the axion density while keeping all other parameters fixed. The effect is a small scale-dependent suppression in the bispectrum, which gets stronger for smaller-scale triangles. However, at the current statistical precision of BOSS data and on the relatively large scales modelled here in the bispectrum ($k < 0.08 h \text{ Mpc}^{-1}$), the effect is negligible. We anticipate that axions will impact the smaller-scale, one-loop bispectrum [137, 138] more strongly; we will investigate this in future work.

3 Data

In Table 1, we give a summary of the data used in this work. In § 3.1 to 3.3, we give more details about the data and, in § 3.4, we give details on our parameter inference method

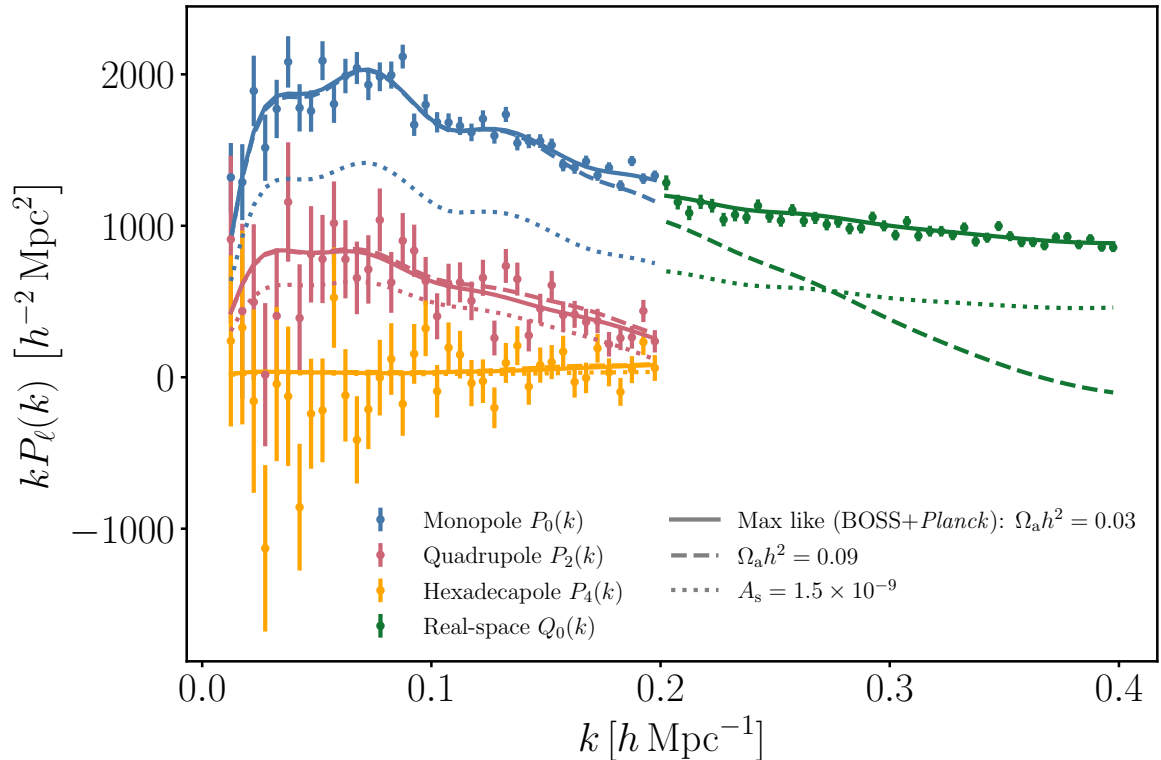


Figure 4. The effect of ultra-light axions (mass $m_a = 10^{-25}$ eV, axion energy density $\Omega_a h^2 = 0.09$, *dashed lines*) on the Baryon Oscillation Spectroscopic Survey (BOSS) galaxy power spectrum, compared to maximum-likelihood model parameters (with $\Omega_a h^2 = 0.03$, *solid lines*; all other parameters fixed to maximum-likelihood values). The solid line shows the maximum likelihood given BOSS galaxy power spectrum and *Planck* cosmic microwave background (CMB) data; here, we maximise the likelihood with respect to all cosmological and EFT of LSS parameters, including those that are usually analytically marginalised. We also show the case (*dotted lines*) where we lower the primordial power spectrum amplitude from its best-fit value given *Planck* + BOSS ($A_s = 2.15 \times 10^{-9}$) to its best-fit value given only BOSS galaxy power spectra ($A_s = 1.53 \times 10^{-9}$). This illustrates the lack of degeneracy with heavier axions ($m_a = 10^{-25}$ eV); nonetheless, a good fit to BOSS data is maintained given the addition of *Planck* data by reducing the best-fit linear galaxy bias (see also Fig. 16). We anticipate degeneracy between high A_s (and also high linear galaxy bias b_1) and high $\Omega_a h^2$ for $m_a \leq 10^{-28}$ eV since the large Jeans scale suppresses all BOSS wavenumbers in a similar way as reducing A_s (or b_1). We show the galaxy power spectrum monopole $P_0(k)$ (*blue*), quadrupole $P_2(k)$ (*red*), hexadecapole $P_4(k)$ (*orange*), and the reconstructed real-space galaxy power spectrum $Q_0(k)$ (*green*), as a function of wavenumber k . BOSS data are shown as points with 68% c.l. errorbars.

including the prior distribution.

3.1 Cosmic microwave background

3.1.1 *Planck*

We consider baseline *Planck* 2018 CMB temperature, polarisation and lensing angular power spectra [2]. We use: the low-multipole ($2 \leq \ell \leq 29$) temperature TT auto-spectrum likelihood `commander_dx12_v3_2_29`; the low-multipole ($2 \leq \ell \leq 29$) polarisation EE auto-spectrum likelihood `simall_100x143_offlike5_EE_Aplanck_B`; the high-multipole, nuisance-marginalised, TT ($30 \leq \ell \leq 2508$), TE and EE ($30 \leq \ell \leq 1996$)

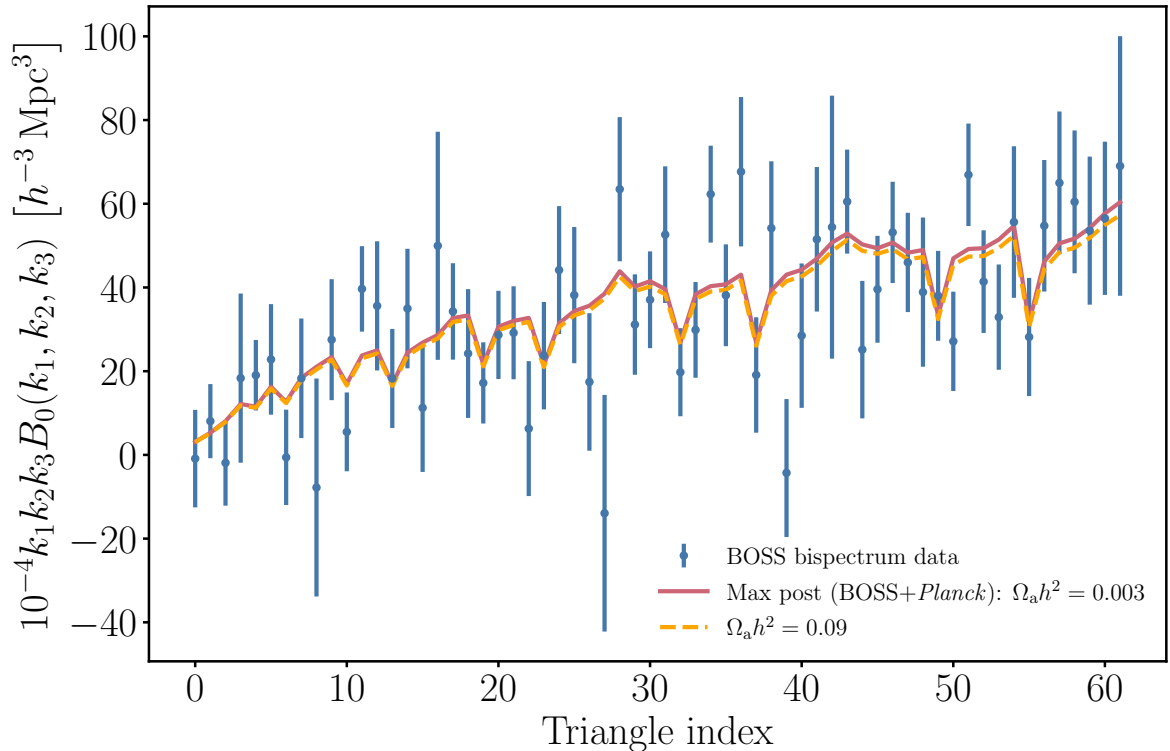


Figure 5. The effect of ultra-light axions ($m_a = 10^{-25}$ eV, $\Omega_a h^2 = 0.09$, *dashed line*) on the BOSS galaxy bispectrum monopole $B_0(k_1, k_2, k_3)$, compared to maximum-posterior model parameters (with negligible axion densities, *solid line*; all other parameters fixed to their maximum posterior values). The solid line shows the maximum posterior given BOSS power spectrum and bispectrum and *Planck* CMB data. We show B_0 as a function of k_1, k_2, k_3 wavenumber triangles, where triangle index increases first with k_1 , then with k_2 , and then with k_3 , for $[k_1, k_2, k_3] \in [0.01, 0.08] h \text{ Mpc}^{-1}$; i. e., wavenumber triangles with smaller sides on the left and larger sides on the right. BOSS data are shown as points with 68% c.l. errorbars.

likelihood `plik_lite_v22_TTTEEE`; and the lensing $\phi\phi$ auto-spectrum likelihood ($8 \leq L \leq 400$) `smicadx12_Dec5_ftl_mv2_ndlcpp_p_teb_consext8`. As we use compressed, nuisance-marginalised likelihoods, we have remaining a single nuisance calibration parameter a_{Planck} . Ref. [23] demonstrated that there is no statistically-significant effect on axion parameter inference if re-marginalising nuisance foreground parameters in an axion model with *Planck* data. The use of *Planck* 2018 data to constrain $\Omega_a h^2$ is an update from Refs. [37, 39], which used *Planck* 2015 data [53], and from Ref. [40], which used *Planck* 2018 data to constrain only m_a in the case where axions are all the dark matter. The main differences from 2015 data are a new low- ℓ polarisation likelihood and a larger-scale cut in the lensing likelihood, i. e., L_{min} goes from 40 to 8. We anticipate improved bounds on the lightest axions from this additional large-scale information (see Fig. 7 for a breakdown of how 2018 data improves axion limits).

3.1.2 Atacama Cosmology Telescope

We consider Atacama Cosmology Telescope (ACT) data release 4 (DR4) temperature and polarisation angular power spectra [54]. We use the baseline nuisance-marginalised (“CMB-only”) likelihood `actpollite`. This includes TT power spectra for $576 \leq \ell \leq 4325$ and

TE and EE power spectra for $326 \leq \ell \leq 4325$. The foreground marginalisation leaves a single nuisance parameter y_p , which is an overall polarisation efficiency that re-scales the TE and EE spectra. Our baseline analysis combines ACT and *Planck* (see § 3.1.1) data. However, the cross-covariance between these data has not yet been released. Therefore, to reduce the amount of cross-covariance that we ignore, we follow Ref. [54] in setting the minimum multipole in the ACT TT spectrum $\ell_{\min} = 1800$, with no cut on the TE and EE spectra. Ref. [54] found that these approximations are sufficient to keep the underestimation of parameter uncertainties to less than 5%, including for one-parameter extensions of the standard cosmological model.

3.1.3 South Pole Telescope

We consider South Pole Telescope (SPT-3G) TE and EE angular power spectra for $300 \leq \ell \leq 2999$ ⁷ [55]. We use the baseline `spt3g_2020` likelihood that has twenty nuisance foreground and calibration parameters⁸. In order to reduce the dimensionality of the parameter space, we fix the nuisance parameters to fiducial values⁹. We confirm that fixing these parameters makes no difference to the inferred cosmological posterior distribution by comparing to the case where all nuisance parameters are marginalised. Our baseline analyses combine SPT with *Planck* (see § 3.1.1) and ACT (see § 3.1.2) data. We follow Ref. [55] in ignoring the cross-covariance between SPT and *Planck* since the survey sky overlap is small; we ignore cross-covariance between SPT and ACT for the same reason [see e.g., 146, for similar assumptions].

3.2 Baryon acoustic oscillations & supernovae

We consider a compendium of galaxy baryon acoustic oscillation (BAO) data from: the 6dF Galaxy Survey (6dFGS) at $z = 0.106$ [139]; the Sloan Digital Sky Survey data release 7 Main Galaxy Sample (SDSS DR7 MGS) at $z = 0.15$ [140]; and the Baryon Oscillation Spectroscopic Survey data release 12 (BOSS DR12) at $z = [0.38, 0.51, 0.61]$ [141]. These galaxy samples are largely independent. In § 3.3, we will consider instead the full-shape galaxy power spectrum and bispectrum as measured from the BOSS DR12 galaxy sample, which captures the BOSS BAO information plus additional information in the full power spectrum and bispectrum. In the data in § 3.3, the BAO information is extracted in the Alcock-Paczynski parameters defined in Eq. (2.6) from the reconstructed power spectrum, taking into account their covariance with the full-shape information [147]. We never combine the full-shape BOSS likelihood in § 3.3 with the “standard” BOSS BAO likelihood (used in this section) as they contain identical BAO information.

We consider a compendium of type Ia supernovae (SNe) data from the Joint Light-curve Analysis (JLA) [142]. We marginalise over the shape parameter α , the colour parameter β and the magnitude parameter δM .

⁷In the latter stages of manuscript preparation, SPT-3G TT angular power spectra were released [143]; we will include these data in a future analysis, although we do not anticipate a significant change to our results since the multipoles contained in this release are already covered by the ACT data that we use (§ 3.1.2).

⁸We write a CosmoSIS [144] wrapper to the Cobaya [145] likelihood available at https://github.com/xgarrido/spt_likelihoods.

⁹We take fiducial values to be the maximum prior probability values from the fiducial SPT-3G analysis: https://github.com/xgarrido/spt_likelihoods/blob/master/spt3g_2020/TEEE.yaml.

3.3 Baryon Oscillation Spectroscopic Survey galaxy power spectrum & bispectrum

We use the twelfth data release of the Baryon Oscillation Spectroscopic Survey (BOSS DR12) [57, 141], which is part of the Sloan Digital Sky Survey (SDSS) [148]. This data release contains $\sim 8 \times 10^5$ galaxies across two redshift slices (LOWZ sample: $0.2 < z < 0.5$; CMASS sample: $0.5 < z < 0.75$) and across both the north and south Galactic cap (NGC/SGC) sky cuts. We use the window-free galaxy power spectrum and bispectrum measurements described in Ref. [56], which are measured respectively with the approaches of Refs. [149] and [150]. We bin in k with $\Delta k = 0.005 h \text{ Mpc}^{-1}$ for power spectra and $\Delta k = 0.01 h \text{ Mpc}^{-1}$ for bispectra, with minimum wavenumber $k_{\min} = 0.01 h \text{ Mpc}^{-1}$ to avoid large-scale systematics [e.g., 151]. As discussed in § 2.2, we fix the maximum wavenumber $k_{\max} = 0.2 h \text{ Mpc}^{-1}$ for the power spectrum (using the $\ell = 0, 2, 4$ multipoles) $P_\ell(k, z)$ [56, 152], $k_{\max} = 0.08 h \text{ Mpc}^{-1}$ for the bispectrum monopole [56, 136] $B_0(k, z)$, and we include the $Q_0(k, z)$ statistic for $k \in [0.2, 0.4] h \text{ Mpc}^{-1}$ following Ref. [129]. We extract from the BOSS galaxy power spectrum information on the post-reconstructed BAO feature using the AP parameters (Eq. (2.6)). We use power spectrum, bispectrum and AP measurements for each of the four redshift/sky cuts (NGC and SGC, both in redshift samples with central redshifts 0.38 and 0.61). The BOSS power spectrum and bispectrum data for the North Galactic cap at $z = 0.38$ are respectively shown in Figs. 4 and 5. These data are analysed with the EFT of LSS model presented in § 2.2; we use the existing public BOSS likelihood¹⁰, with the covariance estimated from 2048 MultiDark-Patchy simulations [153, 154]. The EFT of LSS nuisance parameters (see § 2.2) are allowed to differ independently for each of the four BOSS data cuts due to their different redshifts and calibrations. Only b_1, b_2 and $b_{\mathcal{G}_2}$ enter the model non-linearly: the others are analytically marginalized and only this partially-marginalised likelihood is numerically sampled (see § 3.4 for details about our numerical sampling approach).

3.4 Parameter inference

All the likelihoods presented in § 3.1 to 3.3 are implemented in the cosmological parameter estimation code CosmoSIS [144]. We infer the posterior distribution for an axion cosmological model with uniform prior distributions on: the Hubble parameter h ; the baryon energy density $\Omega_b h^2$; the cold dark matter energy density $\Omega_c h^2$; the axion energy density $\Omega_a h^2$; the primordial power spectrum amplitude A_s ; the primordial power spectrum tilt n_s ; and the reionisation optical depth τ ¹¹. We fix the neutrino energy density $\Omega_\nu h^2 = 0.0006442$ with one massive neutrino at its minimally-allowed mass; Refs. [74, 127, 155] discuss degeneracies between axion and neutrino density parameters. We consistently calculate the helium abundance given the baryon density and number of neutrinos using the `bbn_consistency` module [156]. We often show the posterior for derived cosmological parameters: the total matter energy density today Ω_m (to which axions always contribute); and the matter clumping factor $S_8 \equiv \sqrt{\frac{\Omega_m}{0.3}} \sigma_8$, where σ_8 is the amplitude of the linear matter power spectrum averaged over $8 h^{-1} \text{ Mpc}$ scales. We do not vary the axion mass m_a , but rather follow Refs. [37, 39] by inferring the posterior for fixed values of $m_a \in [10^{-32} \text{ eV}, 10^{-24} \text{ eV}]$. This is because the full posterior projected in the $m_a - \Omega_a h^2$ plane has a highly non-trivial degeneracy, which is difficult to sample numerically in a converged manner. There is no impact on our conclusions

¹⁰https://github.com/oliverphilcox/full_shape_likelihoods.

¹¹When considering BOSS data alone, we do not vary τ since large-scale structure data are insensitive to this parameter.

as we are still able to determine our main results, which are constraints on $\Omega_a h^2$ and S_8 as a function of m_a . The main limitation from our approach is that we cannot marginalise m_a . However, we find no need to do so in our analysis in the same way that it is not useful to marginalise dark matter parameters like mass, cross section or coupling in experimental searches. We therefore defer solving this sampling problem to future work. We consider neither lighter axions as these are indistinguishable from a cosmological constant, nor heavier axions as these are indistinguishable from cold dark matter on the scales probed by the data we use [see 40, for more discussion and tests on axion prior choices].

We use a uniform prior on the ACT calibration parameter y_p and the three supernovae standardisation parameters $[\alpha, \beta, \delta M]$. We use a Gaussian prior on the *Planck* calibration parameter $a_{\text{Planck}} \sim \mathcal{N}(1, 0.0025)$. For the EFT of LSS nuisance parameters (see § 2.2), we use the following priors (from Ref. [56]):

$$\begin{aligned} b_1 &\sim \mathcal{U}(0, 4), \quad b_2 \sim \mathcal{N}(0, 1^2), \quad b_{\mathcal{G}_2} \sim \mathcal{N}(0, 1^2), \quad b_{\Gamma_3} \sim \mathcal{N}\left(\frac{23}{42}(b_1 - 1), 1^2\right) \\ \frac{c_0}{[h^{-1} \text{Mpc}]^2} &\sim \mathcal{N}(0, 30^2), \quad \frac{c_2}{[h^{-1} \text{Mpc}]^2} \sim \mathcal{N}(30, 30^2), \quad \frac{c_4}{[h^{-1} \text{Mpc}]^2} \sim \mathcal{N}(0, 30^2), \\ \frac{\tilde{c}}{[h^{-1} \text{Mpc}]^4} &\sim \mathcal{N}(500, 500^2), \quad \frac{c_1}{[h^{-1} \text{Mpc}]^2} \sim \mathcal{N}(0, 5^2), \\ P_{\text{shot}} &\sim \mathcal{N}(0, \bar{n}^{-2}), \quad B_{\text{shot}} \sim \mathcal{N}(1, \bar{n}^{-2}), \quad a_0 \sim \mathcal{N}(0, \bar{n}^{-2}), \quad a_2 \sim \mathcal{N}(0, \bar{n}^{-2}), \end{aligned} \quad (3.1)$$

where the inverse galaxy number density $\bar{n}^{-1} = 5000 [h^{-1} \text{Mpc}]^3$ for the high- z samples and $\bar{n}^{-1} = 3500 [h^{-1} \text{Mpc}]^3$ for the low- z samples. For discussion on these priors and a comparison to the choices made in the *PyBird* implementation of the EFT of LSS model (whose parameters are a linear combination of the above and which was used in a previous axion analysis [39]), see § 5 and Refs. [157] and [158].

We numerically sample posterior distributions using the importance nested sampling algorithm *MultiNest* [159, 160]. We use 480 live points and we stop chains when posterior weights reach a tolerance of 1% of their maximum, thus ensuring that we sample the bulk of the posterior weight. We check that our chains are converged with respect to the number of live points and tolerance by running test chains with 3600 live points and a tolerance of 10^{-5} and determining no shift in inferred distributions.

4 Results

4.1 Cosmic microwave background, baryon acoustic oscillations & supernovae

4.1.1 *Planck*

We first search for ultra-light axions (ULAs) in baseline *Planck* 2018 CMB temperature, polarisation and lensing data (see § 3.1.1 for a description of the data). We note that this is an update from Refs. [37, 39] which considered older *Planck* 2015 data. We now have access to a more robust measurement of the large-scale polarisation signal, and large-scale lensing anisotropies not previously released (L_{min} goes from 40 to 8). We anticipate improved bounds on the lightest axions that we consider since their effect is strong on large scales. Fig. 6 shows the 95% upper limit on the axion energy density allowed by *Planck* 2018 as a function of mass (it also compares to joint constraints from *Planck* CMB and BOSS galaxy clustering data and constraints from BOSS alone, which we discuss in § 4.2; these results are also shown in Table 2). We see the typical “u”-shaped constraints [161] where axions in the “belly”

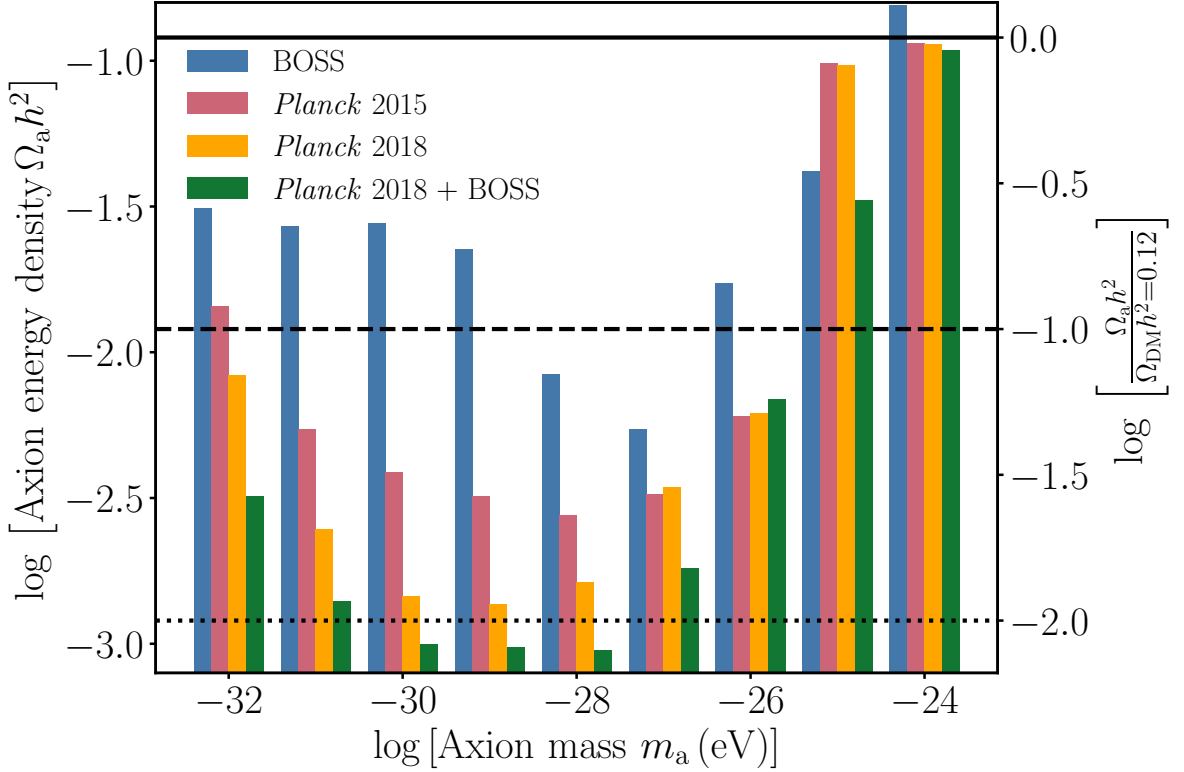


Figure 6. 95% credible upper limits on axion energy density $\Omega_a h^2$, as a function of axion mass m_a , as inferred: from BOSS galaxy clustering data (blue; see § 4.2); from *Planck* 2015 CMB data (red; [37]); from *Planck* 2018 CMB data (orange; see § 4.1); and as jointly inferred from *Planck* 2018 CMB and BOSS galaxy clustering data (green; see § 4.2). On the right-hand side, we show the 95% upper limit on the ratio of the axion energy density to the best-fit dark matter (DM) energy density as inferred from *Planck* in the Λ CDM model $\Omega_{\text{DM}} h^2 = 0.12$. The black horizontal dashed and dotted lines respectively indicate the energy densities at which axions form 10% and 1% of the DM today.

m_a	$\Omega_a h^2$ (<i>Planck</i>)	S_8 (<i>Planck</i>)	$\Omega_a h^2$ (<i>Planck</i> +BOSS)	S_8 (<i>Planck</i> +BOSS)
Λ CDM	–	$0.834^{+0.014}_{-0.013}$	–	0.827 ± 0.011
10^{-24} eV	< 0.11399	0.831 ± 0.014	< 0.10858	$0.826^{+0.011}_{-0.012}$
10^{-25} eV	< 0.09667	$0.811^{+0.025}_{-0.039}$	< 0.03306	$0.818^{+0.015}_{-0.017}$
10^{-26} eV	< 0.00615	0.819 ± 0.020	< 0.00689	$0.804^{+0.020}_{-0.024}$
10^{-27} eV	< 0.00344	$0.822^{+0.016}_{-0.020}$	< 0.00181	$0.819^{+0.013}_{-0.014}$
10^{-28} eV	< 0.00163	$0.831^{+0.014}_{-0.012}$	< 0.00095	0.824 ± 0.011
10^{-29} eV	< 0.00136	0.836 ± 0.014	< 0.00097	0.826 ± 0.011
10^{-30} eV	< 0.00145	$0.837^{+0.014}_{-0.013}$	< 0.00099	0.827 ± 0.011
10^{-31} eV	< 0.00247	$0.838^{+0.015}_{-0.014}$	< 0.00140	0.827 ± 0.011
10^{-32} eV	< 0.00833	$0.843^{+0.019}_{-0.016}$	< 0.00321	$0.829^{+0.012}_{-0.011}$

Table 2. Constraints on axion energy density $\Omega_a h^2$ and the matter clumping factor S_8 , as a function of axion mass m_a (top to bottom), as inferred from *Planck* CMB data (left; see § 4.1) and as jointly inferred from *Planck* CMB and BOSS galaxy clustering data (right; see § 4.2). For $\Omega_a h^2$, we give the 95% upper c.l.; for S_8 , we give the maximum marginalised posterior with the asymmetric 68% c.l.

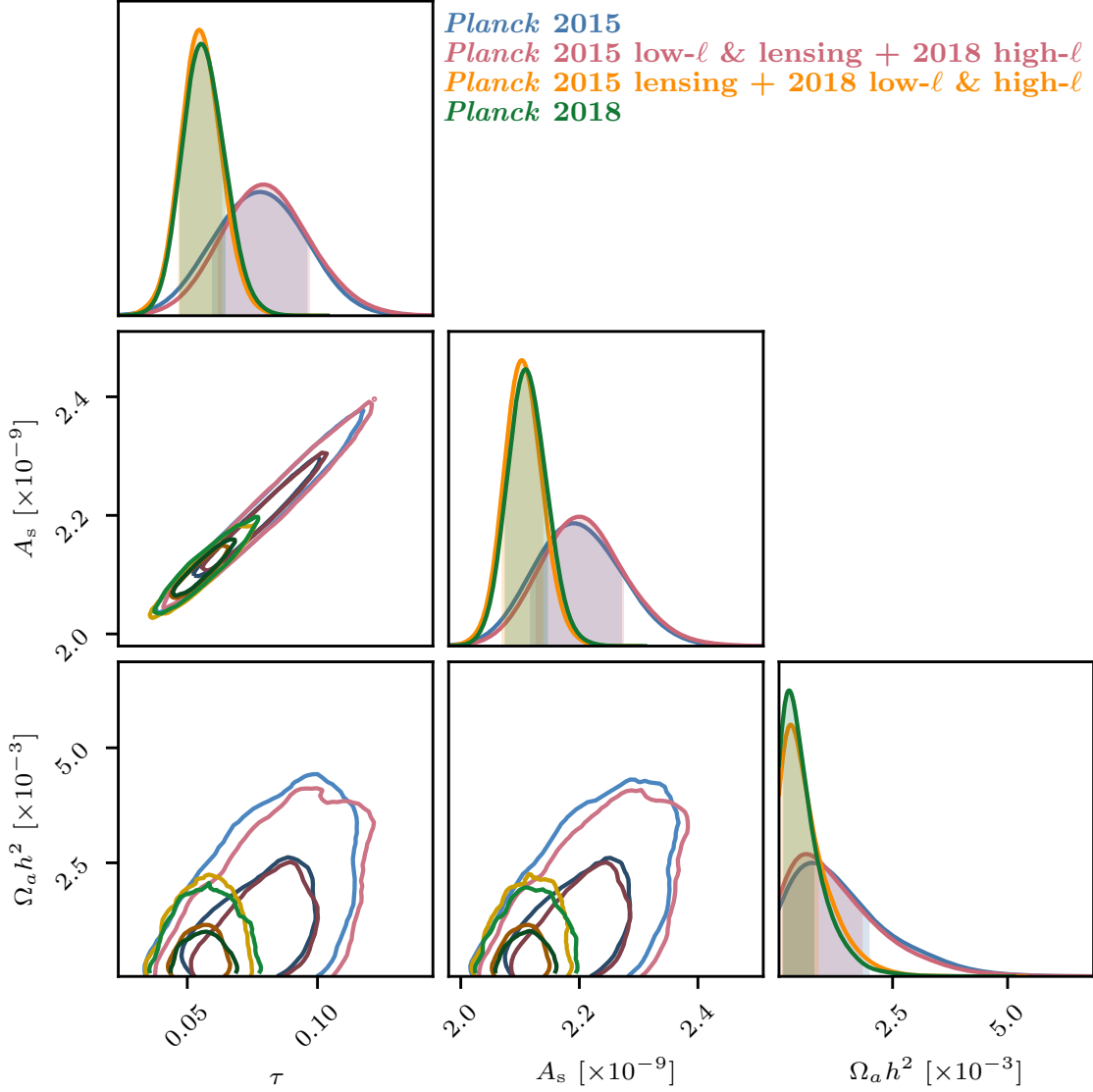


Figure 7. The effect of updating from *Planck* 2015 (blue) to *Planck* 2018 CMB data on axion constraints for $m_a = 10^{-30}$ eV. We systematically update parts of the 2015 data with 2018 results: first the high-multipole ℓ likelihood (red), then also the low- ℓ likelihood (orange), and then finally also the lensing likelihood (green). We find that the vast majority of improvement in the axion energy density bound comes from 2018 low- ℓ information, i.e., the measurement of the large-scale reionisation bump breaks degeneracies between the reionisation optical depth τ , the primordial power spectrum amplitude A_s and the axion energy density $\Omega_a h^2$. For each set, the inner and outer contours respectively indicate the 68% and 95% credible regions of the 2D marginalised posterior distribution, with the 1D marginalised posteriors on the diagonal, where 68% credible regions are shaded.

(10^{-30} eV $\leq m_a \leq 10^{-28}$ eV) are heavily constrained, but dark energy (DE)-like axions for $m_a < 10^{-30}$ eV and dark matter (DM)-like axions for $m_a \geq 10^{-27}$ eV can still be a significant cosmological component. In particular, *Planck* data lose sensitivity for $m_a \geq 10^{-25}$ eV as the scale-dependent suppression is on scales smaller than those that *Planck* probes and the

background evolution is the same as Λ CDM deep into the radiation epoch.

Our *Planck* 2018 results are consistent with previous *Planck* 2015 limits [37] for $m_a \geq 10^{-27}$ eV, but stronger for $m_a \leq 10^{-28}$ eV (see Fig. 6). Fig. 7 investigates which parts of the updated 2018 data are most important in improving axion constraints. In systematically replacing parts of the 2015 likelihood¹² with 2018 updates, we find that it is the inclusion of the 2018 low- ℓ likelihood that accounts for the vast majority of the improvement in the axion energy density bound. The main difference at low ℓ in 2018 data, arising from an analysis of high (electromagnetic) frequency polarisation modes, is a stronger and slightly lower constraint on the reionisation optical depth τ thanks to measurement of the large-scale reionisation bump in the EE power spectrum. This τ measurement breaks degeneracies with the primordial power spectrum amplitude A_s and the axion energy density $\Omega_a h^2$. We show results for $m_a = 10^{-30}$ eV. These are indicative for all $m_a \leq 10^{-28}$ eV, since the effect of the lightest DE-like axions in CMB data is restricted to the largest scales (through the integrated Sachs-Wolfe effect) that are degenerate with the primordial amplitude [23]. Hence, the improved τ measurement does not improve axion constraints for heavier DM-like axions ($m_a \geq 10^{-27}$ eV), whose effect is restricted to smaller scales.

Figure 8 shows the *Planck* constraints on other cosmological parameters. DE-like axions ($m_a < 10^{-27}$ eV) are consistent with lower values of h as they drive accelerated expansion after matter-radiation equality [23]¹³. As DE-like axions have all started oscillating (and so behave like DM) by today, they count towards the total matter energy density Ω_m , but are not degenerate with cold DM in the CMB. Thus, for $m_a \leq 10^{-27}$ eV, larger values of Ω_m are allowed. This also drives compatibility with larger values of the matter clumping factor since $S_8 \propto \sqrt{\Omega_m}$. Conversely, DM-like axions ($m_a > 10^{-27}$ eV) are degenerate with cold DM (CDM) in the CMB and so, in the high-mass limit where axions are poorly constrained, the CDM density is also poorly constrained. Further, DM-like axions suppress the matter power spectrum on scales below their de Broglie wavelength. Thus, when DM-like axions can comprise a significant fraction ($\gtrsim 2\%$) of the total DM budget (10^{-27} eV $\leq m_a \leq 10^{-25}$ eV), *Planck* data are compatible with lower values of S_8 than in the Λ CDM model, since S_8 integrates over lower-amplitude modes. For $m_a > 10^{-25}$ eV, the power spectrum suppression is on scales smaller than those to which the S_8 parameter is most sensitive and so Λ CDM values of S_8 are returned. This suggests that axions with $m_a \in [10^{-27}, 10^{-25}]$ eV could help to resolve the so-called S_8 tension by bringing CMB data into compatibility with the lower S_8 values inferred from large-scale structure data. Fig. 9 explicitly illustrates that it is degeneracy with the axion energy density that allows lower values of h and higher values of Ω_m for DE-like axions ($m_a \sim 10^{-30}$ eV), and lower values of S_8 for DM-like axions ($m_a \sim [10^{-26} - 10^{-25}]$ eV).

Although axions with $m_a = 10^{-25}$ eV can comprise the dark matter according to *Planck* data, there is no preference for such a model compared to Λ CDM according to the Bayesian evidence. The log-ratio of model evidences (or Bayes factor) given *Planck* data is 1.8 in favour of Λ CDM (see Table 3). This amounts to “positive” evidence in favour of Λ CDM according to the Jeffreys scale as given by Ref. [163]. This lack of preference for extended cosmological

¹²We consider the same *Planck* 2015 CMB likelihood as used in Ref. [37]: the low- ℓ likelihood `lowl_SMW_70_dx11d_2014_10_03_v5c_Ap` for $2 \leq \ell \leq 29$, the high- ℓ likelihood `plik_lite_v18_TTTEEE` for $30 \leq \ell \leq 2508$ (TT power spectrum) and $30 \leq \ell \leq 1996$ (TE and EE power spectra), and the lensing likelihood `smica_g30_ftl_full_pp` for $40 \leq L \leq 400$.

¹³We are considering different axion models than those that are typically invoked to *increase* h (and so address the Hubble parameter tension). These so-called “early dark energy” axions are contrived to induce a burst of accelerated expansion *before* recombination and typically require non-trivial axion potentials [see e.g., 162].

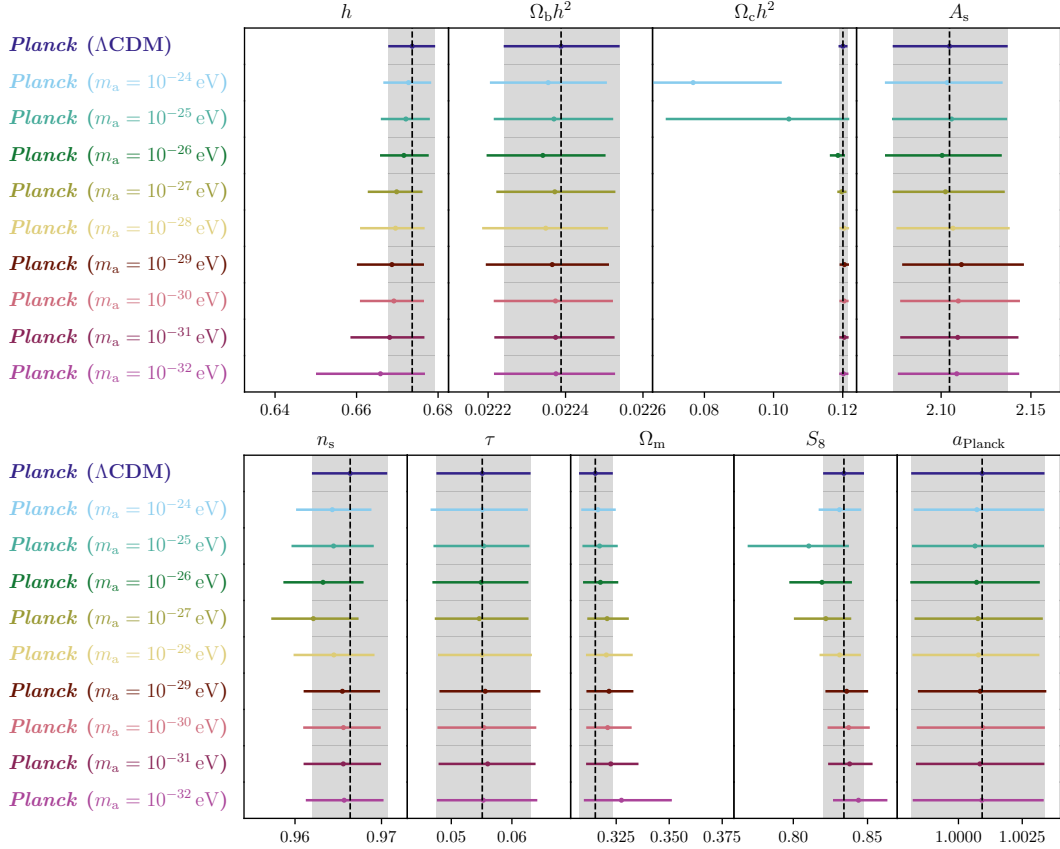


Figure 8. The effect of axion mass m_a on cosmological parameter constraints from *Planck* CMB data. We see how dark energy-like axions ($m_a < 10^{-27}$ eV) have degeneracy with lower values of the Hubble parameter h , while dark matter (DM)-like axions ($m_a \geq 10^{-27}$ eV) have degeneracy with the cold DM density $\Omega_c h^2$ and lower values of the matter clumping factor S_8 . These degeneracies are explored further in Fig. 9. Each point indicates the maximum marginalised posterior, while the errorbar indicates the marginalised 68% c.l. A_s is in units of 10^{-9} .

models is consistent with previous studies [e.g., 164], and there is no improvement in the maximum likelihood (or minimum chi-squared).

4.1.2 All CMB, BAO & supernovae

For the first time in a ULA search, we consider the addition of higher-resolution CMB data from the ACT and SPT experiments. We defer a systematic search of the axion mass parameter space to future work, in anticipation of upcoming high-resolution lensing data. In this study, we focus on the impact of current ACT (see § 3.1.2) and SPT (see § 3.1.3) data (and a compendium of low- z galaxy BAO and supernovae; see § 3.2) on DM-like axions that most significantly increase compatibility with low values of S_8 : $m_a = 10^{-25}$ eV. Fig. 10 illustrates the effect on the $S_8 - \Omega_m - \Omega_a h^2$ planes from adding these data to the *Planck* data considered above. The posterior shifts with respect to *Planck* alone are small. There is a $\sim 0.5\sigma$ decrease in Ω_m when adding BAO and SNe data ($\sim 1\sigma$ decrease seen in the Λ CDM case; see Fig. 11). In particular, the axion energy density bounds at $m_a = 10^{-25}$ eV are slightly weakened with the addition of these data (see also Table 4). Correspondingly, there is a shift to even lower values of S_8 driven by its parameter degeneracy with $\Omega_a h^2$. This weakening of constraints

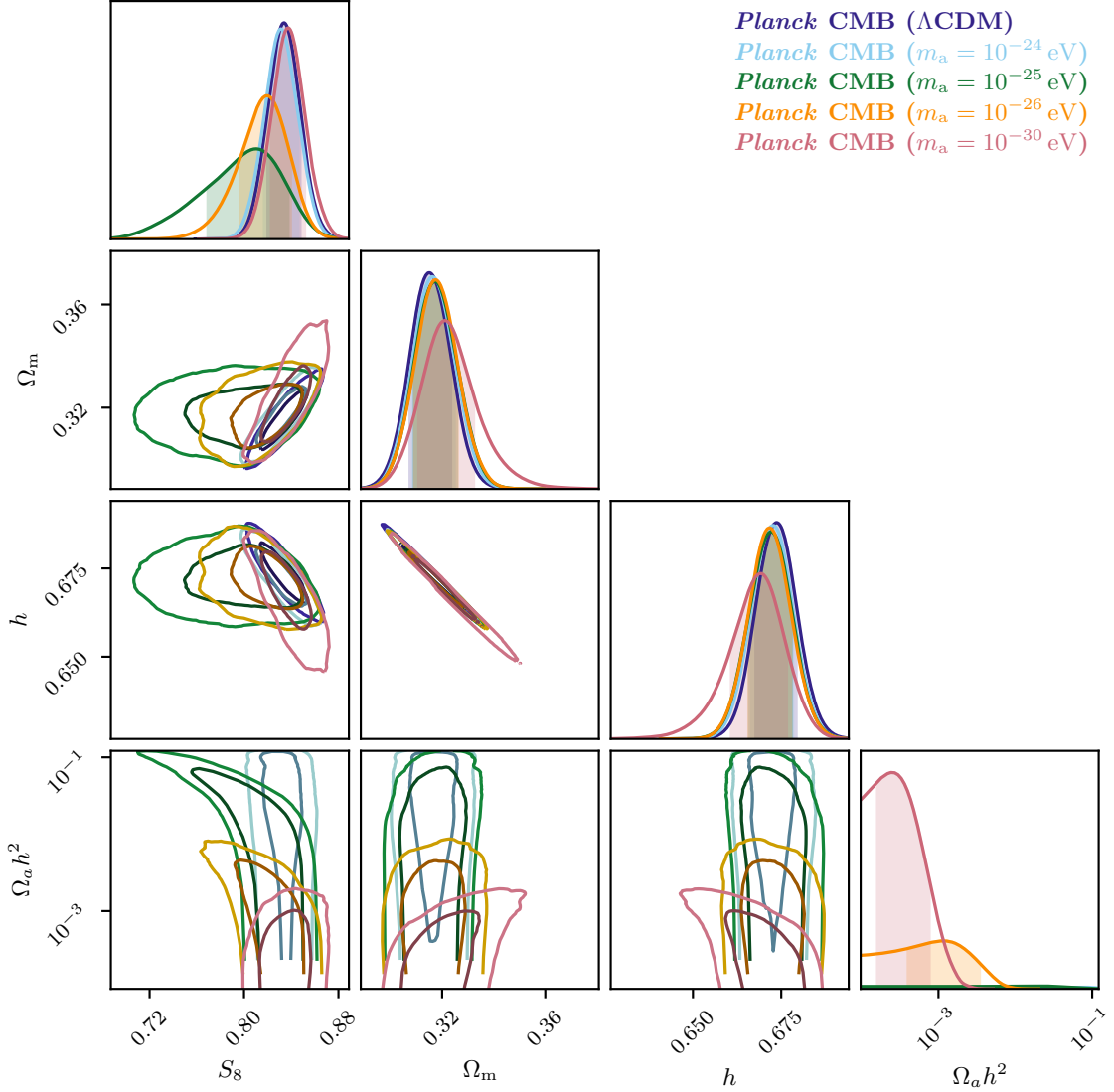


Figure 9. The effect of ultra-light axions on the matter clumping factor S_8 , matter energy density Ω_m and Hubble parameter h , inferred from *Planck*, as a function of axion mass m_a . Dark matter (DM)-like axions for $m_a \in [10^{-26}, 10^{-25}]$ eV give lower S_8 values by a scale-dependent power spectrum suppression, while dark energy-like axions (e.g., $m_a = 10^{-30}$ eV) give lower h values by causing accelerated expansion after matter-radiation equality. DM-like axions with $m_a = 10^{-24}$ eV have a negligible effect on S_8 as the power spectrum suppression is on scales smaller than those to which S_8 is sensitive. For each set, the inner and outer contours respectively indicate the 68% and 95% credible regions of the 2D marginalised posterior distribution, with the 1D marginalised posteriors on the diagonal, where 68% credible regions are shaded.

is consistent with previous searches for massive neutrinos in high-resolution CMB data [e.g., 54]. Similarly to neutrinos, DM-like axions are constrained in primary CMB anisotropy power spectra through the lensing-induced smoothing of acoustic peaks. Here, gravitational lensing by lower-redshift (mostly $z < 2$) large-scale structure dampens the amplitude of peaks in

Data	m_a	Bayes factor relative to Λ CDM
<i>Planck</i>		-1.8
<i>Planck</i> + ACT-DR4	10^{-25} eV	-0.6
<i>Planck</i> + SPT-3G		-1.8
All CMB + BAO + SNe		-0.4
	10^{-24} eV	-1.5
	10^{-25} eV	-2.6
	10^{-26} eV	-1.6
	10^{-27} eV	-4.0
<i>Planck</i> + BOSS	10^{-28} eV	-3.1
	10^{-29} eV	-3.1
	10^{-30} eV	-3.2
	10^{-31} eV	-2.5
	10^{-32} eV	-2.6

Table 3. Bayes factor (log-ratio of model evidences; *right column*) for the indicated data (*left column*) given the indicated axion model (*middle column*) relative to the Λ CDM model. For all the data combinations shown, the Bayesian evidence favours the Λ CDM model; although we find that axions can improve consistency between datasets (see § 4.2), there is no preference for an extension beyond Λ CDM given these data.

Data	S_8 (Λ CDM)	$\Omega_a h^2$ ($m_a = 10^{-25}$ eV)	S_8 ($m_a = 10^{-25}$ eV)
<i>Planck</i>	$0.834^{+0.014}_{-0.013}$	< 0.09667	$0.811^{+0.025}_{-0.039}$
<i>Planck</i> + ACT-DR4	$0.835^{+0.013}_{-0.012}$	< 0.10745	$0.789^{+0.027}_{-0.041}$
<i>Planck</i> + SPT-3G	$0.828^{+0.014}_{-0.011}$	< 0.10580	$0.799^{+0.027}_{-0.046}$
All CMB + BAO + SNe	0.827 ± 0.010	< 0.10610	$0.774^{+0.032}_{-0.037}$

Table 4. Constraints on axion energy density $\Omega_a h^2$ and the matter clumping factor S_8 , for different CMB, galaxy BAO and supernovae data combinations (see § 3.1 for a description of the data). For $\Omega_a h^2$, we give the 95% upper c.l.; for S_8 , we give the maximum marginalised posterior with the asymmetric 68% c.l.

angular power spectra. It follows that the amount of lensing-induced smoothing is sensitive to the presence of ultra-light axions or neutrinos which suppress the growth of structure and thus reduce the amount of smoothing. The amount of lensing relative to the best-fit Λ CDM expectation is quantified by the multiplicative correction to the theoretical expectation A_L . In particular, both ACT-DR4 ($A_L = 1.01 \pm 0.11$) [54] and SPT-3G ($A_L = 0.98 \pm 0.12$) [55] prefer lower values of A_L compared to *Planck* ($A_L = 1.180 \pm 0.065$) [2]. This means that when adding ACT or SPT data to *Planck*, constraints on models that suppress structure and lower the lensing signal are weakened, e. g., massive neutrinos [54] or ultra-light axions. Fig. 11 shows marginalised constraints on all other cosmological parameters, also comparing to the Λ CDM case. We see the typical degeneracy for DM-like axions with standard cold DM meaning that weakened constraints on $\Omega_a h^2$ lead to correspondingly-weakened constraints on $\Omega_c h^2$. We note a $\sim 1\sigma$ increase in the *Planck* calibration parameter a_{Planck} when adding ACT data which is seen in both Λ CDM and axion models. Similarly as for *Planck* data, there is no preference given these combined datasets for an axion model compared to Λ CDM according to the Bayesian evidence (see Table 3). The Bayes factors amount to evidence in favour of Λ CDM that ranges from “positive” to “not worth more than a bare mention” according to the

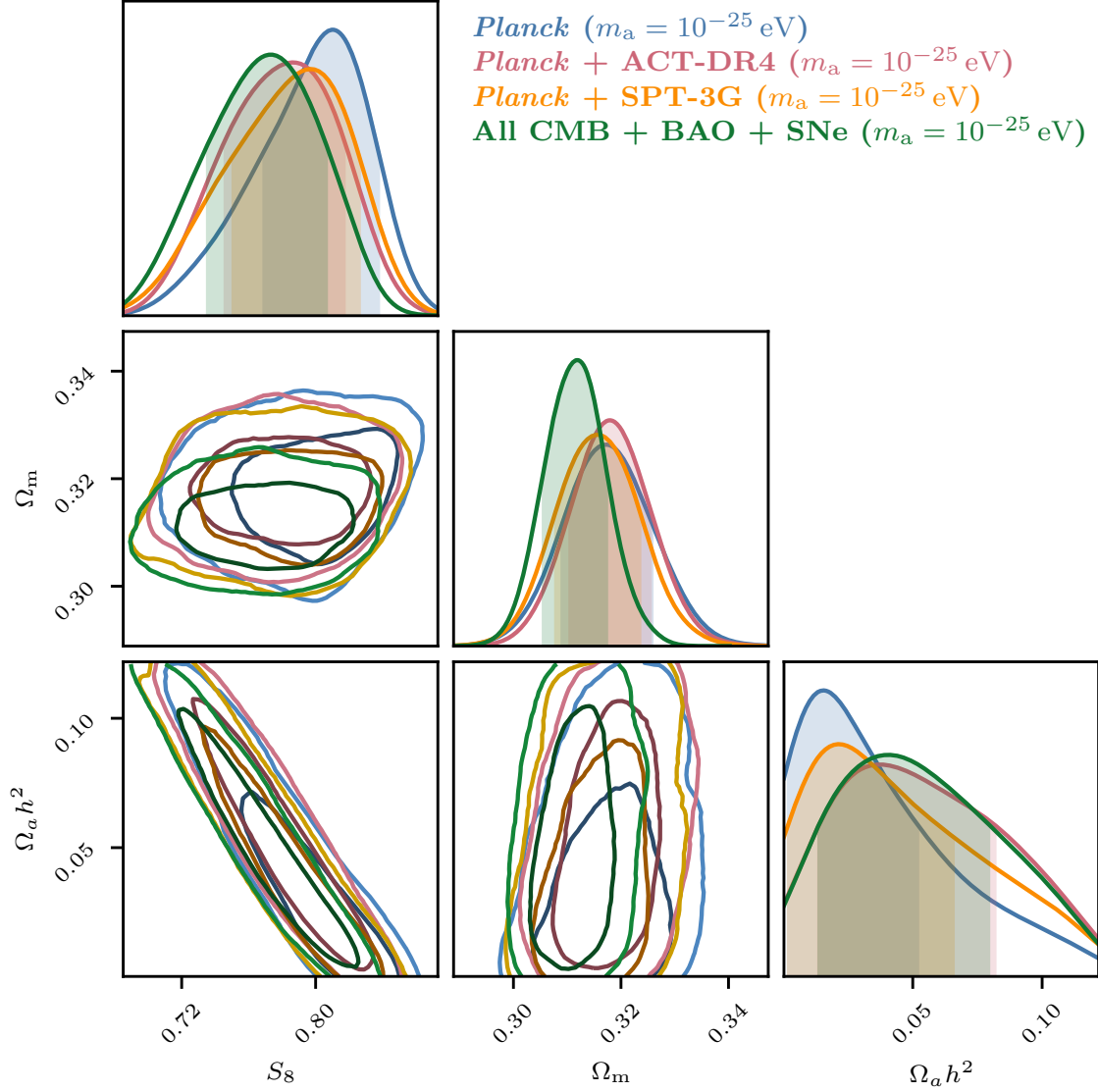


Figure 10. The effect of current higher-resolution CMB data (*Planck* and ACT-DR4 in red; *Planck* and SPT-3G in orange), galaxy baryon acoustic oscillations (BAO) and supernovae (SNe) (all combined with *Planck* in green; *Planck* only in blue) on axion constraints for $m_a = 10^{-25}$ eV. For each set, the inner and outer contours respectively indicate the 68% and 95% credible regions of the 2D marginalised posterior distribution, with the 1D marginalised posteriors on the diagonal, where 68% credible regions are shaded. From left to right, S_8 is the matter clumping factor, Ω_m is the matter energy density and $\Omega_a h^2$ is the physical axion energy density.

Jeffreys scale [163].

We demonstrate above that, in an axion model with $m_a = 10^{-25}$ eV, the combination of *Planck*, ACT-DR4 and SPT-3G CMB, galaxy BAO and supernovae data are compatible with lower values of the matter clumping factor ($S_8 = 0.774^{+0.032}_{-0.037}$) than in Λ CDM ($S_8 = 0.827 \pm 0.010$). Fig. 12 compares this result to fiducial Λ CDM constraints from combined galaxy weak lensing and clustering (3×2) data. We consider Λ CDM constraints (with fixed

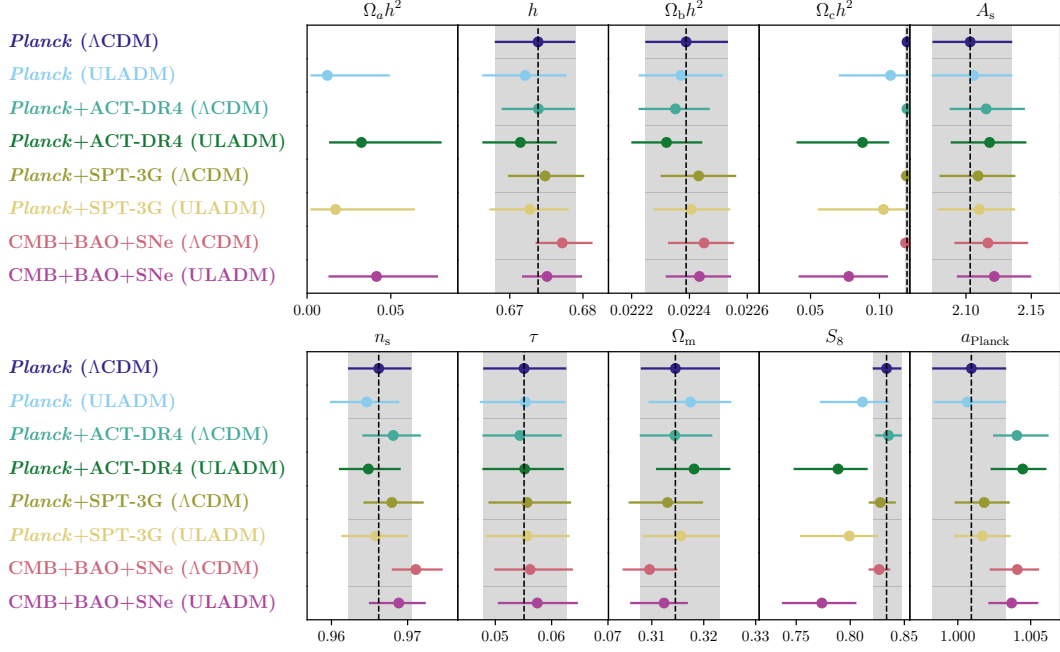


Figure 11. The effect of current higher-resolution CMB data (ACT-DR4, SPT-3G), galaxy BAO and supernovae (SNe) on ultra-light axion and cosmological constraints for $m_a = 10^{-25}$ eV (ULA DM), also comparing to Λ CDM and *Planck*-only constraints. Each point indicates the marginalised mean, while the errorbar indicates the marginalised 68% c.l. A_s is in units of 10^{-9} .

neutrino energy density) from the combination of galaxy clustering, galaxy lensing shear and galaxy – galaxy lensing two-point correlation functions (3×2) as measured by the Dark Energy Survey (DES) [165]¹⁴. We also consider Λ CDM constraints (with fixed neutrino energy density) from the same combination of three \times two-point correlation functions as measured by the Kilo-Degree Survey (KiDS) [166], which includes redshift-space galaxy clustering data from BOSS [167] and galaxy – galaxy lensing data from the survey overlap between KiDS, BOSS and the spectroscopic 2-degree Field Lensing Survey (2dFLenS) [168]¹⁵. We note that the KiDS 3×2 constraints are therefore not entirely independent of the CMB + BAO + SNe compendium we consider, since part of the BAO measurements we use is derived from the same BOSS data (see § 3.2) as goes into the KiDS 3×2 measurement. However, we note that the addition of BAO and SNe data makes only a small difference to the S_8 constraint from *Planck* + ACT and *Planck* + SPT (see e.g., Fig. 10). We anticipate that, in § 4.2, we will consider the full-shape galaxy clustering power spectrum from BOSS, which will be much more significantly correlated with the KiDS 3×2 analysis. Despite this proviso, Fig. 12 illustrates how, in the Λ CDM model, 3×2 analyses from both DES ($S_8 = 0.783 \pm 0.020$) and KiDS ($S_8 = 0.765 \pm 0.017$) prefer systematically lower values of S_8 than the compendium of CMB, BAO and SNe data ($S_8 = 0.827 \pm 0.010$). This is a manifestation of the so-called “ S_8 tension”, where many galaxy clustering, weak lensing and galaxy cluster observations prefer lower values of S_8 than is inferred from CMB observations, with statistical significance ranging from 2 to 3 σ depending on the data comparison [see e.g., 90, for a recent review]. However, when axions of $m_a = 10^{-25}$ eV contribute to the energy budget, the CMB, BAO

¹⁴This is the publicly-released posterior chain `chain_3x2pt_fixednu_lcdm`.

¹⁵This is the publicly-released posterior chain `samples_multinest_blindC_EE_nE_w`.

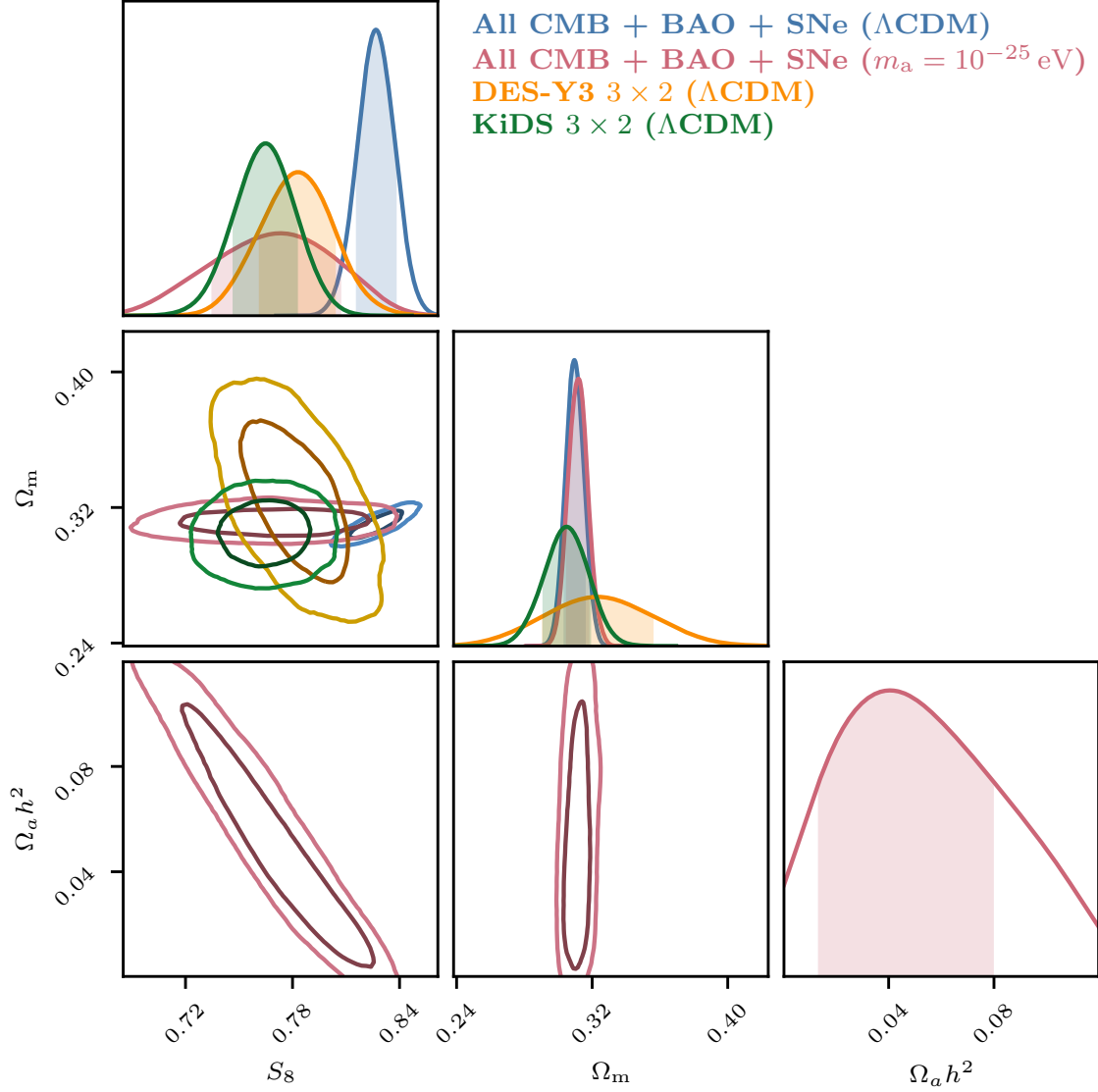


Figure 12. Comparison of CMB (*Planck*, ACT-DR4, SPT-3G), galaxy BAO and supernovae (SNe) constraints with fiducial galaxy weak lensing and clustering (3×2) Λ CDM constraints from the Dark Energy Survey (DES) and the Kilo-Degree Survey (KiDS) (all with fixed neutrino mass). In Λ CDM, CMB, BAO and SNe data prefer systematically higher values of the matter clumping factor S_8 than is inferred from fiducial 3×2 analyses. When axions of $m_a = 10^{-25}$ eV contribute to the energy budget with energy density $\Omega_a h^2$, CMB, BAO and SNe data are consistent with lower values of S_8 . In order to assess consistency between data in an axion model, it is necessary to re-analyse the 3×2 data in the presence of axions; in § 4.2, we consider the first part with galaxy clustering from BOSS. For each set, the inner and outer contours respectively indicate the 68% and 95% credible regions of the 2D marginalised posterior distribution, with the 1D marginalised posteriors on the diagonal, where 68% credible regions are shaded. *From left to right*, S_8 is the matter clumping factor, Ω_m is the matter energy density and $\Omega_a h^2$ is the physical axion energy density.

and SNe compendium is compatible with the low S_8 values preferred by DES and KiDS in the Λ CDM model. We therefore hypothesise that axions could resolve the S_8 tension. In order

to assess this, we must reanalyse the 3×2 data in the axion model. In this work, we consider the first part of this in analysing full-shape galaxy clustering information from BOSS. We present these results in § 4.2.

4.2 Baryon Oscillation Spectroscopic Survey galaxy power spectrum & bispectrum

We now consider the effect on ultra-light axion constraints from the galaxy power spectrum and bispectrum as measured from the Baryon Oscillation Spectroscopic Survey (BOSS; see § 3.3 for a description of the data).

4.2.1 Λ CDM

Before studying the combination of *Planck* CMB and BOSS galaxy clustering data, we assess constraints independently from each dataset. Fig. 13 shows Λ CDM cosmological constraints from the BOSS galaxy power spectrum only (P_0, P_2, P_4, Q_0 and the post-reconstructed BAO Alcock-Paczynski parameters), the BOSS galaxy power spectrum and bispectrum monopole (additionally B_0), and *Planck* CMB data (previously shown in § 4.1). In particular, we consider BOSS constraints without a prior on the baryon energy density $\Omega_b h^2$ or any other cosmological parameters. It is striking how much more constraining is *Planck* data on the full cosmological model than BOSS data alone. However, as is typical of large-scale structure experiments, BOSS provides more competitive constraints when projected onto the plane of derived parameters Ω_m and S_8 .

4.2.2 Parameter tension metrics

In order to assess consistency between datasets in their cosmological constraints, we consider three metrics of parameter tension (the difference in S_8 only, the difference in the $S_8 - \Omega_m$ plane, and the difference in the full posterior distribution). We now describe these metrics in more detail. The first metric, which is most widely quoted in the literature, is the discrepancy in the marginalised S_8 constraint from two datasets (labelled 1 and 2), defined as

$$\frac{\Delta S_8}{\sigma_{S_8}} = \frac{\mu_1 - \mu_2}{\sqrt{\sigma_1^2 + \sigma_2^2}}. \quad (4.1)$$

Here, μ_i and σ_i are respectively the parameter posterior mean and standard deviation given experiment i . This metric is given in the third column of Table 5. We also consider a second metric, which is an extension of Eq. (4.1) to higher dimensions:

$$\chi^2 = (\boldsymbol{\mu}_1 - \boldsymbol{\mu}_2)^T (C_1 + C_2)^{-1} (\boldsymbol{\mu}_1 - \boldsymbol{\mu}_2). \quad (4.2)$$

Here, $\boldsymbol{\mu}_i$ is now the vector of parameter posterior means and C_i is the posterior covariance, both given experiment i . We then calculate the probability p to exceed χ^2 (for a χ^2 distribution with degrees of freedom equal to the number of parameters) and convert this to a number N of σ using the standard Gaussian interpretation¹⁶.

Both Eqs. (4.1) and (4.2) are good measures of parameter discrepancy in the limit of Gaussian posterior distributions. We therefore give, in the fourth column of Table 5, the metric defined in Eq. (4.2) evaluated for the marginalised posterior in the $S_8 - \Omega_m$ plane. In this plane, the BOSS data are most constraining and the distribution is reasonably Gaussian. It is important nonetheless also to consider consistency in the full set of parameters

¹⁶ $N = \sqrt{2} \operatorname{erf}^{-1}(p)$.

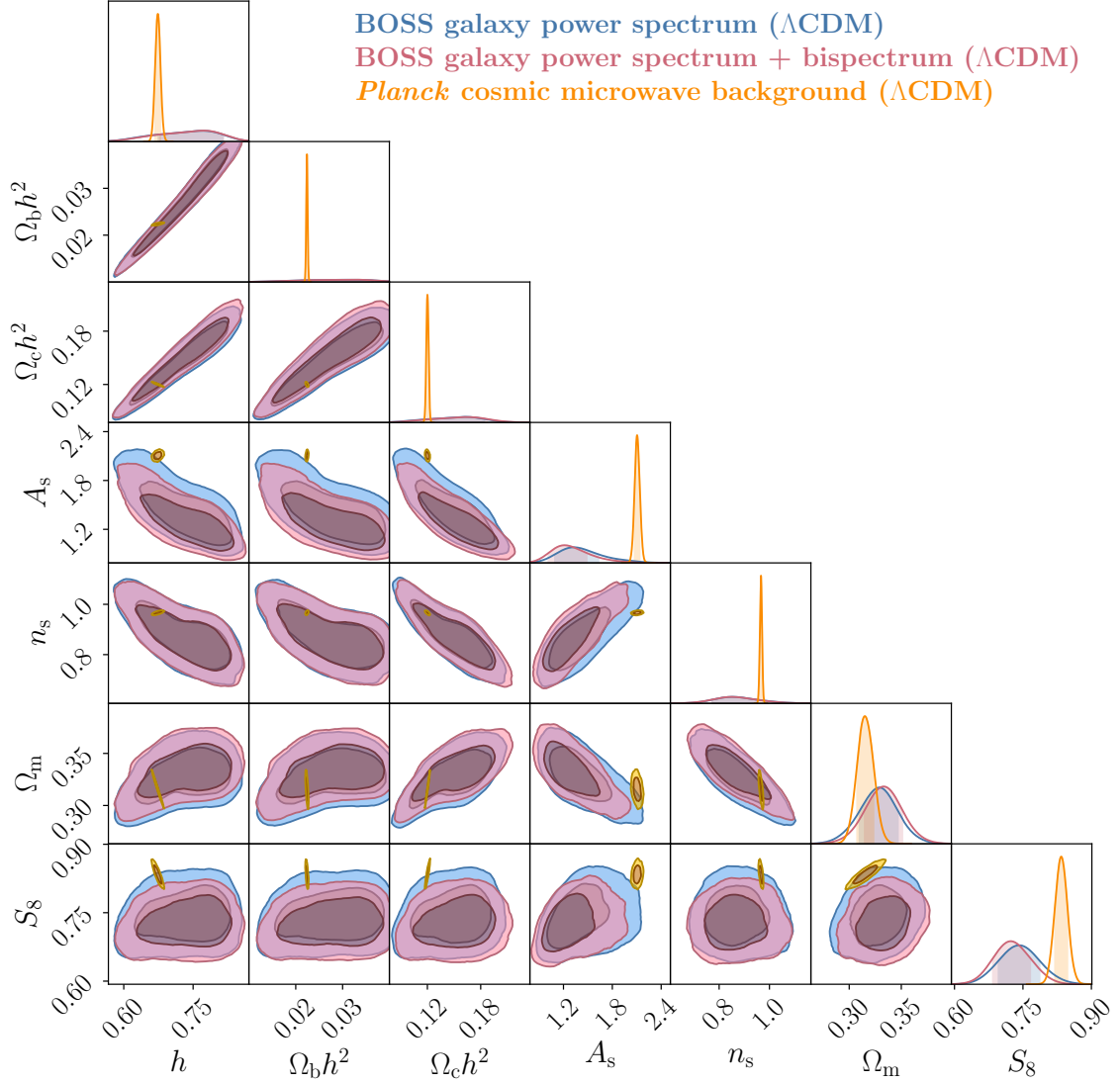


Figure 13. Comparison of BOSS galaxy clustering and *Planck* CMB constraints on Λ CDM cosmological parameters. BOSS data alone (in particular without an $\Omega_b h^2$ prior) are much less constraining than *Planck* data on the standard cosmological model. For each set, the darker and lighter shaded contours respectively indicate the 68% and 95% credible regions of the 2D marginalised posterior distribution, with the 1D marginalised posteriors on the diagonal, where 68% credible regions are shaded. A_s is in units of 10^{-9} .

constrained by both datasets. However, the full BOSS posterior distribution appears highly non-Gaussian and so the metrics defined above will not be a good measure of consistency in the full parameter space. We therefore elect to calculate the full posterior distribution of the parameter difference $\Delta\theta$ (marginalised over the parameters θ) [169]:

$$\mathcal{P}(\Delta\theta) = \int d\theta \mathcal{P}_1(\theta) \mathcal{P}_2(\theta - \Delta\theta). \quad (4.3)$$

Data	Model	S_8 (σ)	$S_8 - \Omega_m$ (σ)	All parameters (σ)
<i>Planck</i> , BOSS [no B_0]	Λ CDM	2.1	2.02	1.77
	$m_a = 10^{-25}$ eV	1.32	1.14	2.14
<i>Planck</i> , BOSS	Λ CDM	2.70	2.82	4.36
	$m_a = 10^{-25}$ eV	1.63	1.57	3.70
	$m_a = 10^{-26}$ eV	3.63	3.81	5.38
	$m_a = 10^{-27}$ eV	2.28	2.11	3.63
	$m_a = 10^{-28}$ eV	1.78	1.76	3.31
	$m_a = 10^{-29}$ eV	1.74	2.44	3.19
	$m_a = 10^{-30}$ eV	2.22	2.82	4.11
	$m_a = 10^{-31}$ eV	2.24	2.73	2.95
	$m_a = 10^{-32}$ eV	2.58	2.78	3.19

Table 5. Discrepancy in parameters (given in the top row) as inferred from the two datasets given in the first column, for the model given in the second column. The third column is the discrepancy in the marginalised S_8 constraint, and the fourth column is the discrepancy in the marginalised $S_8 - \Omega_m$ plane, both with the reasonable approximation of a Gaussian posterior distribution. The final column is the discrepancy in the marginalised constraint on all cosmological (and axion) parameters, where we account for non-Gaussianity by calculating the full parameter difference posterior. The full details of the tension metrics that we use are given in § 4.2.

Here, $\mathcal{P}_i(\boldsymbol{\theta})$ is the posterior distribution given experiment i . We can then calculate the significance of the inferred parameter shift (relative to none) by integrating $\mathcal{P}(\Delta\boldsymbol{\theta})$ above the iso-probability contour that goes through $\Delta\boldsymbol{\theta} = 0$ (this probability to exceed can be converted to a number of σ as above)¹⁷. In this way, this third tension metric accounts for non-Gaussianities in the parameter posterior distribution. We therefore give, in the final column of Table 5, the metric derived from Eq. (4.3) as evaluated in the volume of all parameters constrained by both *Planck* and BOSS [$h, \Omega_b h^2, \Omega_c h^2, A_s, n_s, \Omega_m, S_8$ and $\Omega_a h^2$ when part of the model].

There are many proposed approaches to evaluating parameter consistency in high-dimensional and non-Gaussian distributions. Although these different approaches tend to agree in terms of trend (i.e., they typically agree with respect to an increasing or decreasing tension) [see e.g., 170], they typically disagree as to the particular value of tension. We therefore urge caution when interpreting Table 5 that it is most useful as a measure of relative tension given different models. All three metrics considered in Table 5 (and Fig. 13) illustrate that the addition of BOSS bispectrum data B_0 increases the discrepancy with respect to *Planck* mostly by preferring slightly lower values of the primordial power spectrum amplitude A_s . This in turn pushes S_8 to slightly lower values.

4.2.3 BOSS-only axion constraints

Figure 14 shows the same set of posterior contours as in Fig. 13 but for an axion model with $m_a = 10^{-25}$ eV. Although BOSS is less constraining than *Planck* on Λ CDM parameters, it is significantly more constraining on the axion energy density. This is driven by the addition of smaller-scale data in the reconstructed real-space galaxy power spectrum Q_0 (see Fig. 19 and discussion below). However, since *Planck* alone is unconstraining on the axion energy

¹⁷We numerically evaluate this integral using the `tensiometer` package: <https://github.com/mraveri/tensiometer>.

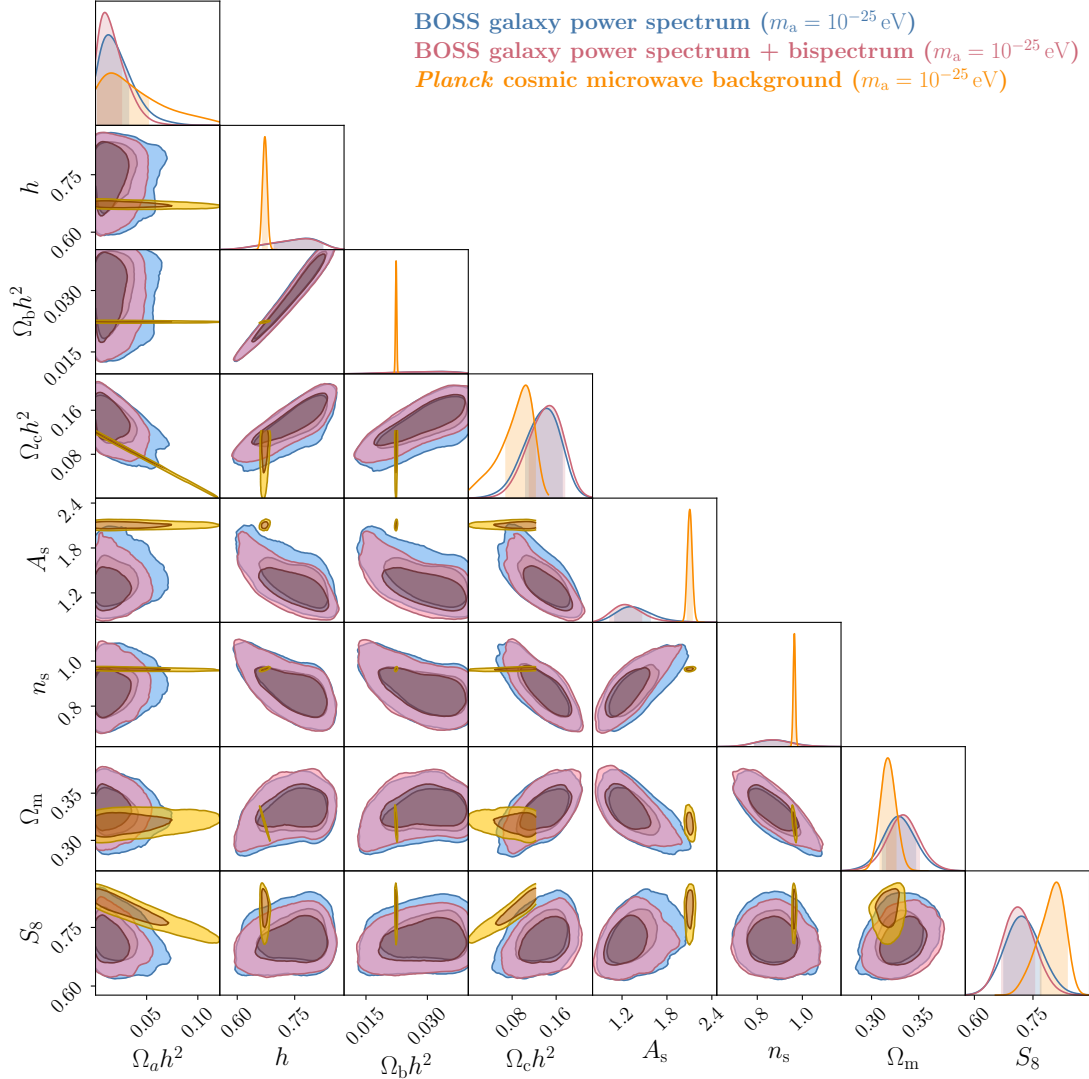


Figure 14. Comparison of BOSS galaxy clustering and *Planck* CMB constraints on axion and cosmological parameters, for axion mass $m_a = 10^{-25}$ eV. BOSS data alone are more constraining than *Planck* data on axion energy density $\Omega_a h^2$ since BOSS probes smaller scales ($k < 0.4 h \text{ Mpc}^{-1}$); in the extended axion model, there is more posterior overlap in the $S_8 - \Omega_m$ plane than in ΛCDM (see Fig. 13). For each set, the darker and lighter shaded contours respectively indicate the 68% and 95% credible regions of the 2D marginalised posterior distribution, with the 1D marginalised posteriors on the diagonal, where 68% credible regions are shaded. A_s is in units of 10^{-9} .

density at this mass (see also § 4.1), it is more consistent with the lower values of S_8 that BOSS (and indeed other large-scale structure experiments) prefer. This means that there is more posterior overlap in the $S_8 - \Omega_m$ plane and this is reflected in the improved tension metrics in Table 5. Notably, the tension in S_8 when comparing *Planck* to full BOSS data is reduced from 2.70σ (ΛCDM) to 1.63σ (for $m_a = 10^{-25}$ eV). However, there is no degeneracy between $\Omega_a h^2$ and A_s at $m_a = 10^{-25}$ eV. This is because $\Omega_a h^2$ largely affects the small-scale

m_a	$\Omega_a h^2$ (BOSS)	S_8 (BOSS)
Λ CDM	–	$0.723^{+0.041}_{-0.037}$
10^{-24} eV	< 0.15539	$0.718^{+0.038}_{-0.039}$
10^{-25} eV	< 0.04174	$0.709^{+0.043}_{-0.037}$
10^{-26} eV	< 0.01717	0.653 ± 0.040
10^{-27} eV	< 0.00542	$0.719^{+0.040}_{-0.038}$
10^{-28} eV	< 0.00842	$0.742^{+0.050}_{-0.040}$
10^{-29} eV	< 0.02259	$0.759^{+0.044}_{-0.043}$
10^{-30} eV	< 0.02771	$0.745^{+0.041}_{-0.040}$
10^{-31} eV	< 0.02706	$0.744^{+0.040}_{-0.042}$
10^{-32} eV	< 0.03126	$0.737^{+0.040}_{-0.038}$

Table 6. Constraints on axion energy density $\Omega_a h^2$ and the matter clumping factor S_8 , as a function of axion mass m_a (*top to bottom*), as inferred from BOSS galaxy clustering data. For $\Omega_a h^2$, we give the 95% upper c.l.; for S_8 , we give the maximum marginalised posterior with the asymmetric 68% c.l. For consistency with other masses, at $m_a = 10^{-26}$ eV, we give the upper limit on the axion density; nonetheless, $\Omega_a h^2 = 0$ is disfavoured at $\sim 2.7\sigma$, i.e., the maximum marginalised posterior $\Omega_a h^2 = 0.0100^{+0.0048}_{-0.0037}$.

power spectrum, while A_s is constrained by the overall normalisation at all wavenumbers (see Fig. 4). This means there is no improvement in the A_s discrepancy between *Planck* and BOSS even in the presence of axions at $m_a = 10^{-25}$ eV and this is reflected in the full parameter space tension metric given in Table 5. Indeed, when not including bispectrum data, the full parameter tension increases slightly.

In Fig. 6, we show the 95 % upper limits on $\Omega_a h^2$ derived from BOSS data across the full mass range that we consider (see also Table 6). For $m_a < 10^{-25}$ eV, the BOSS-only constraints are weaker than *Planck*, although the BOSS data are crucial in strengthening the combined CMB and galaxy clustering limit at nearly all masses (see below). Nonetheless, we see the typical “u”-shaped constraints (that we see with CMB data) also given BOSS alone: at higher mass, BOSS loses sensitivity since the scale-dependent suppression manifests at larger wavenumbers than those we model in BOSS (crucially, BOSS probes smaller scales than *Planck* and so we have improved sensitivity for $m_a = 10^{-25}$ eV); at lower mass, BOSS loses sensitivity owing to degeneracy with A_s . The degeneracy with A_s for $m_a \leq 10^{-28}$ eV is illustrated in Fig. 15, where we show how axions impact BOSS constraints on all cosmological parameters. This degeneracy arises at low mass since the axion Jeans wavenumber is then smaller than the smallest wavenumber that we model in BOSS. This means that axions suppress all BOSS wavenumbers, which is degenerate with lowering A_s and so lowering the overall power amplitude. BOSS data are therefore compatible with higher values of S_8 (driven by higher A_s and also higher Ω_m) than for Λ CDM for $m_a \leq 10^{-28}$ eV (the effects of higher A_s and $\Omega_a h^2$ do not cancel perfectly at the scales to which S_8 is sensitive). This drives an increase in compatibility between BOSS and *Planck* around $m_a \sim 10^{-29}$ eV, including (unlike with heavier axions) with regards to the A_s discrepancy (see Table 5). Beyond degeneracy with A_s , we also see the typical degeneracy with $\Omega_c h^2$ for (heavier) DM-like axions and degeneracy with Ω_m for (lighter) DE-like axions since they additionally count as matter by today. Fig. 15 also reveals that at $m_a = 10^{-26}$ eV, rather than an upper limit on the axion density, BOSS data alone disfavour no axions at $\sim 2.7\sigma$ significance; we discuss this in more detail below (see Fig. 18 and surrounding discussion).

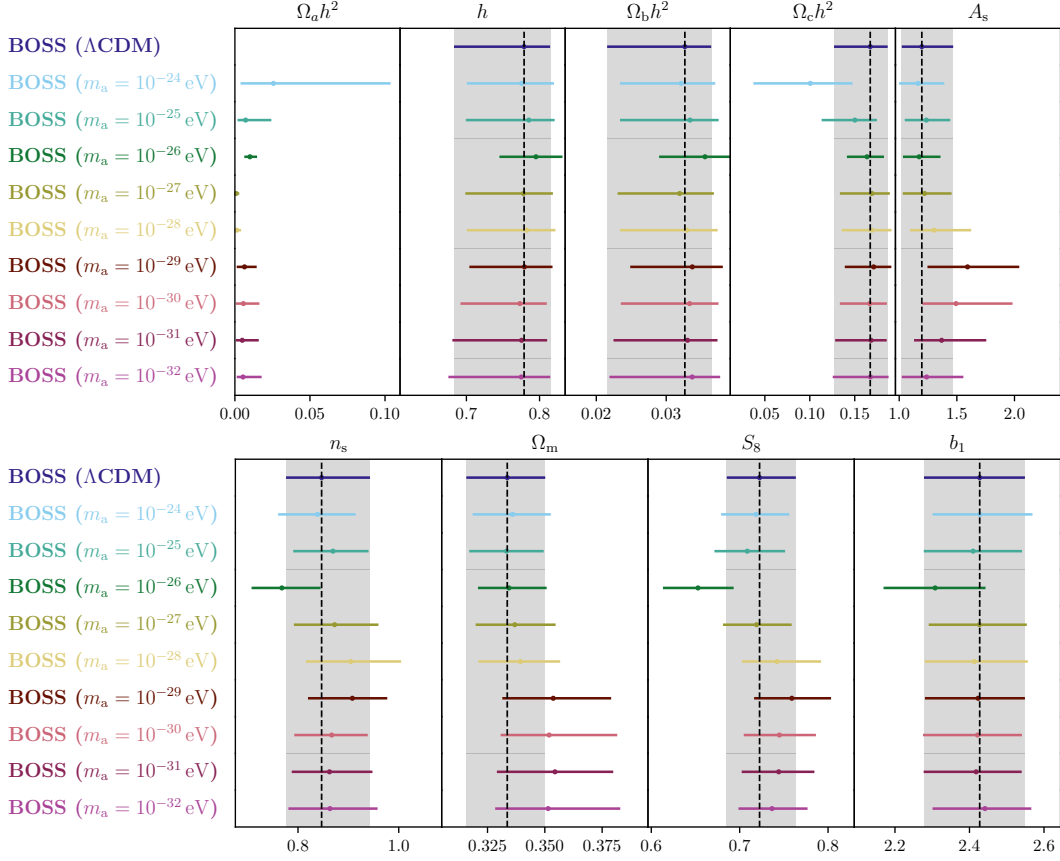


Figure 15. The effect of axion mass m_a on cosmological parameter constraints from BOSS galaxy clustering data. We stress that even the Λ CDM constraints differ from those reported in Ref. [56] as, in this work, we do not use a Big Bang nucleosynthesis (BBN) prior on the baryon energy density $\Omega_b h^2$. Each point indicates the marginalised mean, while the errorbar indicates the marginalised 68% c.l. A_s is in units of 10^{-9} ; b_1 is the linear galaxy bias at $z = 0.61$ in the north Galactic cap (NGC; similar values are found in all four redshift/sky samples).

4.2.4 Joint *Planck* and BOSS axion constraints

In Fig. 16, we show the joint constraint from *Planck* and the BOSS galaxy power spectrum on axions for $m_a = 10^{-25}$ eV. The strongest limit on the axion energy density comes from combining the datasets. Since *Planck* is significantly more constraining than BOSS alone on Λ CDM parameters, the joint constraint on those parameters is largely driven by *Planck* (see also Fig. 17). BOSS (and galaxy clustering data in general) are constraining on a degenerate combination $b_1 S_8$ of the power spectrum amplitude S_8 and the linear galaxy bias b_1 , since this combination scales the large-scale galaxy power spectrum (see § 2.2; although this degeneracy is partly broken by the quadrupole’s sensitivity to $f\sigma_8$, where f is the growth rate). It follows that, in the joint constraint, since *Planck* drives higher values of the power spectrum amplitude (even in the presence of axions) that a good fit to BOSS data is maintained by preferring a lower value of b_1 . This is illustrated in Fig. 16, where the joint constraint on b_1 is lower than for BOSS alone (moving along the $b_1 S_8$ degeneracy), but still has a value $b_1 \sim 2$ that is consistent with previous findings. This behaviour is observed at other axion masses and in the Λ CDM case (see Fig. 17).

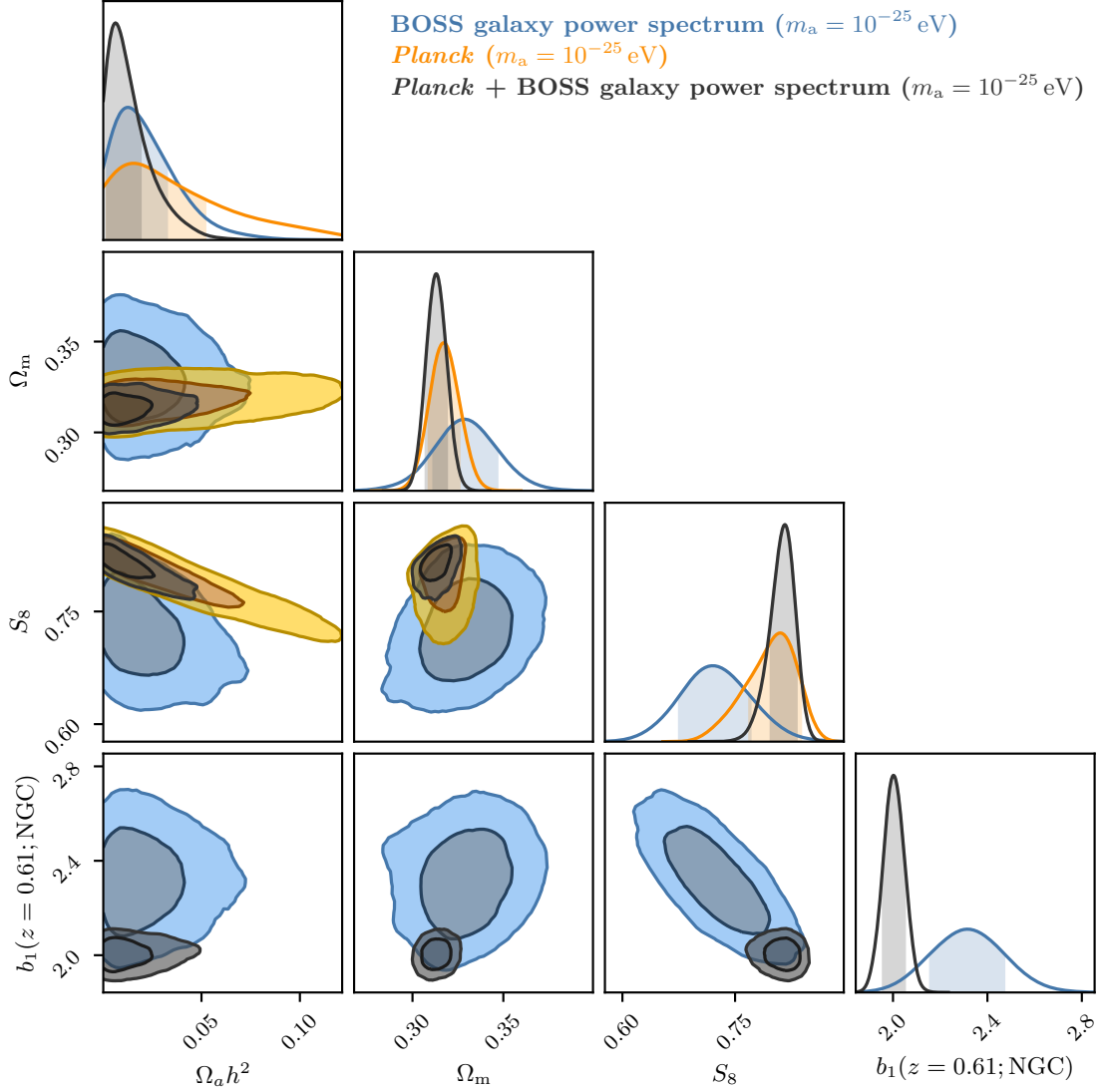


Figure 16. Comparison of BOSS galaxy power spectrum (*blue*), *Planck* CMB (*orange*) and joint (*black*) constraints on axion and cosmological parameters, for axion mass $m_a = 10^{-25}$ eV. The strongest bound on the axion energy density $\Omega_a h^2$ comes from combining the datasets; in order to maintain a good fit to the galaxy data in the joint constraint, lower (though still physically plausible) values of the linear galaxy bias b_1 are preferred. For each set, the darker and lighter shaded contours respectively indicate the 68% and 95% credible regions of the 2D marginalised posterior distribution, with the 1D marginalised posteriors on the diagonal, where 68% credible regions are shaded. *From left to right*, $\Omega_a h^2$ is the physical axion energy density, Ω_m is the matter energy density, S_8 is the matter clumping factor and $b_1(z = 0.61; \text{NGC})$ is the linear galaxy bias at redshift $z = 0.61$ in the north Galactic cap (NGC; similar values are found in all four redshift/sky samples).

Figure 6 shows the joint limit from *Planck* and BOSS on the axion energy density across the full axion mass range to which we are sensitive (10^{-32} eV $\leq m_a \leq 10^{-24}$ eV; see also Table 2). At nearly all masses, the strongest bound comes from combining the

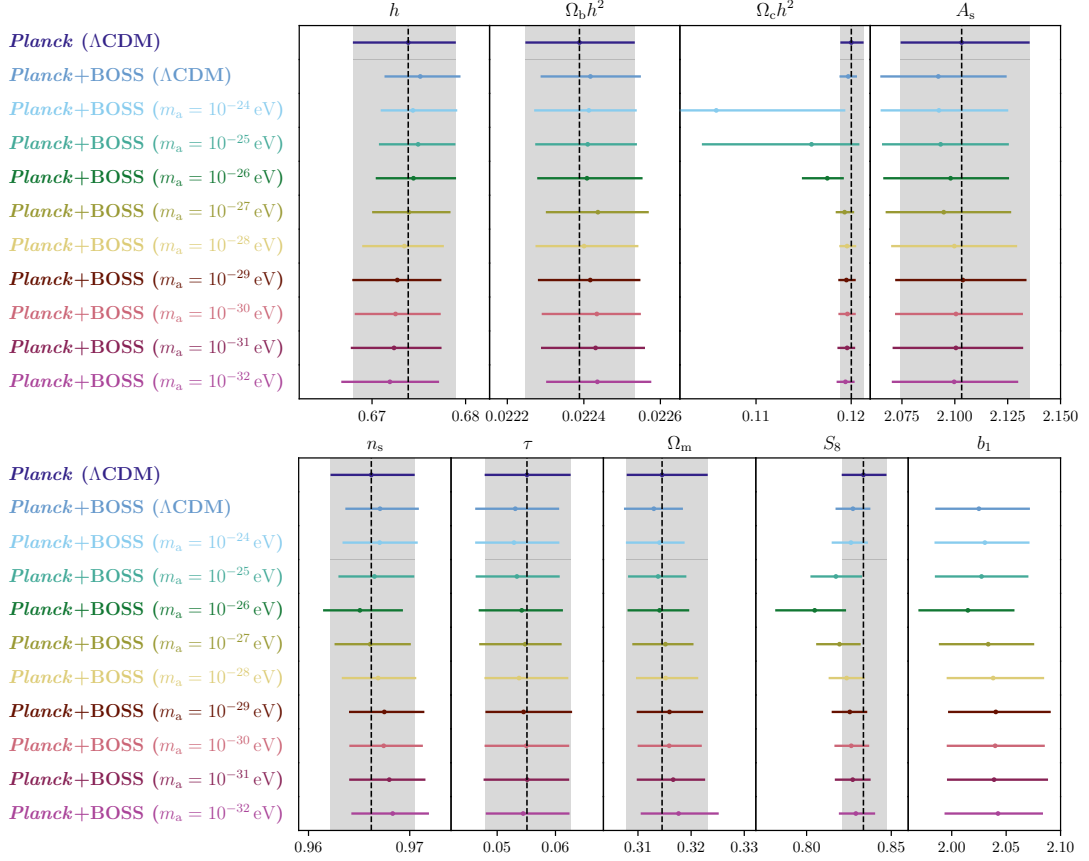


Figure 17. The effect of axion mass m_a on cosmological parameter constraints from the joint inference of *Planck* CMB and BOSS galaxy clustering data, and a comparison to the *Planck* Λ CDM inference. Since *Planck* is much more constraining than BOSS alone on Λ CDM cosmological parameters, the joint constraints on these parameters are broadly consistent with the *Planck* Λ CDM case. Each point indicates the marginalised mean, while the errorbar indicates the marginalised 68% c.l. A_s is in units of 10^{-9} ; b_1 is the linear galaxy bias at $z = 0.61$ in the north Galactic cap (NGC; similar values are found in all four redshift/sky samples). The $\Omega_c h^2$ constraint at $m_a = 10^{-24}$ eV extends to 0.05; we zoom-in for clarity at other masses.

datasets. Fig. 17 shows the joint constraints on the other cosmological parameters and the linear galaxy bias. As discussed above (Fig. 16), since *Planck* is much more constraining on Λ CDM parameters, the joint *Planck* + BOSS constraints on these parameters is largely driven by *Planck*. Nonetheless, we note the typical degeneracy of $\Omega_a h^2$ with, for DE-like axions, lower values of h and higher values of Ω_m , and for DM-like axions, with lower values of $\Omega_c h^2$ (see also *Planck* data in § 4.1). BOSS, in general, strengthens the limit on the amount of axions. However, in the DM-like mass range to which we are sensitive (10^{-27} eV $\leq m_a \leq 10^{-25}$ eV), the joint bound leaves enough axions still to drive consistency with lower values of S_8 (see also Table 2). Below, we consider which parts of the BOSS data are most responsible for improving constraints (Fig. 19) and discuss further the implications of these results for the S_8 tension (Figs. 20 and 21). Similarly as for the CMB data considered in § 4.1, with the addition of BOSS data, there remains no preference for axion models according to the Bayesian evidence (see Table 3). The Bayes factors amount to evidence in favour of Λ CDM ranging from “positive” to “strong” [163].

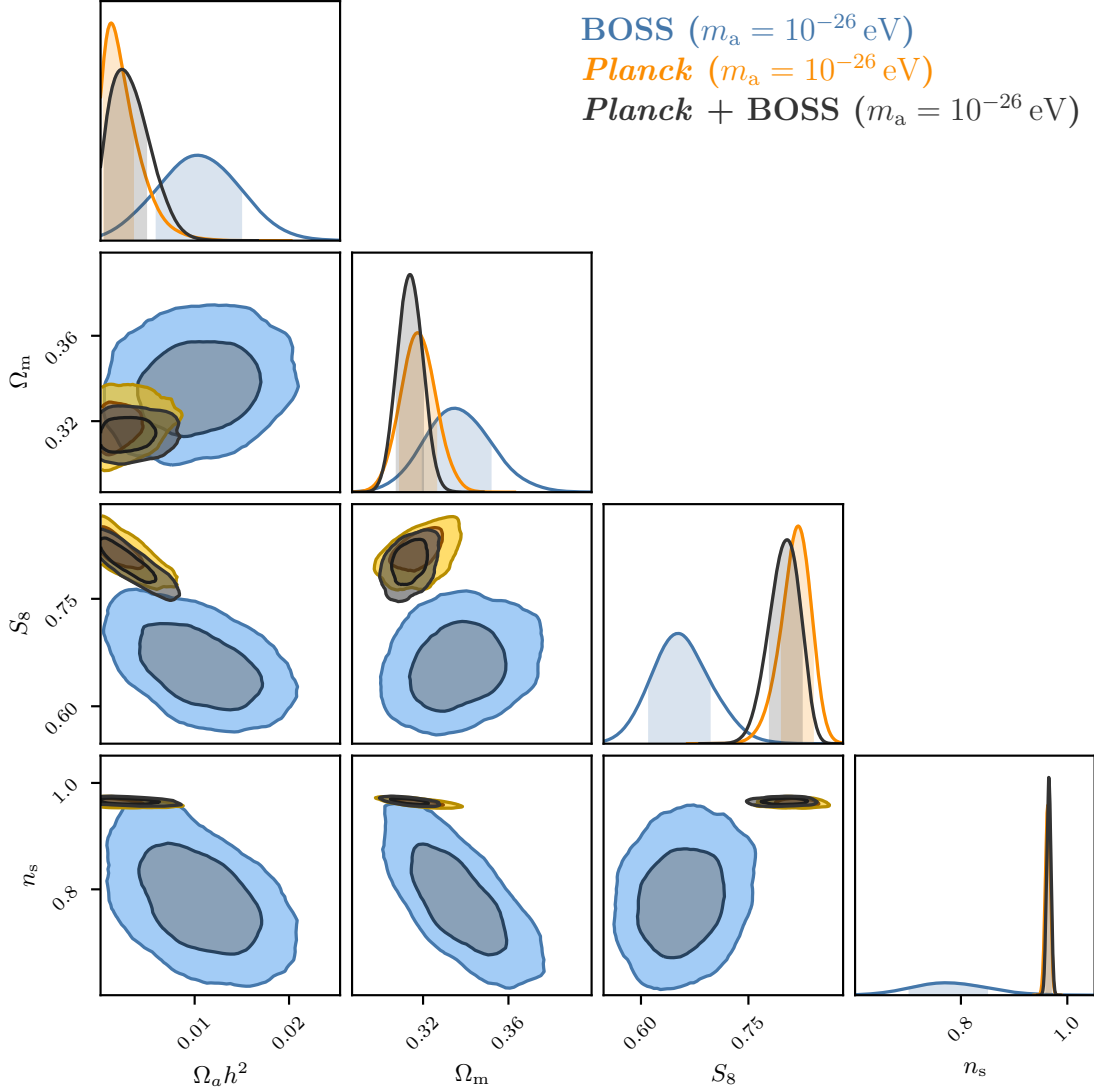


Figure 18. Comparison of BOSS galaxy clustering (all data; *blue*), *Planck* CMB (*orange*) and joint (*black*) constraints on axion and cosmological parameters, for axion mass $m_a = 10^{-26}$ eV. Although BOSS data give a hint of a significant axion energy density at this mass, *Planck* data disfavour this scenario. The consequence is that the joint axion constraint is weaker than for *Planck* data alone. However, we note that, unlike axions at other masses, axions with $m_a = 10^{-26}$ eV increase the discrepancy between *Planck* and BOSS data with respect to Λ CDM (see Table 5) and so the joint constraint should be considered with caution. For each set, the darker and lighter shaded contours respectively indicate the 68% and 95% credible regions of the 2D marginalised posterior distribution, with the 1D marginalised posteriors on the diagonal, where 68% credible regions are shaded. *From left to right*, $\Omega_a h^2$ is the physical axion energy density, Ω_m is the matter energy density, S_8 is the matter clumping factor and n_s is the primordial power spectrum tilt.

It is striking that the addition of BOSS data strengthens axion bounds at all masses apart from $m_a = 10^{-26}$ eV, where in fact the bound is weakened. Fig. 18 breaks down the constraint

at this mass into its constituent parts. While *Planck* alone sets a 95% credible upper limit $\Omega_a h^2 < 0.00615$, BOSS alone actually favours a contribution of axions $\Omega_a h^2 = 0.0100^{+0.0048}_{-0.0037}$, which excludes no axions at $\sim 2.7\sigma$ (the best-fit model with respect to BOSS data has a chi-squared reduced by $\Delta\chi^2 = -7.7$). This discrepancy in the axion constraint, however, increases the tension between all parameters inferred from *Planck* and BOSS, as seen in all three tension metrics shown in Table 5. In particular, the preference in BOSS data for axions of $m_a = 10^{-26}$ eV increases the discrepancy in S_8 from 2.70σ in the Λ CDM case to 3.63σ . This is because the power suppression of axions combines with the already-low value of A_s ($\Omega_a h^2$ and A_s are constrained from different parts of the galaxy power spectrum; see, e.g., Fig. 4) to lower further the power spectrum amplitude S_8 that is inferred from BOSS. For completeness, we show the joint constraint although we caution that it derives from two datasets that are in more discrepancy than in the Λ CDM case. As before, *Planck* dominates the constraint on Λ CDM parameters, while the joint limit on $\Omega_a h^2$ is slightly weaker than for *Planck* alone. Ref. [39] in their analysis of previous BOSS data do not report a preference for axions at this mass. There are a number of differences with respect to this study (summarised at the start of § 4.2). However, in particular, previously, the primordial power spectrum tilt was fixed: $n_s = 0.9611$. Fig. 18 illustrates that fixing n_s at this value will break degeneracy with $\Omega_a h^2$ such that the preference for a non-zero contribution is removed (this degeneracy with n_s in this mass range is also seen in *Planck* data; see Fig. 8)¹⁸. This preference for axions is not seen at any other mass. At all other masses, BOSS data strengthen the axion limit and also increase consistency between *Planck* and BOSS datasets (see Table 5). The fixed axion masses which we consider are arbitrary. Thus, this result means that there is a preference in BOSS data alone for a contribution of axions with a mass in a window $m_a \in [10^{-27}, 10^{-25}]$ eV, which motivates future work where we additionally sample m_a .

Notwithstanding $m_a = 10^{-26}$ eV, BOSS data otherwise always improve axion limits with respect to *Planck* alone, and axions improve consistency between the datasets. Fig. 19 illustrates which parts of the BOSS data are most constraining at $m_a = 10^{-25}$ eV. We systematically add different parts of the BOSS data to a joint constraint with *Planck*. We find that it is the addition of the small-scale reconstructed real-space galaxy power spectrum Q_0 for $0.2 h \text{ Mpc}^{-1} < k < 0.4 h \text{ Mpc}^{-1}$ which drives the vast majority of the improvement in the bound. This arises because the power suppression effect of axions is always stronger on smaller scales.

Figure 20 illustrates the degeneracy between $\Omega_a h^2$ and S_8 within the 95% credible upper limits on $\Omega_a h^2$ that are allowed by the joint analysis of *Planck* and BOSS. As we saw above, there is no such degeneracy for DE-like axions ($m_a < 10^{-28}$ eV) or for DM-like axions where the power suppression scale is too small ($m_a \geq 10^{-24}$ eV). In the mass window ($10^{-28} \text{ eV} \leq m_a \leq 10^{-25} \text{ eV}$) however, the joint constraint still allows enough axions to drive consistency with lower values of S_8 . Although more axions are allowed at higher masses (in the DM-like regime), since the suppression scale is smaller at higher mass, there is less total power suppression at the wavenumbers to which S_8 is sensitive. The lowest values of S_8 are in fact found at $m_a = 10^{-26}$ eV ($S_8 = 0.804^{+0.020}_{-0.024}$; see also Table 2 and Fig. 17). However we caution that this constraint arises from two datasets that are in stronger tension than the Λ CDM case.

¹⁸Using a Big Bang nucleosynthesis (BBN) prior on the baryon energy density $\Omega_b h^2 \sim \mathcal{N}(0.02268, 0.00038)$ [171] reduces the significance for an axion component at $m_a = 10^{-26}$ eV to 2.1σ ; further adding a *Planck*-motivated prior $n_s \sim \mathcal{N}(0.9649, 0.0042)$ [2] reduces the significance to 1.7σ . Weakening the prior on the EFT of LSS bias and counterterm parameters (see § 3.3 and 3.4) (by doubling the standard deviation in Gaussian prior distributions and doubling the width in uniform prior distributions) increases the significance to 3.2σ .

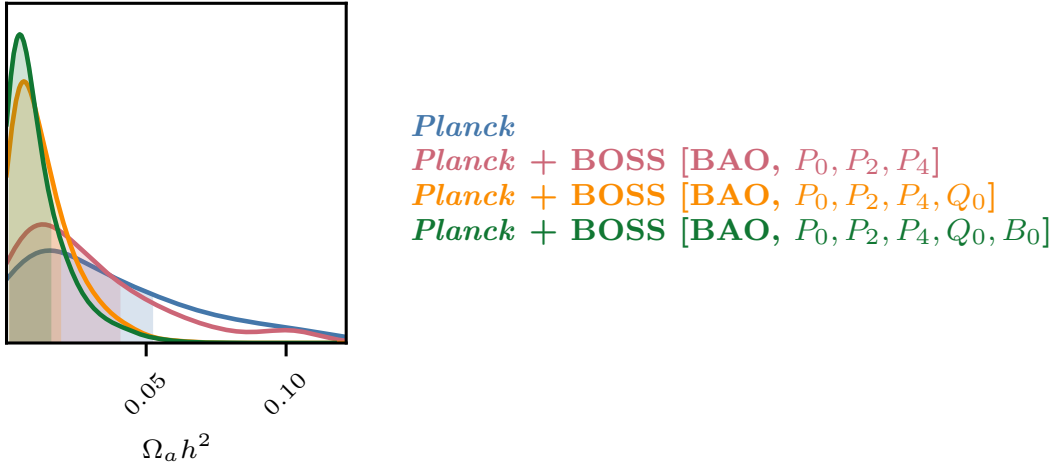


Figure 19. The effect of adding different parts of the BOSS galaxy clustering data on axion energy density $\Omega_a h^2$ constraints for $m_a = 10^{-25}$ eV. We systematically add to the *Planck* CMB likelihood (blue) different parts of the BOSS likelihood: first, BAO and power spectrum multipoles $[P_0, P_2, P_4]$ up to maximum wavenumber $k_{\text{max}} = 0.2 \, h \, \text{Mpc}^{-1}$ (red); then, also the reconstructed real-space power spectrum Q_0 for $k \in [0.2, 0.4] \, h \, \text{Mpc}^{-1}$ (orange); and finally, also the bispectrum monopole B_0 (green). We find that the vast majority of the improvement in the bound comes from the addition of smaller-scale information in the Q_0 likelihood, since the suppression effect of axions is stronger on smaller scales (see Fig. 4). For each data cut, we show the 1D marginalised posterior for $\Omega_a h^2$, where the 68% credible region is shaded.

Nonetheless, at $m_a = 10^{-25}$ eV ($S_8 = 0.818_{-0.017}^{+0.015}$) and $m_a = 10^{-27}$ eV ($S_8 = 0.819_{-0.014}^{+0.013}$), the parameter discrepancy between *Planck* and BOSS is reduced and the joint constraint on S_8 is shifted to lower values than the Λ CDM case ($S_8 = 0.827 \pm 0.011$). Fig. 21 updates Fig. 12 with the joint *Planck* + BOSS constraints (see § 4.1 for details about the DES and KiDS Λ CDM contours that we show). In comparison to Fig. 12, we note how the addition of BOSS data more strongly constrains the axion energy density and in turn reduces the extent to which low values of S_8 are allowed. Nonetheless, there remains a tail in the posterior to lower values of S_8 in the presence of axions with $m_a = 10^{-25}$ eV. Fully assessing the consistency with galaxy weak lensing experiments like DES and KiDS requires re-analysing these data in the axion models we consider here. We discuss the prospects for this in § 5.

5 Discussion

In § 4, we present several new results in searching for ultra-light axions in a compendium of CMB and large-scale structure data. In § 4.1, we present legacy constraints on the axion energy density from *Planck* 2018 CMB temperature, polarisation and lensing anisotropies. We find that, compared to previous *Planck* 2015 results [37], a new measurement of the optical depth to reionisation (through large-scale polarisation) breaks parameter degeneracies and improves energy density bounds for DE-like axions ($m_a \leq 10^{-28}$ eV; see Fig. 7). Further, we search for axions in a compendium of higher-resolution CMB data (ACT-DR4, SPT-3G), galaxy BAO and supernovae data. We find that the addition of these data marginally weakens the axion energy density bound for $m_a = 10^{-25}$ eV (see Table 4).

In § 4.2, we present axion constraints from BOSS galaxy clustering data. We find that the addition of BOSS to *Planck* improves axion energy density bounds at nearly all

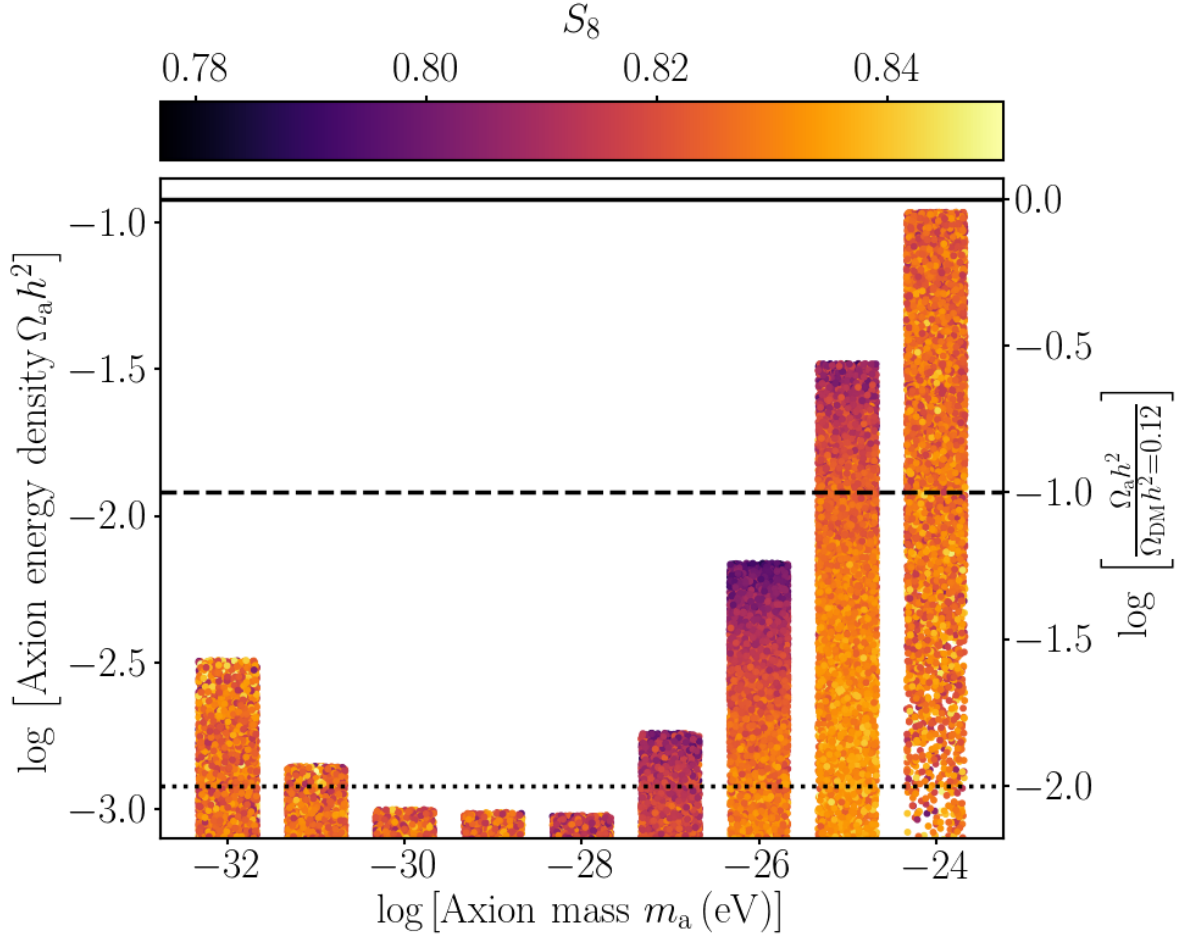


Figure 20. 95% credible upper limits on axion energy density $\Omega_a h^2$, as a function of axion mass m_a , as jointly inferred from *Planck* CMB and BOSS galaxy clustering data. We illustrate the degeneracy with the matter clumping factor S_8 by colouring (unweighted) posterior samples according to their S_8 value. The lowest values of S_8 are allowed for dark matter-like axions with $m_a \in [10^{-27}, 10^{-25}]$ eV. On the right-hand side, we show the 95% upper limit on the ratio of the axion energy density to the best-fit dark matter (DM) energy density as inferred from *Planck* $\Omega_{\text{DM}} h^2 = 0.12$.

axion masses that we consider ($10^{-32} \text{ eV} \leq m_a \leq 10^{-25} \text{ eV}$). Crucially, we find that the inclusion of new small-scale modes (Q_0 for $k \in [0.2, 0.4] h \text{ Mpc}^{-1}$) strengthens the constraint at $m_a = 10^{-25} \text{ eV}$ with respect to *Planck* only (see Fig. 19). This is driven by gaining sensitivity to larger wavenumbers where the power suppression of heavier axions manifests. Gains in sensitivity from BOSS data to lighter, DE-like axions ($m_a \leq 10^{-28} \text{ eV}$) are limited by degeneracy between $\Omega_a h^2$ and A_s at those masses. This arises since the axion-induced power suppression occurs at wavenumbers smaller than we model in BOSS data and so the axion effect is degenerate with an overall re-scaling of the galaxy power spectrum amplitude (e.g., see Fig. 15). This suggests that robustly modelling larger-volume galaxy surveys can improve sensitivity to DE-like axions. Robustly modelling smaller-scale correlations in galaxy positions will be extremely challenging owing to the non-trivial way that galaxies trace dark matter on small scales (i.e., non-linear galaxy bias). We therefore suggest alternative probes like galaxy and CMB weak lensing (that are insensitive to galaxy bias) to increase sensitivity

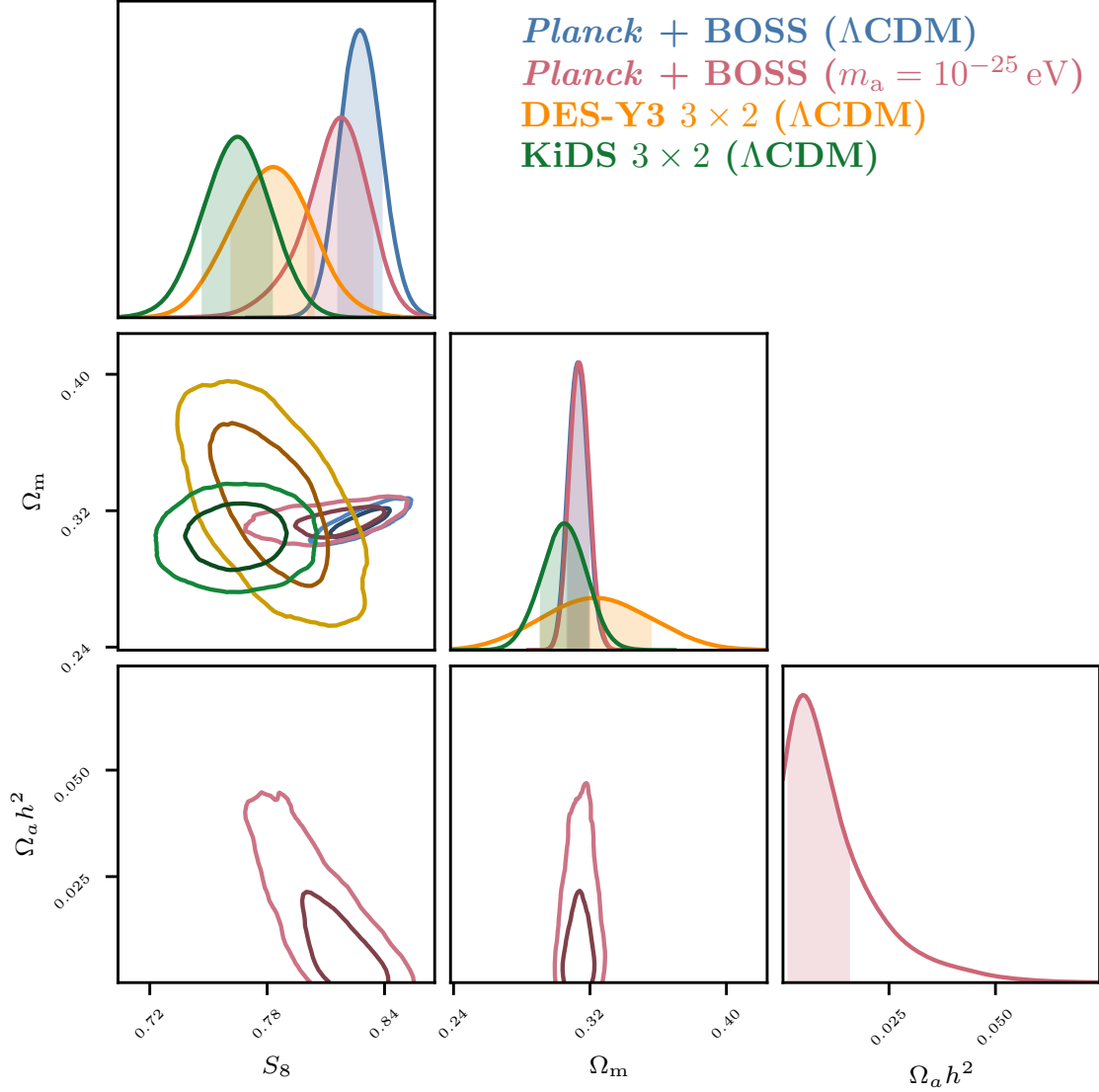


Figure 21. Comparison of joint *Planck* CMB and BOSS galaxy clustering constraints (in both axion and Λ CDM models) with fiducial galaxy weak lensing and clustering (3×2) Λ CDM constraints from the Dark Energy Survey (DES) and the Kilo-Degree Survey (KiDS) (all with fixed neutrino mass). *Planck* and BOSS data are consistent with lower values of S_8 in the presence of axions with mass $m_a = 10^{-25}$ eV compared to the Λ CDM case. In order to assess consistency between all data in an axion model, it is necessary to re-analyse the 3×2 data in the presence of axions; we discuss the future analysis of cosmic shear data in § 5. We note caution in assessing parameter tension by eye, especially as the *Planck* + BOSS and KiDS datasets are not independent, since KiDS uses BOSS clustering information in their 3×2 measurement. For each set, the inner and outer contours respectively indicate the 68% and 95% credible regions of the 2D marginalised posterior distribution, with the 1D marginalised posteriors on the diagonal, where 68% credible regions are shaded. *From left to right*, S_8 is the matter clumping factor, Ω_m is the matter energy density and $\Omega_a h^2$ is the physical axion energy density.

at $m_a \geq 10^{-24}$ eV (see above and below for more discussion about probes complementary to galaxy correlations). Nonetheless, our results demonstrate the power in combining CMB and large-scale structure data when constraining dark matter models beyond standard CDM.

5.1 Comparison to previous work

There are a number of differences between this study and a previous BOSS analysis presented in Ref. [39]. First, as discussed above, we model more of the BOSS data, in particular, additionally, the galaxy power spectrum hexadecapole P_4 , the small-scale real-space galaxy power spectrum Q_0 (where we conservatively project away hard-to-model non-linear redshift-space distortions) and the galaxy bispectrum monopole B_0 . Further, we choose less informative priors on cosmological parameters, i.e., we do not use BBN information to place a prior on the baryon energy density $\Omega_b h^2$ and, importantly, we do not fix the primordial power spectrum tilt n_s . The latter is important as we do in general observe degeneracy between $\Omega_a h^2$ and n_s (e.g., see Fig. 15) and this degeneracy will be broken by fixing n_s . We thus find that our bounds from BOSS alone are weaker than those reported in Ref. [39]. Ref. [39] combined *Planck* and BOSS through a *Planck*-motivated prior on cosmological and axion parameters (except n_s which remained fixed) combined with the BOSS likelihood. Instead, in this work, for the first time, we jointly sample the *Planck* and BOSS likelihoods in a full axion and cosmological model in setting axion constraints. We find in general that our combined constraints are stronger than those reported in Ref. [39]. We attribute a large degree of this to the information gained by updating to *Planck* 2018 data (*Planck* 2015 data was previously considered) for low masses (see above) and using the small-scale Q_0 statistic for higher masses. The results in Ref. [39] are affected by an error in the BOSS data weights, which has since been corrected and does not affect the results presented here.

There are further pipeline differences between the two analyses. In particular, beyond the different and more complete compression of the BOSS data discussed above, we use different implementations of the BOSS likelihood and EFT of LSS theory calculations (namely, `CLASS-PT/full_shape_likelihoolds` and, previously, `PyBird`) and, correspondingly, different EFT of LSS parameter priors (namely, so-called “East Coast” and, previously, “West Coast” priors). In general, the different prior choices will lead to differences in parameter inference given the same set of BOSS data (in Λ CDM, the cosmological constraints are consistent within $\sim 1\sigma$; see Ref. [158]). Importantly, Refs. [157] and [158] demonstrated that, with external CMB information from *Planck*, the prior sensitivity is significantly reduced, while future larger-volume galaxy surveys will have sufficient constraining power also to lose prior sensitivity. We defer to future work a detailed study of the effect of EFT of LSS priors on BOSS axion constraints since, in this work, it is non-trivial to disentangle the other analysis differences.

5.2 $m_a = 10^{-26}$ eV

A striking difference between this work and Ref. [39] is the axion constraint at $m_a = 10^{-26}$ eV. Unlike at other axion masses that we consider, at $m_a = 10^{-26}$ eV, rather than setting an upper limit on the axion energy density, we find, given BOSS data only, $\Omega_a h^2 = 0.0100^{+0.0048}_{-0.0037}$ that excludes no axions at $\sim 2.7\sigma$ significance. However, such a large contribution of axions at this mass is disfavoured by *Planck* ($\Omega_a h^2 < 0.00615$) and so the tension in parameter inference between these datasets is increased at this axion mass with respect to Λ CDM (at all other masses, the tension is reduced; see more discussion below). For completeness, we consider the joint constraint (which is thus weaker than *Planck* alone) although we caution that this

derives from two datasets in greater discrepancy than in the standard CDM model. We find that the preference for axions at this mass opens up degeneracy with other cosmological parameters, in particular n_s and b_1 (although in an opposite sense as at other masses; e.g., see Figs. 15 and 18). This explains why this preference was not observed in Ref. [39] where n_s was fixed; indeed, when giving a BBN prior on $\Omega_b h^2$ and a *Planck* prior on n_s , the significance of the axion preference is reduced to only 1.7σ . Further, if an inflation-motivated prior that excluded low values of n_s was imposed, we anticipate that the significance would also be reduced.

The anomalous (with respect to other masses) degeneracy between higher $\Omega_a h^2$ and lower n_s and b_1 suggests an effect from marginalisation over other EFT of LSS parameters; indeed, weakening the prior on EFT of LSS bias and counterterm parameters increases the axion preference to 3.2σ . As discussed in § 3.3, in order to reduce the dimensions of the sampling task, we analytically marginalise over a number of bias and counterterm parameters. We therefore leave for future work a detailed study of the effect of nuisance parameter marginalisation by numerically sampling the full joint cosmological and EFT of LSS posterior distribution. We stress, nonetheless, owing to the way that we consider axion masses only at a number of fixed values, that there is an element of the look-elsewhere effect where it is not surprising to find one of the nine axion masses has a mild preference unlike the others. Future galaxy data (e.g., from the Dark Energy Spectroscopic Instrument [172] or the *Rubin* Observatory [173]) will be crucial in determining if this preference is only a statistical anomaly or otherwise. Reconciliation with the *Planck* bound may be connected to the A_L anomaly. As discussed above, we find that CMB datasets with lower (and theoretically-consistent) amounts of lensing weaken axion bounds and so we hypothesise that the A_L anomaly in *Planck* is strengthening the bound and increasing the discrepancy with BOSS at $m_a = 10^{-26}$ eV. We will investigate this hypothesis in future work.

5.3 Comparison to other axion probes and future prospects

Notwithstanding the mild preference for axions at $m_a = 10^{-26}$ eV given BOSS data only, our *Planck* and joint *Planck* and BOSS analyses set strong limits on the axion energy density for $m_a \leq 10^{-25}$ eV. Axions are well-motivated in a range of particle masses and can be produced in a mixture with other axions (the so-called “axiverse” [e.g., 22]) and/or with other DM and DE particle candidates. This motivates a search for axions across a wide range of masses and for sub-dominant energy densities so that an axion of a particular mass is not prematurely excluded by assuming that it constitutes the entirety of the DM or DE. Fig. 22¹⁹ compares our new bounds for $m_a \leq 10^{-25}$ eV to other cosmological bounds across the mass range where the gravitational effect of axions is distinguishable in the large-scale structure from standard cold DM (10^{-32} eV $\leq m_a \leq 10^{-18}$ eV)²⁰. The details of each experiment and current and projected bounds are given in the caption. We stress that, to probe across the parameter space, it is necessary to use complementary probes of large- and small-scale structure to search for, respectively, lighter and heavier axions. We anticipate progress in this regard from ongoing, upcoming and proposed CMB (e.g., ACT, SPT, Simons Observatory, CMB-S4 [176], CMB-HD), large-scale structure (e.g., *Rubin*, DESI), intensity mapping (e.g., SKA) and pulsar timing array observations.

¹⁹An up-to-date version of Fig. 22 is maintained at https://keirkwame.github.io/DM_limits.

²⁰There are many ongoing and proposed experimental efforts to probe axions at and above this mass range; see Refs. [51, 52] for recent reviews; Fig. 22 shows only cosmological probes.

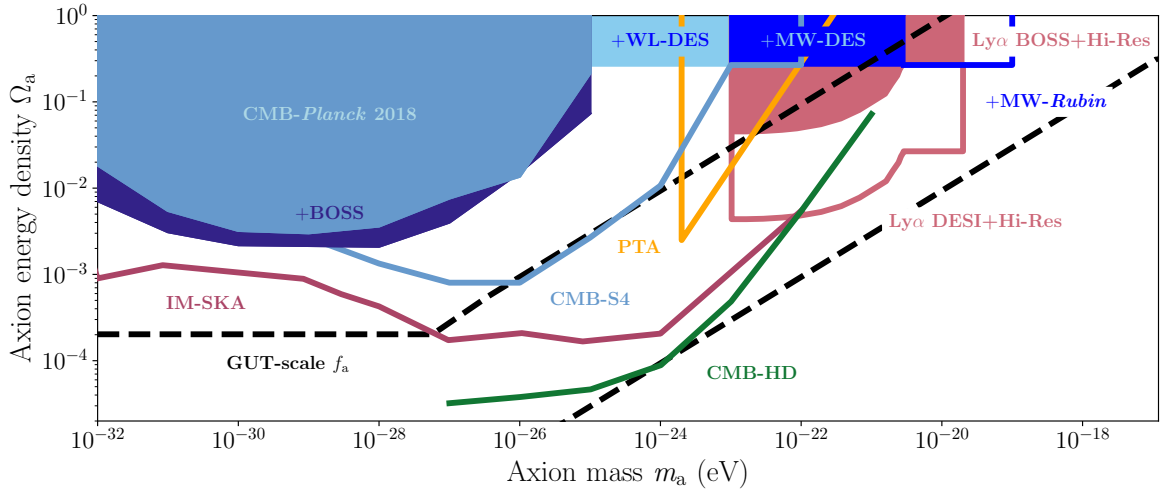


Figure 22. 95% c.l. axion energy density Ω_a bounds presented in this work from *Planck* 2018 CMB data (*top left*) and from a joint analysis of *Planck* CMB and BOSS galaxy clustering data (+BOSS) compared to other cosmological bounds (*shaded solid*) and projected bounds (*thick lines*). Our results are complementary to existing bounds at higher masses derived from probes of smaller-scale structure: a joint analysis of *Planck* CMB and galaxy weak lensing data from the Dark Energy Survey (+WL-DES) [40]; the Milky Way sub-halo mass function from DES (+MW-DES) [30]; the strongest lower limit for axions being all the DM ($m_a > 2 \times 10^{-20}$ eV) comes from high-resolution Lyman-alpha forest data (Ly α Hi-Res) [29, 32], while Ref. [43] considered a sub-dominant axion contribution (see also Ref. [44] for a BOSS Lyman-alpha forest analysis). We show projected bounds for: the CMB-S4 experiment [127]; the CMB-HD experiment using the Ostriker-Vishniac signal [38]; the *Rubin* Observatory using the MW sub-halo mass function [174]; future Lyman-alpha forest data from the Dark Energy Spectroscopic Instrument (DESI) and high-resolution quasar spectra (Hi-Res) [175]; intensity mapping from the Square Kilometre Array (IM-SKA) [49]; and pulsar timing array (PTA) residuals [175]. We indicate (*between the black dotted lines*) the parameter space where the axion decay constant f_a is at the Grand Unified Theory (GUT) scale (see Eq. (2.2)). Where bounds exclude axions being all the DM, we additionally exclude higher energy densities (up to $\Omega_a = 1$) by enforcing that the Universe is not over-closed. The projections rely on different assumptions and have varying degrees of rigour and so are only indicative of future progress.

5.4 Axions as a resolution to the S_8 parameter tension

A key aim of this study is not only to search for axions as a DM and DE candidate, but also to consider the extent to which axions can improve consistency between CMB and large-scale structure datasets in their parameter inference, in particular with respect to the so-called S_8 tension. The cosmological parameter S_8 , through its dependence on the matter power spectrum amplitude σ_8 , is a measure of the clustering of matter at $z = 0$ when averaged over $8 h^{-1}$ Mpc scales. CMB experiments prefer higher values of S_8 than various large-scale structure analyses with statistical significance ranging from 2 to 3 σ depending on the data comparison [see e. g., 90, for a recent review]. Since CMB experiments generally probe structure at higher redshift (even CMB lensing is more sensitive to structure at earlier times than current galaxy surveys), most concrete model solutions to the S_8 tension invoke a redshift-dependent suppression in the growth of structure, e. g., decaying dark matter [e. g., 96, 98]. In this way, it is argued that this explains why probes of later-time structure have lower amplitude. In this work, we investigate the hypothesis that the S_8 tension is a discrepancy

between probes of larger- and smaller-scale structure, with axions as a concrete model, and with no need to invoke a late-time decay in the nature of DM.

Fig. 1 illustrates our hypothesis by showing how *Planck* CMB data lose sensitivity to small-scale modes to which S_8 is sensitive. It follows that it is possible to invoke a scale-dependent suppression in the matter power spectrum that is consistent with current CMB data on large scales, while lowering the value of S_8 to improve compatibility with galaxy surveys (in particular, galaxy weak lensing) as a more direct probe of the scales to which S_8 is sensitive. Indeed, we find (in § 4.1) axions with $m_a \in [10^{-28}, 10^{-25}]$ eV as a good candidate where they are compatible with a compendium of “large-scale” probes (CMB, galaxy BAO and supernovae) and the lower values of S_8 that are inferred from fiducial galaxy clustering and weak lensing (3×2) analyses (see Fig. 12). Lighter axions are largely incompatible with *Planck* data (except as a highly sub-dominant contribution that does little to S_8), while heavier axions are unconstrained by these data but suppress wavenumbers larger than those to which S_8 is sensitive.

In order to assess whether axions can resolve parameter tensions between CMB and large-scale structure data, it is necessary also to analyse large-scale structure data in an axion model. In § 4.2, we analyse BOSS galaxy clustering data and model the effect of axions in the mildly non-linear regime using the effective field theory of large-scale structure (see § 2.2 for details). We find two regimes in which the S_8 discrepancy between *Planck* and BOSS is reduced. The first is for $m_a \sim 10^{-25}$ eV, where, as discussed above, large axion contributions are unconstrained by CMB data and so bring CMB data into compatibility with lower values of S_8 : the S_8 discrepancy is reduced from 2.70σ in Λ CDM to 1.63σ . The second regime is for $m_a \sim 10^{-28}$ eV, where, instead, the effect of axions in BOSS data is partly degenerate with the overall amplitude of the galaxy power spectrum since all BOSS wavenumbers are suppressed by axions of this mass. This weakens BOSS constraints on the lightest axions, while allowing higher values of the primordial power spectrum amplitude A_s and also S_8 (the effects of higher A_s and higher $\Omega_a h^2$ not cancelling exactly). Thus, the S_8 discrepancy is reduced to 1.78σ , but, importantly, values of A_s (which are low in this BOSS analysis; see Ref. [158] for a discussion on the effect of EFT of LSS priors on cosmological parameter inference) are brought into greater compatibility with the higher values inferred from *Planck*.

Indeed, although S_8 is a reasonably good compression of the information contained in large-scale structure data (though not necessarily optimal for all experiments), it is necessary to assess tension in the full posterior, in particular accounting for non-Gaussianity in the distribution (which one-parameter tension metrics do not capture). In this work, in order better to capture tension in the full parameter space, we estimate the posterior distribution of the parameter difference [169] inferred given the two experiments (*Planck* and BOSS). If the two experiments are in perfect agreement, the parameter difference posterior will peak at zero; we assign the significance of the discrepancy between experiments to the amount of shift from perfect agreement (see § 4.2 for more details). We find that this measure of tension improves from Λ CDM at nearly all axion masses apart from $m_a = 10^{-26}$ eV (as discussed above). There is no single tension metric on which the community has converged; different metrics tend to disagree in terms of absolute value though they agree with regards to increasing or decreasing tension [see e.g., 170]. The metrics we use in this work (and quite generally) depend on the parameterisation of the model. Since S_8 and σ_8 may not be optimal measures of the matter clustering information directly probed by CMB and even many large-scale structure experiments, we defer to future work studies of the agreement

between datasets directly in the linear matter power spectrum using Bayesian metrics like the posterior predictive distribution.

Nonetheless, our results suggest that axions with masses in a window $[10^{-28}, 10^{-25}]$ eV can be a promising candidate to improve consistency between CMB and large-scale structure observations, in particular by bringing *Planck* CMB and BOSS galaxy clustering data into consistency with lower values of S_8 that are preferred by galaxy weak lensing data (see e.g., Figs. 20 and 21). We stress, though, that this is achieved through only upper limits on the axion energy density and there is no preference for model extensions beyond Λ CDM given these data according to the Bayesian evidence in any of our analysis (see Table 3). A more stringent test of the ability for axions to address cosmological parameter tension is the inclusion of galaxy weak lensing data. It is common in the literature to include the effect of weak lensing through a prior on S_8 derived from Λ CDM S_8 constraints, see e.g. [103, 177]. This is a good measure of the information content in the Λ CDM model, but we caution that this may not be the case in extended models like axions which affect in a non-trivial way the non-linear modes probed by galaxy shear (indeed, we see with BOSS how the S_8 constraint changes with axions). We therefore leave for future work an analysis of galaxy shear and 3×2 clustering and shear data using a fully non-linear halo model of axion structure formation [e.g., 74]. This will build on initial studies of DES cosmic shear in the limited case that axions comprise the entirety of the DM [40].

6 Conclusions

We present a comprehensive search for ultra-light axions as a well-motivated dark matter and dark energy particle candidate using a compendium of CMB and large-scale structure data. We set the strongest bounds to date on the axion energy density for axion masses $m_a \in [10^{-32}, 10^{-25}]$ eV through a joint analysis of *Planck* 2018 CMB and BOSS full-shape galaxy power spectrum and bispectrum data, modelling the effect of axions in the mildly non-linear regime using the effective field theory of large-scale structure. We exclude axions being more than 10% of the DM today for $m_a \leq 10^{-26}$ eV and more than 1% for $m_a \in [10^{-30}, 10^{-28}]$ eV. We give legacy constraints from *Planck* 2018 CMB data and find that measurements of the optical depth to reionisation break parameter degeneracies and improve bounds for DE-like axions ($m_a \leq 10^{-28}$ eV). For the first time, we consider high-resolution CMB data from the Atacama Cosmology Telescope and the South Pole Telescope (in combination with galaxy BAO and supernovae data), which we find to weaken marginally axion bounds at $m_a = 10^{-25}$ eV. Similarly to the effect of massive neutrinos, we attribute this weakening to the lower (and theoretically-consistent) amounts of lensing observed in ACT and SPT angular power spectra, which allow more structure suppression arising from axions. In the first full joint analysis of *Planck* 2018 and BOSS full-shape data, we find that galaxy clustering information strengthens axion energy density limits at nearly all masses that we consider. The exception is at $m_a = 10^{-26}$ eV, where BOSS data alone have a mild preference for a non-zero axion contribution, excluding no axions at $\sim 2.7\sigma$. The significance is reduced to only 1.7σ when including Big Bang nucleosynthesis constraints on the baryon energy density $\Omega_b h^2$ and *Planck* constraints on the primordial power spectrum tilt n_s . Such an axion contribution is, further, disfavoured by *Planck* and we caution that the look-elsewhere effect applies owing to the large number of axion masses that we consider. Future galaxy data (e.g., DESI, *Rubin*) will be crucial in assessing the significance of this result.

We propose axions as a candidate to address the so-called “ S_8 tension”, where CMB experiments infer systematically higher values of S_8 (which is sensitive to the matter power spectrum amplitude at $z = 0$) than various large-scale structure datasets, with significance ranging from 2 to 3 σ [e.g., 90]. We hypothesise that the scale-dependent power spectrum suppression (relative to standard cold DM) arising from axion DM can reconcile current CMB data (which probe larger scales and prefer higher amplitude) with the more direct probes of smaller-scale structure in galaxy clustering and weak lensing that prefer lower amplitude. We indeed find that a compendium of “large-scale” data (CMB, galaxy BAO and supernovae) are compatible with lower values of $S_8 = 0.774^{+0.032}_{-0.037}$ for $m_a = 10^{-25}$ eV than in Λ CDM ($S_8 = 0.827 \pm 0.010$). This is achieved since this data combination is not sensitive to the small-scale suppression arising from axions of this mass, while the axion suppression still occurs at wavenumbers to which S_8 is sensitive, thus lowering its value. Although BOSS full-shape data, in general, strengthen axion density bounds (apart from at $m_a = 10^{-26}$ eV), we find that axions can improve inferred parameter consistency between *Planck* and BOSS and that the joint *Planck* and BOSS constraint is still consistent with lower values of S_8 than Λ CDM in a window of masses $[10^{-28}, 10^{-25}]$ eV. In future work, we will assess consistency with upcoming CMB and galaxy weak lensing data using a fully non-linear (halo) model of axion structure formation [e.g., 40, 74].

Acknowledgments

The authors thank Daniel Grin for valuable discussions. The Dunlap Institute is funded through an endowment established by the David Dunlap family and the University of Toronto. RH is a CIFAR Azrieli Global Scholar (Gravity & the Extreme Universe Program 2019) and a 2020 Alfred P. Sloan Research Fellow; and is supported by the Natural Sciences and Engineering Research Council of Canada Discovery Grant Program and the Connaught Fund. MMI is supported by the National Aeronautics and Space Administration (NASA) through the NASA Hubble Fellowship grant #HST-HF2-51483.001-A awarded by the Space Telescope Science Institute, which is operated by the Association of Universities for Research in Astronomy, Incorporated, under NASA contract NAS5-26555. OHEP is a Junior Fellow of the Simons Society of Fellows and thanks the Institute for Advanced Study for their hospitality and abundance of baked goods. KA is supported by Japan Society for the Promotion of Science (JSPS) Overseas Research Fellowships. DJEM is supported by an Ernest Rutherford Fellowship from the Science and Technologies Facilities Council (ST/T004037/1).

References

- [1] D. Brout, D. Scolnic, B. Popovic, A. G. Riess, A. Carr, J. Zuntz et al., *The Pantheon+ Analysis: Cosmological Constraints*, [ApJ **938** \(2022\) 110 \[2202.04077\]](#).
- [2] Planck Collaboration, N. Aghanim, Y. Akrami, M. Ashdown, J. Aumont, C. Baccigalupi et al., *Planck 2018 results. VI. Cosmological parameters*, [A&A **641** \(2020\) A6 \[1807.06209\]](#).
- [3] C. L. Bennett, D. Larson, J. L. Weiland, N. Jarosik, G. Hinshaw, N. Odegard et al., *Nine-year Wilkinson Microwave Anisotropy Probe (WMAP) Observations: Final Maps and Results*, [ApJS **208** \(2013\) 20 \[1212.5225\]](#).
- [4] Z. Hou, C. L. Reichardt, K. T. Story, B. Follin, R. Keisler, K. A. Aird et al., *Constraints on Cosmology from the Cosmic Microwave Background Power Spectrum of the 2500 deg² SPT-SZ Survey*, [ApJ **782** \(2014\) 74 \[1212.6267\]](#).

- [5] M. S. Madhavacheril, N. Sehgal and T. R. Slatyer, *Current dark matter annihilation constraints from CMB and low-redshift data*, *Phys. Rev. D* **89** (2014) 103508 [[1310.3815](#)].
- [6] J. L. Sievers, R. A. Hlozek, M. R. Nolta, V. Acquaviva, G. E. Addison, P. A. R. Ade et al., *The Atacama Cosmology Telescope: cosmological parameters from three seasons of data*, *J. Cosmology Astropart. Phys.* **2013** (2013) 060 [[1301.0824](#)].
- [7] M. B. Wise, H. Georgi and S. L. Glashow, *SU(5) and the Invisible Axion*, *Phys. Rev. Lett.* **47** (1981) 402.
- [8] M. Dine, W. Fischler and M. Srednicki, *A simple solution to the strong CP problem with a harmless axion*, *Physics Letters B* **104** (1981) 199.
- [9] M. Dine, *Axions: Visible and Invisible*, in *Novel Results in Particle Physics - 1982: Fifth International Conference on Particle Physics*, vol. 93 of *American Institute of Physics Conference Series*, pp. 66–76, Nov., 1982, [DOI](#).
- [10] M. Dine and W. Fischler, *The Not So Harmless Axion*, *Phys. Lett. B* **120** (1983) 137.
- [11] L. F. Abbott, *Axion Cosmology*, in *Relativity, Cosmology, Topological Mass and Supergravity; SILARG IV*, p. 100, Jan., 1983.
- [12] J. Preskill, M. B. Wise and F. Wilczek, *Cosmology of the invisible axion*, *Physics Letters B* **120** (1983) 127.
- [13] P. J. Steinhardt and M. S. Turner, *Saving the invisible axion*, *Phys. Lett. B* **129** (1983) 51.
- [14] J. E. Kim, *Light pseudoscalars, particle physics and cosmology.*, *Phys. Rep.* **150** (1987) 1.
- [15] Z. G. Berezhiani, A. S. Sakharov and M. Y. Khlopov, *Primordial background of cosmological axions.*, *Soviet Journal of Nuclear Physics* **55** (1992) 1063.
- [16] R. Peccei and H. R. Quinn, *CP Conservation in the Presence of Instantons*, *Phys. Rev. Lett.* **38** (1977) 1440.
- [17] S. Weinberg, *A New Light Boson?*, *Phys. Rev. Lett.* **40** (1978) 223.
- [18] F. Wilczek, *Problem of Strong p and t Invariance in the Presence of Instantons*, *Phys. Rev. Lett.* **40** (1978) 279.
- [19] E. Witten, *Some properties of O(32) superstrings*, *Physics Letters B* **149** (1984) 351.
- [20] P. Svrcek and E. Witten, *Axions In String Theory*, *JHEP* **06** (2006) 051 [[hep-th/0605206](#)].
- [21] S. Weinberg, *A new light boson?*, *Phys. Rev. Lett.* **40** (1978) 223.
- [22] A. Arvanitaki, S. Dimopoulos, S. Dubovsky, N. Kaloper and J. March-Russell, *String Axiverse*, *Phys. Rev. D* **81** (2010) 123530 [[0905.4720](#)].
- [23] R. Hlozek, D. Grin, D. J. E. Marsh and P. G. Ferreira, *A search for ultralight axions using precision cosmological data*, *Phys. Rev. D* **91** (2015) 103512 [[1410.2896](#)].
- [24] J. S. Bullock and M. Boylan-Kolchin, *Small-Scale Challenges to the Λ CDM Paradigm*, *ARA&A* **55** (2017) 343 [[1707.04256](#)].
- [25] D. H. Weinberg, J. S. Bullock, F. Governato, R. Kuzio de Naray and A. H. G. Peter, *Cold dark matter: Controversies on small scales*, *Proceedings of the National Academy of Science* **112** (2015) 12249 [[1306.0913](#)].
- [26] L. Hui, J. P. Ostriker, S. Tremaine and E. Witten, *Ultralight scalars as cosmological dark matter*, *Phys. Rev. D* **95** (2017) 043541 [[1610.08297](#)].
- [27] A. Pontzen and F. Governato, *Cold dark matter heats up*, *Nature* **506** (2014) 171 [[1402.1764](#)].
- [28] A. Drlica-Wagner, K. Bechtol, S. Mau, M. McNanna, E. O. Nadler, A. B. Pace et al., *Milky Way Satellite Census. I. The Observational Selection Function for Milky Way Satellites in DES Y3 and Pan-STARRS DR1*, *ApJ* **893** (2020) 47 [[1912.03302](#)].

- [29] K. K. Rogers and H. V. Peiris, *Strong Bound on Canonical Ultralight Axion Dark Matter from the Lyman-Alpha Forest*, *Phys. Rev. Lett.* **126** (2021) 071302 [[2007.12705](#)].
- [30] E. O. Nadler, A. Drlica-Wagner, K. Bechtol, S. Mau, R. H. Wechsler, V. Gluscevic et al., *Constraints on Dark Matter Properties from Observations of Milky Way Satellite Galaxies*, *Phys. Rev. Lett.* **126** (2021) 091101 [[2008.00022](#)].
- [31] A. Laguë, J. R. Bond, R. Hložek, D. J. E. Marsh and L. Söding, *Evolving ultralight scalars into non-linearity with Lagrangian perturbation theory*, *MNRAS* **504** (2021) 2391 [[2004.08482](#)].
- [32] K. K. Rogers and H. V. Peiris, *General framework for cosmological dark matter bounds using N -body simulations*, *Phys. Rev. D* **103** (2021) 043526 [[2007.13751](#)].
- [33] T. Dome, A. Fialkov, P. Mocz, B. M. Schäfer, M. Boylan-Kolchin and M. Vogelsberger, *On the Cosmic Web Elongation in Fuzzy Dark Matter Cosmologies*, *arXiv e-prints* (2022) arXiv:2208.03827 [[2208.03827](#)].
- [34] S. May and V. Springel, *The halo mass function and filaments in full cosmological simulations with fuzzy dark matter*, *arXiv e-prints* (2022) arXiv:2209.14886 [[2209.14886](#)].
- [35] M. Nori, A. V. Macciò and M. Baldi, *Fuzzy Aquarius: evolution of a Milky-way like system in the Fuzzy Dark Matter scenario*, *arXiv e-prints* (2022) arXiv:2210.08022 [[2210.08022](#)].
- [36] S. M. L. Vogt, D. J. E. Marsh and A. Laguë, *Improved Mixed Dark Matter Halo Model for Ultralight Axions*, *arXiv e-prints* (2022) arXiv:2209.13445 [[2209.13445](#)].
- [37] R. Hložek, D. J. E. Marsh and D. Grin, *Using the full power of the cosmic microwave background to probe axion dark matter*, *MNRAS* **476** (2018) 3063 [[1708.05681](#)].
- [38] G. S. Farren, D. Grin, A. H. Jaffe, R. Hložek and D. J. Marsh, *Ultralight axions and the kinetic sunyaev-zel'dovich effect*, *Physical Review D* **105** (2022) .
- [39] A. Laguë, J. R. Bond, R. Hložek, K. K. Rogers, D. J. E. Marsh and D. Grin, *Constraining ultralight axions with galaxy surveys*, *J. Cosmology Astropart. Phys.* **2022** (2022) 049 [[2104.07802](#)].
- [40] M. Dentler, D. J. E. Marsh, R. Hložek, A. Laguë, K. K. Rogers and D. Grin, *Fuzzy dark matter and the Dark Energy Survey Year 1 data*, *MNRAS* **515** (2022) 5646 [[2111.01199](#)].
- [41] A. Kunkel, T. Chiueh and B. M. Schäfer, *A weak lensing perspective on nonlinear structure formation with fuzzy dark matter*, *arXiv e-prints* (2022) arXiv:2211.01523 [[2211.01523](#)].
- [42] V. Iršič, M. Viel, M. G. Haehnelt, J. S. Bolton and G. D. Becker, *First constraints on fuzzy dark matter from Lyman- α forest data and hydrodynamical simulations*, *ArXiv e-prints* (2017) [[1703.04683](#)].
- [43] T. Kobayashi, R. Murgia, A. De Simone, V. Iršič and M. Viel, *Lyman-alpha Constraints on Ultralight Scalar Dark Matter: Implications for the Early and Late Universe*, *ArXiv e-prints* (2017) [[1708.00015](#)].
- [44] E. Armengaud, N. Palanque-Delabrouille, C. Yèche, D. J. E. Marsh and J. Baur, *Constraining the mass of light bosonic dark matter using SDSS Lyman- α forest*, *ArXiv e-prints* (2017) [[1703.09126](#)].
- [45] J. Baur, N. Palanque-Delabrouille, C. Yèche, C. Magneville and M. Viel, *Lyman-alpha forests cool warm dark matter*, *J. Cosmology Astropart. Phys.* **8** (2016) 012 [[1512.01981](#)].
- [46] N. Dalal and A. Kravtsov, *Excluding fuzzy dark matter with sizes and stellar kinematics of ultrafaint dwarf galaxies*, *Phys. Rev. D* **106** (2022) 063517.
- [47] I. S. Goldstein, S. M. Koushiappas and M. G. Walker, *Viability of ultralight bosonic dark matter in dwarf galaxies*, *Phys. Rev. D* **106** (2022) 063010 [[2206.05244](#)].
- [48] S. C. Hotinli, D. J. E. Marsh and M. Kamionkowski, *Probing ultralight axions with the 21-cm signal during cosmic dawn*, *Phys. Rev. D* **106** (2022) 043529 [[2112.06943](#)].

- [49] J. B. Bauer, D. J. E. Marsh, R. Hložek, H. Padmanabhan and A. Laguë, *Intensity mapping as a probe of axion dark matter*, [*MNRAS* **500** \(2021\) 3162](#) [[2003.09655](#)].
- [50] J. Flitter and E. D. Kovetz, *Closing the window on fuzzy dark matter with the 21-cm signal*, [*Phys. Rev. D* **106** \(2022\) 063504](#) [[2207.05083](#)].
- [51] D. Antypas, A. Banerjee, C. Bartram, M. Baryakhtar, J. Betz, J. J. Bollinger et al., *New Horizons: Scalar and Vector Ultralight Dark Matter*, *arXiv e-prints* (2022) [arXiv:2203.14915](#) [[2203.14915](#)].
- [52] C. B. Adams et al., *Axion Dark Matter*, in *2022 Snowmass Summer Study*, 3, 2022, [2203.14923](#).
- [53] Planck Collaboration, P. A. R. Ade, N. Aghanim, M. Arnaud, M. Ashdown, J. Aumont et al., *Planck 2015 results. XIII. Cosmological parameters*, [*A&A* **594** \(2016\) A13](#) [[1502.01589](#)].
- [54] S. Aiola, E. Calabrese, L. Maurin, S. Naess, B. L. Schmitt, M. H. Abitbol et al., *The Atacama Cosmology Telescope: DR4 maps and cosmological parameters*, [*J. Cosmology Astropart. Phys.* **2020** \(2020\) 047](#) [[2007.07288](#)].
- [55] D. Dutcher, L. Balkenhol, P. A. R. Ade, Z. Ahmed, E. Anderes, A. J. Anderson et al., *Measurements of the E -mode polarization and temperature- E -mode correlation of the CMB from SPT-3G 2018 data*, [*Phys. Rev. D* **104** \(2021\) 022003](#) [[2101.01684](#)].
- [56] O. H. E. Philcox and M. M. Ivanov, *BOSS DR12 full-shape cosmology: Λ CDM constraints from the large-scale galaxy power spectrum and bispectrum monopole*, [*Phys. Rev. D* **105** \(2022\) 043517](#) [[2112.04515](#)].
- [57] BOSS collaboration, K. S. Dawson et al., *The Baryon Oscillation Spectroscopic Survey of SDSS-III*, [*Astron. J.* **145** \(2013\) 10](#) [[1208.0022](#)].
- [58] D. Grin, D. J. E. Marsh and R. Hložek, “axionCAMB: Modification of the CAMB Boltzmann code.” Astrophysics Source Code Library, record ascl:2203.026, Mar., 2022.
- [59] D. Blas, J. Lesgourgues and T. Tram, *The Cosmic Linear Anisotropy Solving System (CLASS). Part II: Approximation schemes*, [*J. Cosmology Astropart. Phys.* **7** \(2011\) 34](#) [[1104.2933](#)].
- [60] T. Cookmeyer, J. Cookmeyer, D. Grin and T. L. Smith, *How sound are our ultralight axion approximations?*, [*Phys. Rev. D* **101** \(2020\) 023501](#) [[1909.11094](#)].
- [61] S. Passaglia and W. Hu, *Accurate effective fluid approximation for ultralight axions*, [*Phys. Rev. D* **105** \(2022\) 123529](#) [[2201.10238](#)].
- [62] D. Baumann, A. Nicolis, L. Senatore and M. Zaldarriaga, *Cosmological non-linearities as an effective fluid*, [*J. Cosmology Astropart. Phys.* **2012** \(2012\) 051](#) [[1004.2488](#)].
- [63] M. Simonović, T. Baldauf, M. Zaldarriaga, J. J. Carrasco and J. A. Kollmeier, *Cosmological perturbation theory using the FFTLog: formalism and connection to QFT loop integrals*, [*J. Cosmology Astropart. Phys.* **2018** \(2018\) 030](#) [[1708.08130](#)].
- [64] G. Cabass, M. M. Ivanov, M. Lewandowski, M. Mirbabayi and M. Simonović, *Snowmass White Paper: Effective Field Theories in Cosmology*, in *2022 Snowmass Summer Study*, 3, 2022, [2203.08232](#).
- [65] G. D’Amico, L. Senatore and P. Zhang, *Limits on w CDM from the EFTofLSS with the PyBird code*, [*JCAP* **01** \(2021\) 006](#) [[2003.07956](#)].
- [66] G. d’Amico, J. Gleyzes, N. Kokron, K. Markovic, L. Senatore, P. Zhang et al., *The cosmological analysis of the SDSS/BOSS data from the Effective Field Theory of Large-Scale Structure*, [*J. Cosmology Astropart. Phys.* **2020** \(2020\) 005](#) [[1909.05271](#)].

- [67] T. Colas, G. d’Amico, L. Senatore, P. Zhang and F. Beutler, *Efficient cosmological analysis of the SDSS/BOSS data from the Effective Field Theory of Large-Scale Structure*, *J. Cosmology Astropart. Phys.* **2020** (2020) 001 [[1909.07951](#)].
- [68] M. M. Ivanov, M. Simonović and M. Zaldarriaga, *Cosmological Parameters from the BOSS Galaxy Power Spectrum*, *JCAP* **05** (2020) 042 [[1909.05277](#)].
- [69] M. M. Ivanov, M. Simonović and M. Zaldarriaga, *Cosmological Parameters and Neutrino Masses from the Final Planck and Full-Shape BOSS Data*, *Phys. Rev. D* **101** (2020) 083504 [[1912.08208](#)].
- [70] A. Chudaykin, M. M. Ivanov, O. H. E. Philcox and M. Simonović, *Nonlinear perturbation theory extension of the Boltzmann code CLASS*, *Phys. Rev. D* **102** (2020) 063533 [[2004.10607](#)].
- [71] M. M. Ivanov, *Effective Field Theory for Large Scale Structure*, [2212.08488](#).
- [72] L. Senatore and M. Zaldarriaga, *The Effective Field Theory of Large-Scale Structure in the presence of Massive Neutrinos*, *arXiv e-prints* (2017) arXiv:1707.04698 [[1707.04698](#)].
- [73] D. J. E. Marsh, *WarmAndFuzzy: the halo model beyond CDM*, *ArXiv e-prints* (2016) [[1605.05973](#)].
- [74] S. M. L. Vogt, D. J. E. Marsh and A. Laguë, *Improved Mixed Dark Matter Halo Model for Ultralight Axions*, *arXiv e-prints* (2022) arXiv:2209.13445 [[2209.13445](#)].
- [75] K. Heitmann, D. Higdon, M. White, S. Habib, B. J. Williams, E. Lawrence et al., *The Coyote Universe. II. Cosmological Models and Precision Emulation of the Nonlinear Matter Power Spectrum*, *ApJ* **705** (2009) 156 [[0902.0429](#)].
- [76] K. Heitmann, E. Lawrence, J. Kwan, S. Habib and D. Higdon, *The Coyote Universe Extended: Precision Emulation of the Matter Power Spectrum*, *ApJ* **780** (2014) 111 [[1304.7849](#)].
- [77] E. Lawrence, K. Heitmann, J. Kwan, A. Upadhye, D. Bingham, S. Habib et al., *The Mira-Titan Universe. II. Matter Power Spectrum Emulation*, *ApJ* **847** (2017) 50 [[1705.03388](#)].
- [78] Z. Zhai, J. L. Tinker, M. R. Becker, J. DeRose, Y.-Y. Mao, T. McClintock et al., *The Aemulus Project. III. Emulation of the Galaxy Correlation Function*, *ApJ* **874** (2019) 95 [[1804.05867](#)].
- [79] Euclid Collaboration, M. Knabenhans, J. Stadel, S. Marelli, D. Potter, R. Teyssier et al., *Euclid preparation: II. The EUCLIDEMULATOR - a tool to compute the cosmology dependence of the nonlinear matter power spectrum*, *MNRAS* **484** (2019) 5509 [[1809.04695](#)].
- [80] S. Bird, K. K. Rogers, H. V. Peiris, L. Verde, A. Font-Ribera and A. Pontzen, *An emulator for the Lyman- α forest*, *J. Cosmology Astropart. Phys.* **2019** (2019) 050 [[1812.04654](#)].
- [81] K. K. Rogers, H. V. Peiris, A. Pontzen, S. Bird, L. Verde and A. Font-Ribera, *Bayesian emulator optimisation for cosmology: application to the Lyman-alpha forest*, *J. Cosmology Astropart. Phys.* **2019** (2019) 031 [[1812.04631](#)].
- [82] C. Pedersen, A. Font-Ribera, K. K. Rogers, P. McDonald, H. V. Peiris, A. Pontzen et al., *An emulator for the Lyman- α forest in beyond- Λ CDM cosmologies*, *J. Cosmology Astropart. Phys.* **2021** (2021) 033 [[2011.15127](#)].
- [83] K. K. Rogers, C. Dvorkin and H. V. Peiris, *Limits on the Light Dark Matter-Proton Cross Section from Cosmic Large-Scale Structure*, *Phys. Rev. Lett.* **128** (2022) 171301 [[2111.10386](#)].
- [84] M. Nori and M. Baldi, *AX-GADGET: a new code for cosmological simulations of Fuzzy Dark Matter and Axion models*, *MNRAS* **478** (2018) 3935 [[1801.08144](#)].
- [85] H.-Y. Schive, T. Chiueh and T. Broadhurst, *Cosmic structure as the quantum interference of a coherent dark wave*, *Nature Physics* **10** (2014) 496 [[1406.6586](#)].

- [86] P. Mocz, A. Fialkov, M. Vogelsberger, F. Becerra, M. A. Amin, S. Bose et al., *First Star-Forming Structures in Fuzzy Cosmic Filaments*, *Phys. Rev. Lett.* **123** (2019) 141301 [[1910.01653](#)].
- [87] X. Li, L. Hui and G. L. Bryan, *Numerical and perturbative computations of the fuzzy dark matter model*, *Phys. Rev. D* **99** (2019) 063509 [[1810.01915](#)].
- [88] B. Schwabe, M. Gosenca, C. Behrens, J. C. Niemeyer and R. Easther, *Simulating mixed fuzzy and cold dark matter*, *Phys. Rev. D* **102** (2020) 083518 [[2007.08256](#)].
- [89] M. Kulkarni, E. Visbal, G. L. Bryan and X. Li, *If dark matter is fuzzy, the first stars form in massive pancakes*, *arXiv e-prints* (2022) arXiv:2210.11515 [[2210.11515](#)].
- [90] E. Abdalla, G. F. Abellán, A. Aboubrahim, A. Agnello, Ö. Akarsu, Y. Akrami et al., *Cosmology intertwined: A review of the particle physics, astrophysics, and cosmology associated with the cosmological tensions and anomalies*, *Journal of High Energy Astrophysics* **34** (2022) 49 [[2203.06142](#)].
- [91] M. Lucca, *Dark energy-dark matter interactions as a solution to the S_8 tension*, *Physics of the Dark Universe* **34** (2021) 100899 [[2105.09249](#)].
- [92] V. Poulin, J. L. Bernal, E. Kovetz and M. Kamionkowski, *The Sigma-8 Tension is a Drag*, *arXiv e-prints* (2022) arXiv:2209.06217 [[2209.06217](#)].
- [93] D. E. Kaplan, G. Z. Krnjaic, K. R. Rehermann and C. M. Wells, *Atomic dark matter*, *J. Cosmology Astropart. Phys.* **2010** (2010) 021 [[0909.0753](#)].
- [94] F.-Y. Cyr-Racine and K. Sigurdson, *Cosmology of atomic dark matter*, *Phys. Rev. D* **87** (2013) 103515 [[1209.5752](#)].
- [95] S. Bansal, J. Barron, D. Curtin and Y. Tsai, *Precision Cosmological Constraints on Atomic Dark Matter*, *arXiv e-prints* (2022) arXiv:2212.02487 [[2212.02487](#)].
- [96] K. Enqvist, S. Nadathur, T. Sekiguchi and T. Takahashi, *Decaying dark matter and the tension in σ_8* , *J. Cosmology Astropart. Phys.* **2015** (2015) 067 [[1505.05511](#)].
- [97] K. L. Pandey, T. Karwal and S. Das, *Alleviating the H_0 and σ_8 anomalies with a decaying dark matter model*, *J. Cosmology Astropart. Phys.* **2020** (2020) 026 [[1902.10636](#)].
- [98] G. F. Abellán, R. Murgia, V. Poulin and J. Lavalle, *Implications of the S_8 tension for decaying dark matter with warm decay products*, *arXiv e-prints* (2020) arXiv:2008.09615 [[2008.09615](#)].
- [99] G. F. Abellán, R. Murgia and V. Poulin, *Linear cosmological constraints on two-body decaying dark matter scenarios and the S_8 tension*, *Phys. Rev. D* **104** (2021) 123533 [[2102.12498](#)].
- [100] T. Simon, G. F. Abellán, P. Du, V. Poulin and Y. Tsai, *Constraining decaying dark matter with BOSS data and the effective field theory of large-scale structures*, *Phys. Rev. D* **106** (2022) 023516 [[2203.07440](#)].
- [101] T. Driskell, E. O. Nadler, J. Mirocha, A. Benson, K. K. Boddy, T. D. Morton et al., *Structure formation and the global 21-cm signal in the presence of Coulomb-like dark matter-baryon interactions*, *Phys. Rev. D* **106** (2022) 103525 [[2209.04499](#)].
- [102] A. Amon and G. Efstathiou, *A non-linear solution to the S_8 tension?*, *MNRAS* **516** (2022) 5355 [[2206.11794](#)].
- [103] J. C. Hill, E. McDonough, M. W. Toomey and S. Alexander, *Early dark energy does not restore cosmological concordance*, *Phys. Rev. D* **102** (2020) 043507 [[2003.07355](#)].
- [104] G. Ye, J. Zhang and Y.-S. Piao, *Resolving both H_0 and S_8 tensions with AdS early dark energy and ultralight axion*, *arXiv e-prints* (2021) arXiv:2107.13391 [[2107.13391](#)].
- [105] S. Alexander, H. Bernardo and M. W. Toomey, *Addressing the Hubble and S_8 Tensions with a Kinetically Mixed Dark Sector*, *arXiv e-prints* (2022) arXiv:2207.13086 [[2207.13086](#)].

- [106] I. J. Allali, M. P. Hertzberg and F. Rompineve, *Dark sector to restore cosmological concordance*, [*Phys. Rev. D* **104** \(2021\) L081303](#) [[2104.12798](#)].
- [107] U.-H. Zhang and T. Chiueh, *Cosmological Perturbations of Extreme Axion in the Radiation Era*, [*Phys. Rev. D* **96** \(2017\) 063522](#) [[1705.01439](#)].
- [108] F. X. L. Cedeño, A. X. González-Morales and L. A. Ureña López, *Cosmological signatures of ultralight dark matter with an axionlike potential*, [*Phys. Rev. D* **96** \(2017\) 061301](#) [[1703.10180](#)].
- [109] K.-H. Leong, H.-Y. Schive, U.-H. Zhang and T. Chiueh, *Testing extreme-axion wave-like dark matter using the BOSS Lyman-alpha forest data*, [*Mon. Not. Roy. Astron. Soc.* **484** \(2019\) 4273](#) [[1810.05930](#)].
- [110] A. Arvanitaki, S. Dimopoulos, M. Galanis, L. Lehner, J. O. Thompson and K. Van Tilburg, *Large-misalignment mechanism for the formation of compact axion structures: Signatures from the QCD axion to fuzzy dark matter*, [*Phys. Rev. D* **101** \(2020\) 083014](#) [[1909.11665](#)].
- [111] M. Pospelov, A. Ritz, C. Skordis, A. Ritz and C. Skordis, *Pseudoscalar perturbations and polarization of the cosmic microwave background*, [*Phys. Rev. Lett.* **103** \(2009\) 051302](#) [[0808.0673](#)].
- [112] G. Sigl and P. Trivedi, *Axion-like Dark Matter Constraints from CMB Birefringence*, [1811.07873](#).
- [113] M. A. Fedderke, P. W. Graham and S. Rajendran, *Axion Dark Matter Detection with CMB Polarization*, [*Phys. Rev. D* **100** \(2019\) 015040](#) [[1903.02666](#)].
- [114] I. Obata, *Implications of the cosmic birefringence measurement for the axion dark matter search*, [*JCAP* **09** \(2022\) 062](#) [[2108.02150](#)].
- [115] D. G. Levkov, A. G. Panin and I. I. Tkachev, *Radio-emission of axion stars*, [*Phys. Rev. D* **102** \(2020\) 023501](#) [[2004.05179](#)].
- [116] D. Baumann, D. Green and B. Wallisch, *New Target for Cosmic Axion Searches*, [*Phys. Rev. Lett.* **117** \(2016\) 171301](#) [[1604.08614](#)].
- [117] F. D’Eramo, F. Hajkarim and S. Yun, *Thermal Axion Production at Low Temperatures: A Smooth Treatment of the QCD Phase Transition*, [*Phys. Rev. Lett.* **128** \(2022\) 152001](#) [[2108.04259](#)].
- [118] W. Hu, *Structure formation with generalized dark matter*, [*Astrophys. J.* **506** \(1998\) 485](#) [[astro-ph/9801234](#)].
- [119] L. Amendola and R. Barbieri, *Dark matter from an ultra-light pseudo-Goldstone-boson*, [*Phys. Lett. B* **642** \(2006\) 192](#) [[hep-ph/0509257](#)].
- [120] J.-c. Hwang and H. Noh, *Axion as a Cold Dark Matter candidate*, [*Phys. Lett. B* **680** \(2009\) 1](#) [[0902.4738](#)].
- [121] D. J. E. Marsh, *Axion Cosmology*, [*Phys. Rept.* **643** \(2016\) 1](#) [[1510.07633](#)].
- [122] E. Madelung, *Eine anschauliche Deutung der Gleichung von Schrödinger*, [*Naturwissenschaften* **14** \(1926\) 1004](#).
- [123] M. Khlopov, B. A. Malomed and I. B. Zeldovich, *Gravitational instability of scalar fields and formation of primordial black holes*, [*Mon. Not. Roy. Astron. Soc.* **215** \(1985\) 575](#).
- [124] D. J. E. Marsh and P. G. Ferreira, *Ultra-Light Scalar Fields and the Growth of Structure in the Universe*, [*Phys. Rev. D* **82** \(2010\) 103528](#) [[1009.3501](#)].
- [125] W. Hu, R. Barkana and A. Gruzinov, *Fuzzy Cold Dark Matter: The Wave Properties of Ultralight Particles*, [*Physical Review Letters* **85** \(2000\) 1158](#) [[astro-ph/0003365](#)].

- [126] D. J. E. Marsh, D. Grin, R. Hložek and P. G. Ferreira, *Axiverse cosmology and the energy scale of inflation*, *Phys. Rev. D* **87** (2013) 121701 [[1303.3008](#)].
- [127] R. Hložek, D. J. E. Marsh, D. Grin, R. Allison, J. Dunkley and E. Calabrese, *Future CMB tests of dark matter: Ultralight axions and massive neutrinos*, *Phys. Rev. D* **95** (2017) 123511 [[1607.08208](#)].
- [128] J. C. Jackson, *Fingers of God: A critique of Rees' theory of primordial gravitational radiation*, *Mon. Not. Roy. Astron. Soc.* **156** (1972) 1P [[0810.3908](#)].
- [129] M. M. Ivanov, O. H. E. Philcox, M. Simonović, M. Zaldarriaga, T. Nishimichi and M. Takada, *Cosmological constraints without nonlinear redshift-space distortions*, *Phys. Rev. D* **105** (2022) 043531 [[2110.00006](#)].
- [130] G. D'Amico, L. Senatore, P. Zhang and T. Nishimichi, *Taming redshift-space distortion effects in the EFTofLSS and its application to data*, [2110.00016](#).
- [131] N. Kaiser, *Clustering in real space and in redshift space*, *MNRAS* **227** (1987) 1.
- [132] L. Senatore and M. Zaldarriaga, *The IR-resummed Effective Field Theory of Large Scale Structures*, *JCAP* **02** (2015) 013 [[1404.5954](#)].
- [133] D. Blas, M. Garny, M. M. Ivanov and S. Sibiryakov, *Time-Sliced Perturbation Theory II: Baryon Acoustic Oscillations and Infrared Resummation*, *JCAP* **07** (2016) 028 [[1605.02149](#)].
- [134] M. M. Ivanov and S. Sibiryakov, *Infrared Resummation for Biased Tracers in Redshift Space*, *JCAP* **07** (2018) 053 [[1804.05080](#)].
- [135] C. Alcock and B. Paczynski, *An evolution free test for non-zero cosmological constant*, *Nature* **281** (1979) 358.
- [136] M. M. Ivanov, O. H. E. Philcox, T. Nishimichi, M. Simonović, M. Takada and M. Zaldarriaga, *Precision analysis of the redshift-space galaxy bispectrum*, *Phys. Rev. D* **105** (2022) 063512 [[2110.10161](#)].
- [137] O. H. E. Philcox, M. M. Ivanov, G. Cabass, M. Simonović, M. Zaldarriaga and T. Nishimichi, *Cosmology with the redshift-space galaxy bispectrum monopole at one-loop order*, *Phys. Rev. D* **106** (2022) 043530 [[2206.02800](#)].
- [138] G. D'Amico, Y. Donath, M. Lewandowski, L. Senatore and P. Zhang, *The BOSS bispectrum analysis at one loop from the Effective Field Theory of Large-Scale Structure*, [2206.08327](#).
- [139] F. Beutler, C. Blake, M. Colless, D. H. Jones, L. Staveley-Smith, L. Campbell et al., *The 6dF Galaxy Survey: baryon acoustic oscillations and the local Hubble constant*, *MNRAS* **416** (2011) 3017 [[1106.3366](#)].
- [140] A. J. Ross, L. Samushia, C. Howlett, W. J. Percival, A. Burden and M. Manera, *The clustering of the SDSS DR7 main Galaxy sample - I. A 4 per cent distance measure at $z = 0.15$* , *MNRAS* **449** (2015) 835 [[1409.3242](#)].
- [141] S. Alam, M. Ata, S. Bailey, F. Beutler, D. Bizyaev, J. A. Blazek et al., *The clustering of galaxies in the completed SDSS-III Baryon Oscillation Spectroscopic Survey: cosmological analysis of the DR12 galaxy sample*, *MNRAS* **470** (2017) 2617 [[1607.03155](#)].
- [142] M. Betoule, R. Kessler, J. Guy, J. Mosher, D. Hardin, R. Biswas et al., *Improved cosmological constraints from a joint analysis of the SDSS-II and SNLS supernova samples*, *A&A* **568** (2014) A22 [[1401.4064](#)].
- [143] L. Balkenhol, D. Dutcher, A. Spurio Mancini, A. Doussot, K. Benabed, S. Galli et al., *A Measurement of the CMB Temperature Power Spectrum and Constraints on Cosmology from the SPT-3G 2018 TT/TE/EE Data Set*, *arXiv e-prints* (2022) arXiv:2212.05642 [[2212.05642](#)].

- [144] J. Zuntz, M. Paterno, E. Jennings, D. Rudd, A. Manzotti, S. Dodelson et al., *CosmoSIS: Modular cosmological parameter estimation*, *Astronomy and Computing* **12** (2015) 45 [[1409.3409](#)].
- [145] J. Torrado and A. Lewis, *Cobaya: code for Bayesian analysis of hierarchical physical models*, *J. Cosmology Astropart. Phys.* **2021** (2021) 057 [[2005.05290](#)].
- [146] A. La Posta, T. Louis, X. Garrido and J. C. Hill, *Constraints on prerecombination early dark energy from spt-3g public data*, *Phys. Rev. D* **105** (2022) 083519.
- [147] O. H. E. Philcox, M. M. Ivanov, M. Simonović and M. Zaldarriaga, *Combining Full-Shape and BAO Analyses of Galaxy Power Spectra: A 1.6% CMB-independent constraint on H_0* , *JCAP* **05** (2020) 032 [[2002.04035](#)].
- [148] SDSS collaboration, D. J. Eisenstein et al., *SDSS-III: Massive Spectroscopic Surveys of the Distant Universe, the Milky Way Galaxy, and Extra-Solar Planetary Systems*, *Astron. J.* **142** (2011) 72 [[1101.1529](#)].
- [149] O. H. E. Philcox, *Cosmology without window functions: Quadratic estimators for the galaxy power spectrum*, *Phys. Rev. D* **103** (2021) 103504 [[2012.09389](#)].
- [150] O. H. E. Philcox, *Cosmology without window functions. II. Cubic estimators for the galaxy bispectrum*, *Phys. Rev. D* **104** (2021) 123529 [[2107.06287](#)].
- [151] B. Kalus, W. J. Percival, D. J. Bacon, E. M. Mueller, L. Samushia, L. Verde et al., *A map-based method for eliminating systematic modes from galaxy clustering power spectra with application to BOSS*, *Mon. Not. Roy. Astron. Soc.* **482** (2019) 453 [[1806.02789](#)].
- [152] A. Chudaykin, K. Dolgikh and M. M. Ivanov, *Constraints on the curvature of the Universe and dynamical dark energy from the Full-shape and BAO data*, *Phys. Rev. D* **103** (2021) 023507 [[2009.10106](#)].
- [153] F.-S. Kitaura et al., *The clustering of galaxies in the SDSS-III Baryon Oscillation Spectroscopic Survey: mock galaxy catalogues for the BOSS Final Data Release*, *Mon. Not. Roy. Astron. Soc.* **456** (2016) 4156 [[1509.06400](#)].
- [154] S. A. Rodríguez-Torres et al., *The clustering of galaxies in the SDSS-III Baryon Oscillation Spectroscopic Survey: modelling the clustering and halo occupation distribution of BOSS CMASS galaxies in the Final Data Release*, *Mon. Not. Roy. Astron. Soc.* **460** (2016) 1173 [[1509.06404](#)].
- [155] D. J. Marsh, E. Macaulay, M. Trebitsch and P. G. Ferreira, *Ultra-light Axions: Degeneracies with Massive Neutrinos and Forecasts for Future Cosmological Observations*, *Phys. Rev. D* **85** (2012) 103514 [[1110.0502](#)].
- [156] O. Pisanti, A. Cirillo, S. Esposito, F. Iocco, G. Mangano, G. Miele et al., *PARthENoPE: Public algorithm evaluating the nucleosynthesis of primordial elements*, *Computer Physics Communications* **178** (2008) 956 [[0705.0290](#)].
- [157] T. Nishimichi, G. D’Amico, M. M. Ivanov, L. Senatore, M. Simonović, M. Takada et al., *Blinded challenge for precision cosmology with large-scale structure: results from effective field theory for the redshift-space galaxy power spectrum*, *Phys. Rev. D* **102** (2020) 123541 [[2003.08277](#)].
- [158] T. Simon, P. Zhang, V. Poulin and T. L. Smith, *On the consistency of effective field theory analyses of BOSS power spectrum*, [2208.05929](#).
- [159] F. Feroz, M. P. Hobson and M. Bridges, *MULTINEST: an efficient and robust Bayesian inference tool for cosmology and particle physics*, *MNRAS* **398** (2009) 1601 [[0809.3437](#)].
- [160] F. Feroz, M. P. Hobson, E. Cameron and A. N. Pettitt, *Importance Nested Sampling and the MultiNest Algorithm*, *The Open Journal of Astrophysics* **2** (2019) 10 [[1306.2144](#)].

- [161] L. Amendola and R. Barbieri, *Dark matter from an ultra-light pseudo-Goldstone-boson*, *Physics Letters B* **642** (2006) 192 [[hep-ph/0509257](#)].
- [162] V. Poulin, T. L. Smith, T. Karwal and M. Kamionkowski, *Early Dark Energy can Resolve the Hubble Tension*, *Phys. Rev. Lett.* **122** (2019) 221301 [[1811.04083](#)].
- [163] R. E. Kass and A. E. Raftery, *Bayes factors*, *Journal of the American Statistical Association* **90** (1995) 773 [<https://www.tandfonline.com/doi/pdf/10.1080/01621459.1995.10476572>].
- [164] A. Heavens, Y. Fantaye, E. Sellentin, H. Eggers, Z. Hosenie, S. Kroon et al., *No Evidence for Extensions to the Standard Cosmological Model*, *Phys. Rev. Lett.* **119** (2017) 101301 [[1704.03467](#)].
- [165] T. M. C. Abbott, M. Aguena, A. Alarcon, S. Allam, O. Alves, A. Amon et al., *Dark Energy Survey Year 3 results: Cosmological constraints from galaxy clustering and weak lensing*, *Phys. Rev. D* **105** (2022) 023520 [[2105.13549](#)].
- [166] C. Heymans, T. Tröster, M. Asgari, C. Blake, H. Hildebrandt, B. Joachimi et al., *KiDS-1000 Cosmology: Multi-probe weak gravitational lensing and spectroscopic galaxy clustering constraints*, *A&A* **646** (2021) A140 [[2007.15632](#)].
- [167] A. G. Sánchez, R. Scoccimarro, M. Crocce, J. N. Grieb, S. Salazar-Albornoz, C. Dalla Vecchia et al., *The clustering of galaxies in the completed SDSS-III Baryon Oscillation Spectroscopic Survey: Cosmological implications of the configuration-space clustering wedges*, *MNRAS* **464** (2017) 1640 [[1607.03147](#)].
- [168] C. Blake, A. Amon, M. Childress, T. Erben, K. Glazebrook, J. Harnois-Deraps et al., *The 2-degree Field Lensing Survey: design and clustering measurements*, *Monthly Notices of the Royal Astronomical Society* **462** (2016) 4240 [<https://academic.oup.com/mnras/article-pdf/462/4/4240/18517346/stw1990.pdf>].
- [169] M. Raveri and C. Doux, *Non-Gaussian estimates of tensions in cosmological parameters*, *Phys. Rev. D* **104** (2021) 043504 [[2105.03324](#)].
- [170] P. Lemos, M. Raveri, A. Campos, Y. Park, C. Chang, N. Weaverdyck et al., *Assessing tension metrics with dark energy survey and Planck data*, *MNRAS* **505** (2021) 6179 [[2012.09554](#)].
- [171] N. Schöneberg, J. Lesgourgues and D. C. Hooper, *The $ba\bar{o}+bbn$ take on the hubble tension*, *Journal of Cosmology and Astroparticle Physics* **2019** (2019) 029.
- [172] DESI Collaboration, A. Aghamousa, J. Aguilar, S. Ahlen, S. Alam, L. E. Allen et al., *The DESI Experiment Part I: Science, Targeting, and Survey Design*, *arXiv e-prints* (2016) arXiv:1611.00036 [[1611.00036](#)].
- [173] LSST Dark Energy Science Collaboration, *Large Synoptic Survey Telescope: Dark Energy Science Collaboration*, *arXiv e-prints* (2012) arXiv:1211.0310 [[1211.0310](#)].
- [174] K. Bechtol, S. Birrer, F.-Y. Cyr-Racine, K. Schutz, S. Adhikari, A. Banerjee et al., *Snowmass2021 Cosmic Frontier White Paper: Dark Matter Physics from Halo Measurements*, *arXiv e-prints* (2022) arXiv:2203.07354 [[2203.07354](#)].
- [175] D. Grin, M. A. Amin, V. Gluscevic, R. Hlozek, D. J. E. Marsh, V. Poulin et al., *Gravitational probes of ultra-light axions*, *BAAS* **51** (2019) 567 [[1904.09003](#)].
- [176] C. Dvorkin et al., *Dark Matter Physics from the CMB-S4 Experiment*, in *2022 Snowmass Summer Study*, 3, 2022, [2203.07064](#).
- [177] M. M. Ivanov, E. McDonough, J. C. Hill, M. Simonović, M. W. Toomey, S. Alexander et al., *Constraining Early Dark Energy with Large-Scale Structure*, *Phys. Rev. D* **102** (2020) 103502 [[2006.11235](#)].